

**Final Technical Report
ONR Grant N00014-97-1-0014**

**INCORPORATION OF UNCERTAINTY ANALYSIS
IN EXPERIMENTAL/COMPUTATIONAL FLUID DYNAMICS
VALIDATIONS**

**Hugh W. Coleman
Propulsion Research Center
Mechanical and Aerospace Engineering Department
University of Alabama in Huntsville
Huntsville, AL 35899**

April 2002

20020502 099

AQMO2-08-1406

REPORT DOCUMENTATION PAGE			Form Approved OMB No. 0704-0188	
Public reporting burden for this collection of information is estimated to average 1 hour per response, including the time for reviewing instructions, searching existing data sources, gathering and maintaining the data needed, and completing and reviewing the collection of information. Send comments regarding this burden estimate or any other aspect of this collection of information, including suggestions for reducing this burden, to Washington Headquarters Services, Directorate for Information Operations and Reports, 1215 Jefferson Davis Highway, Suite 1204, Arlington, VA 22202-4302, and to the Office of Management and Budget, Paperwork Reduction Project (0704-0188), Washington, DC 20503.				
1. AGENCY USE ONLY (Leave blank)		2. REPORT DATE April 15, 2002		3. REPORT TYPE AND DATES COVERED Final; 01 OCT 1996 - 31DEC 2001
4. TITLE AND SUBTITLE Incorporation of Uncertainty Analysis in Experimental/Computational Fluid Dynamics Validations			5. FUNDING NUMBERS Grant N00014-97-1-0014	
6. AUTHORS Hugh W. Coleman				
7. PERFORMING ORGANIZATION NAME(S) AND ADDRESS(ES) Propulsion Research Center Department of Mechanical and Aerospace Engineering University of Alabama in Huntsville Huntsville, AL 35899			8. PERFORMING ORGANIZATION REPORT NUMBER UAH-PRC-HWC-041502	
9. SPONSORING/MONITORING AGENCY NAME(S) AND ADDRESS(ES) Office of Naval Research Ballston Center Tower One 800 North Quincy Street Arlington, VA 22217-5660			10. SPONSORING/MONITORING AGENCY REPORT NUMBER	
11. SUPPLEMENTARY NOTES				
12a. DISTRIBUTION/AVAILABILITY STATEMENT Approved for Public Release; distribution is Unlimited			12b. DISTRIBUTION CODE	
13. ABSTRACT (Maximum 200 words) A quantitative approach to verification and validation of simulations was developed which properly takes into account the uncertainties in experimental data and the uncertainties in the simulation result. This report includes as appendices the refereed publications which document the research program and its results.				
14. SUBJECT TERMS Verification; Validation; Uncertainty Analysis; Fluid Dynamics; CFD			15. NUMBER OF PAGES 58	
			16. PRICE CODE	
17. SECURITY CLASSIFICATION OF REPORT UNCLASSIFIED	18. SECURITY CLASSIFICATION OF THIS PAGE UNCLASSIFIED	19. SECURITY CLASSIFICATION OF ABSTRACT UNCLASSIFIED	20. LIMITATION OF ABSTRACT UNCLASSIFIED	

This report documents the results of the research program conducted under ONR Grant N00014-97-1-0014 during the period 1 OCT 1996 through 31 DEC 2001. Since the results have been carefully documented in four refereed journal articles and one refereed proceedings paper, those documents are incorporated as appendices and the material therein is not repeated in the body of this report.

Long-term research objective:

The verification and validation (V&V) of simulations is a subject of great current interest across the entire spectrum of computational mechanics. V&V techniques are in their infancy and are the subjects of spirited debate. Our objective was to develop a rigorous V&V methodology that (1) properly includes the effects of uncertainties in the simulations and in the experimental validation data and (2) provides a *quantitative* assessment of the degree of (or lack of) validation of a simulation for a specific configuration and condition.

S&T objective:

Develop V&V techniques for Computational Fluid Dynamics (CFD) codes and Structural Loads and Motions codes supported/developed by ONR. Participate in the application of the V&V techniques to assess the codes and produce *documented solutions* for specific configurations and specific conditions.

Results:

The methodology has been refined and applied in the ONR programs "Verification/Validation of Computational Ship Hydrodynamics," "International Collaboration on Complementary Computational and Experimental Ship Hydrodynamics and Uncertainty Analysis," and "Surface Combatant Accelerated Hydrodynamics S&T Initiative". These programs include collaborative efforts among multiple universities, multiple industrial consortia, U.S. government researchers, and researchers at the Italian Istituto Nazionale Per Studi Ed Esperienze Di Architettura Navale. The results are documented in the following Appendices:

Appendix A

Coleman, H. W. and Stern, F. , "Uncertainties and CFD Code Validation," *J. Fluids Engineering*, Vol. 119, p. 795-803, December 1997. (Also "Discussion and Authors' Closure," Vol.120, p 635-6, September 1998.)

Appendix B

Stern, F., Longo, J., Penna, R., Olivieri, A., Ratcliffe, T., and Coleman, H., "International Collaboration on Benchmark CFD Validation Data for Surface Combatant DTMB Model 5415," Proceedings of the 23rd Symposium on Naval Hydrodynamics, Val de Reuil, France, September 17-22, 2000.

Appendix C

Coleman, H. W., Stern, F., Di Mascio, A., and Campana, E. "The Problem With Oscillatory Behavior in Grid Convergence Studies," ***J. Fluids Engineering***, Vol. 123, No. 2, p438-439, June 2001.

Appendix D

Stern, F., Wilson, R. V., Coleman, H. W., and Paterson, E. G., "Comprehensive Approach to Verification and Validation of CFD Simulations – Part 1: Methodology and Procedures," ***J. Fluids Engineering***, Vol. 123, No. 4, December 2001.

Appendix E

Wilson, R. V., Stern, F., Coleman, H. W., and Paterson, E. G., "Comprehensive Approach to Verification and Validation of CFD Simulations – Part 2: Application for RANS Simulation of a Cargo/Container Ship," ***J. Fluids Engineering***, Vol. 123, No. 4, December 2001.

Appendix A

Coleman, H. W. and Stern, F. , "Uncertainties and CFD Code Validation," *J. Fluids Engineering*, Vol. 119, p. 795-803, December 1997. (Also "Discussion and Authors' Closure," Vol.120, p 635-6, September 1998.)

Uncertainties and CFD Code Validation

H. W. Coleman

Eminent Scholar in Propulsion and
Professor,
Propulsion Research Center,
Mechanical and Aerospace
Engineering Department,
University of Alabama in Huntsville,
Huntsville, AL 35899

F. Stern

Professor,
Iowa Institute of Hydraulic Research,
Department of Mechanical Engineering,
University of Iowa,
Iowa City, IA 52242

A new approach to computational fluid dynamics code validation is developed that gives proper consideration to experimental and simulation uncertainties. The comparison error is defined as the difference between the data and simulation values and represents the combination of all errors. The validation uncertainty is defined as the combination of the uncertainties in the experimental data and the portion of the uncertainties in the CFD prediction that can be estimated. This validation uncertainty sets the level at which validation can be achieved. The criterion for validation is that the magnitude of the comparison error must be less than the validation uncertainty. If validation is not accomplished, the magnitude and sign of the comparison error can be used to improve the mathematical modeling. Consideration is given to validation procedures for a single code, multiple codes and/or models, and predictions of trends. Example results of verification/validation are presented for a single computational fluid dynamics code and for a comparison of multiple turbulence models. The results demonstrate the usefulness of the proposed validation strategy. This new approach for validation should be useful in guiding future developments in computational fluid dynamics through validation studies and in the transition of computational fluid dynamics codes to design.

1 Introduction

Uncertainty considerations involved in using experimental data in validating the predictions of CFD codes (or, more generally, computer simulations) are discussed in this article. The word uncertainty is used in the following sense—the uncertainty U associated with a measured quantity or a predicted quantity defines the $\pm U$ interval about that quantity within which we expect the true (but unknown) value of that quantity to lie 95 times out of 100. It is important to recognize that a validation is restricted to some range, typically the range of conditions of the data used in the (successful) validation effort. This is intended by the authors to be implicit in the discussions in this article.

The comparison process in attempting to validate predictions using experimental data is illustrated schematically in Fig. 1. The hypothetical predictions of result r versus independent variable X from two models (or simulations) are shown along with experimental data points (X_i, r_i) . In part (a) of the figure, no uncertainties are considered, and one might well be tempted to argue that Model 1 is superior to Model 2. The predictions from Model 1 seem to “capture the trend of the data” better than the predictions from the (simplistic, linearized, etc.) Model 2. If the uncertainties in the experimentally-determined values of the result r are considered (Fig. 1(b)), the perspective changes completely, and it is obvious that arguing for one method over another based on comparison with the experimental data is wasted effort since the predictions from both methods fall well within the data uncertainty.

Actually, Fig. 1(b) does not show the complete situation. For the data points, uncertainties in both the experimentally-determined r and the experimentally-determined value of the independent variable X should be considered, giving an uncertainty “box” around each experimental data point. Additionally, the prediction from a model should not be viewed as an infinitesimally thin r vs. X line, but rather as a “fuzzy band” that represents the prediction plus and minus the uncertainty

that should be associated with the simulation/model/code. This is illustrated in Fig. 2, which also shows that, in general, uncertainties in both the data and the predictions can vary (sometimes dramatically) over the range of X . Figure 2 shows the variables and their uncertainties, but the comparison it shows is deceptive because it is two-dimensional. The independent variable X must be considered a vector (\mathbf{X}) of n dimensions—fluid velocity as a function of position and time, $V(x, y, z, t)$, for example—and the “box” around \mathbf{X} will therefore be n -dimensional. The (total) uncertainty in r that should be used in a comparison should include the experimental uncertainty in r and the additional uncertainty in r arising from experimental uncertainties in the measurements of the n independent variables (this is developed in detail in Section 3).

Contributors to the prediction uncertainty $U_r(\mathbf{X})$ can be divided into two broad categories—numerical uncertainty and modeling uncertainty. In fact, insuring that the modeling uncertainty is below some designated value is one purpose of CFD validation through comparisons with benchmark experimental data.

The validation strategy proposed in this article and discussed in detail in Section 3 views the situation from a new perspective, isolating the modeling uncertainty (which the authors do not know how to estimate) from the uncertainties that can be estimated (the data uncertainty and the non-modeling uncertainties in predictions). A direct calculation of the comparison error E (data minus prediction) is made and compared with a validation uncertainty U_v that is composed of the uncertainties in the experimental data and the portion of the uncertainties in the CFD prediction that can be estimated. This validation uncertainty U_v is the best resolution possible in the validation effort (i.e., it sets the “noise level” below which no discrimination is possible). If the absolute value of the calculated comparison error E is less than U_v , then validation is defined as being successful at the U_v level.

From the preceding discussion the authors believe it is evident that (1) the uncertainties in the data and in the predictions set the scale at which validation is possible, and (2) these uncertainties must be considered in determining if validation has been achieved. Obviously, these uncertainties should be considered in planning and implementing a computational/experimental research program for validating CFD codes, al-

Contributed by the Fluids Engineering Division for publication in the JOURNAL OF FLUIDS ENGINEERING. Manuscript received by the Fluids Engineering Division March 31, 1997; revised manuscript received August 4, 1997. Associate Technical Editor: D. P. Telionis.

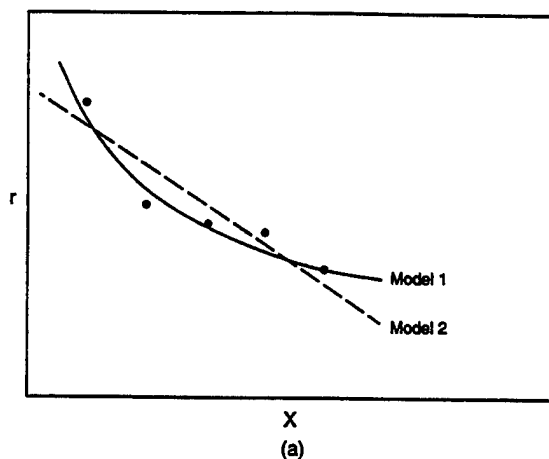


Fig. 1(a) without consideration of experimental uncertainties

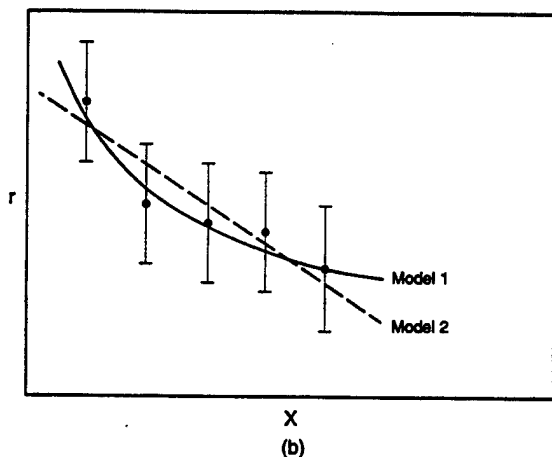


Fig. 1(b) with partial consideration of experimental uncertainties

Fig. 1 Comparisons of experimental data and model predictions

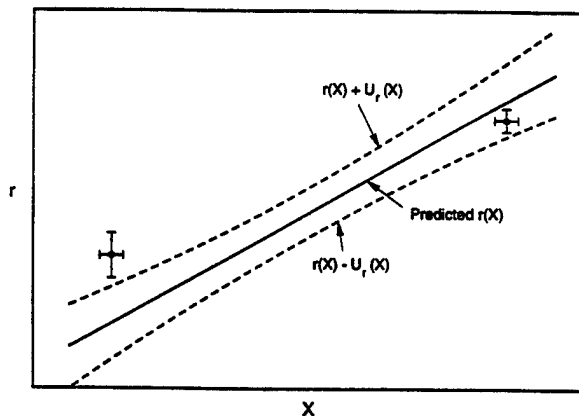


Fig. 2 Uncertainties in data and predictions to be considered in validations

though they typically have not been in the past. Figure 1(a) gives a qualitative view of the way most previous validation efforts have proceeded, with Fig. 1(b) being typical of the few approaches considering uncertainties at all.

This current work is part of a larger program (Rood, 1996) for developing and implementing a strategy for validation of Reynolds-Averaged Navier-Stokes (RANS) computational ship hydrodynamics codes. The program includes complementary computational ship hydrodynamics and towing tank investiga-

tions and considers the uncertainties in both computations and data in assessing the success of validation efforts.

2 Uncertainties in Data and in Simulations

As stated earlier, the uncertainty U associated with a measured quantity or a predicted quantity defines the $\pm U$ interval about that quantity within which we expect the true (but unknown) value of that quantity to lie 95 times out of 100. For detailed discussion of uncertainties associated with experimental data, the reader is referred to Coleman and Steele (1989, 1995). Although the uncertainty in an experimental data point originally comes from both bias (systematic) and precision (random) sources, the uncertainty is "fossilized" into a fixed quantity (a bias) once the value (X_i, r_i) of the data point is recorded and reported. This is logical if one notes that the value of the data point is always the same amount different from the (unknown) true value each time the data point is used.

The uncertainties associated with the predictions of models, simulations, CFD codes, etc. and their role in the validation process have been receiving increasing attention in the last few years, and only a few representative references are cited here. Editorial policies have been set by professional journals (ASME, 1993; AIAA, 1994; Gresho and Taylor, 1994), and standards and guidelines (IAHR, 1994) and recommended practices (ITTC, 1996) have been specified by international organizations. The literature covers a broad range from governmental (Rood, 1996) and industrial (Melnik et al., 1994) perspectives to overall methodology (Coleman, 1996; Marvin, 1995; Mehta, 1996 (also AIAA, 1997); Oberkampf et al., 1995) and detailed application (Blottner, 1990; Roache, 1997; Zingg, 1992). The 1993 ASME Symposium on Quantification of Uncertainty in Computational Fluid Dynamics (Celik et al., 1993) provides a good introduction.

As mentioned in the previous section, uncertainties associated with predictions from simulations can be divided into two broad categories: (1) numerical uncertainties, and (2) modeling uncertainties. The numerical uncertainty category includes uncertainties due to the numerical solution of the mathematical equations (discretization, artificial dissipation, iterative and grid non-convergence, local and global non-conservation of mass, momentum, energy, etc., internal and external boundary non-continuity, computer round-off, etc.) The modeling uncertainty category includes uncertainties due to assumptions and approximations in the mathematical representation of the physical process (geometry, mathematical equation, coordinate transformation approximations, free-surface boundary conditions, turbulence models, etc) and also uncertainties due to the incorporation of previous experimental data into the model (such things as fluid property values and the "constants" in turbulence models). Examples of reported uncertainties associated with property data range from 0.25–0.5 percent for liquid oxygen density (Brown et al., 1994), to 2–5 percent for the thermal conductivity of air at atmospheric pressure (Coleman and Steele, 1989), to huge percentages for properties such as surface tension coefficient that are extremely sensitive to contaminants. A recent study (Beard and Landrum, 1996) utilizing laminar Navier-Stokes computations for hydrogen flow through a solar thermal thruster at temperatures up to 6100 R showed a ± 2 percent variation in computed specific impulse due solely to the range of the available reaction rate data reported by different investigators.

The overall process leading to validation and simulation uncertainty estimation can be categorized as documentation, verification, and validation. Documentation involves detailed presentation of the mathematical equations and numerical method. Verification involves estimation of numerical uncertainty through parametric, convergence, and order-of-accuracy studies. Validation involves estimation of the difference (error) between the simulation's prediction and the truth, and this esti-

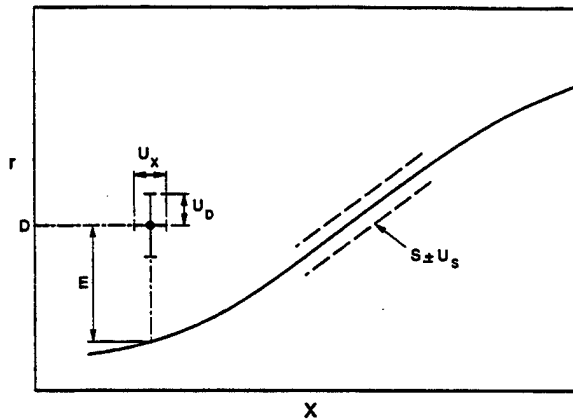


Fig. 3 Definition of comparison error

mate is impossible to make with any confidence without a benchmark. The benchmark can be an analytical solution (with an associated uncertainty) or, more likely and of primary interest here, an experimental value with its associated uncertainty. To paraphrase one reviewer, (verification)/(validation) can be viewed as addressing (equations solved right?)/(right equations solved?).

Although not always available, documentation is relatively straightforward, whereas, in spite of the aforementioned efforts, specific implementation procedures for verification and validation are not yet established. Approaches for verification require procedures for the estimation of the numerical uncertainties. Stern et al. (1996) provided an example approach for their steady RANS CFD method with application to naval surface combatants. In this approach, estimates of uncertainties were provided for both integral and point quantities for iterative and grid nonconvergence and were combined using root sum square. Also, for conditions permitting, order-of-accuracy and Richardson extrapolation studies were conducted.

In the following section, a new approach to CFD validation is developed and discussed with regard to validation of a single CFD code, to validation of a comparison of multiple codes and/or models, and to validation of predictions of trends. Subsequently, in Section 4, example results of validations are presented both for a single CFD code and for a comparison of multiple turbulence models. The CFD code and verification procedures of Stern et al. (1996) are used for two applications for which numerical and experimental uncertainty analyses are available: marine-propulsor flow (Chen, 1996; Jessup, 1994) and two-dimensional turbulent flat-plate boundary-layer flow (Sreedhar and Stern, 1997; Longo, et al., 1998).

3 An Approach to CFD Code Validation

Consider the situation shown in Fig. 3. Using the example mentioned previously, the single-plane representation r versus X might be a mean velocity component V vs. distance (z) normal to a solid surface at a given time and position (x, y, t) on that surface. Define the predicted r -value from the simulation (code) as S , the experimentally determined r -value of the (X_i, r_i) data point as D , and the comparison error, E , as their difference:

$$E = D - S \quad (1)$$

The comparison error E is the resultant of *all* of the errors associated with the experimental data and the errors associated with the simulation. Here it is assumed that a correction has been made for any error whose value is known. Thus, the errors that are the subject of this discussion have unknown sign and magnitude, and the uncertainties are estimates of these errors.

If X_i , r_i , and S share no common error sources, then the uncertainty U_E in the comparison error can be expressed as

$$U_E^2 = \left(\frac{\partial E}{\partial D}\right)^2 U_D^2 + \left(\frac{\partial E}{\partial S}\right)^2 U_S^2 = U_D^2 + U_S^2 \quad (2)$$

where U_D is the uncertainty in the data and U_S the uncertainty in the simulation. The uncertainty U_E should bound the (true) absolute value of the comparison error E 95 times out of 100. The assumptions and approximations made in deriving Eq. (2) are discussed in detail in Coleman and Steele (1995).

Recalling the discussion in Section 2, the simulation uncertainty U_S can be represented as

$$U_S^2 = U_{SN}^2 + U_{SPD}^2 + U_{SMA}^2 \quad (3)$$

where U_{SN} is the simulation numerical solution uncertainty, U_{SPD} is the simulation modeling uncertainty arising from using previous experimental data, and U_{SMA} is the simulation modeling uncertainty arising from modeling assumptions. Substituting Eq. (3) into Eq. (2) gives

$$U_E^2 = U_D^2 + U_{SN}^2 + U_{SPD}^2 + U_{SMA}^2 \quad (4)$$

Ideally, we would like to postulate that if the absolute value of E is less than its uncertainty U_E , then validation is achieved. In reality, the authors know of no approach that gives an estimate of U_{SMA} , so U_E cannot be estimated. That leaves a more stringent validation test as the practical alternative. If we define the validation uncertainty U_V as the combination of all uncertainties that we know how to estimate (i.e., all but U_{SMA}), then

$$U_V^2 = U_E^2 - U_{SMA}^2 = U_D^2 + U_{SN}^2 + U_{SPD}^2 \quad (5)$$

If $|E|$ is less than the validation uncertainty U_V , then the combination of all the errors in D and S is smaller than the estimated validation uncertainty and validation has been achieved at the U_V level. This quantity U_V is the key metric in the validation process. U_V is the validation "noise level" imposed by the uncertainties inherent in the data, the numerical solution, and the previous experimental data used in the simulation model—one cannot discriminate once $|E|$ is less than this, i.e., as long as $|E|$ is less than this one cannot evaluate the effectiveness of proposed model "improvements." Choice of the required level of U_V is associated with the degree of risk deemed acceptable in a program.

To estimate U_{SPD} for a case in which the simulation uses previous data d_i in m instances, one would need to evaluate

$$U_{SPD}^2 = \sum_{i=1}^m \left(\frac{\partial S}{\partial d_i}\right)^2 (U_{d_i})^2 \quad (6)$$

where the U_{d_i} would be estimated using established uncertainty analysis procedures (Coleman and Steele, 1989, 1995).

As discussed in Section 1, for the data point (X_i, r_i), U_D should include both the experimental uncertainty in r_i and the additional uncertainties in r_i arising from experimental uncertainties in the measurements of the n independent variables (X_j), in X_i . The expression for U_D that should be used in the U_V calculation is then

$$U_D^2 = U_{r_i}^2 + \sum_{j=1}^n \left(\frac{\partial r}{\partial X_j}\right)^2 (U_{X_j})^2 \quad (7)$$

In some cases, the terms in the summation in Eq. (7) may be shown to be very small using an order-of-magnitude analysis and then neglected. This would occur in situations in which the U_{X_j} 's are of "reasonable" magnitude and gradients in r are small. In regions of the flow with high gradients (near a surface in a turbulent flow), however, these terms may be very significant.

There is also a very real possibility that measurements of different variables might share identical bias errors. This is easy to imagine for measurements of x , y , and z . Another possibility is D and S sharing an identical error source, for example if r is drag coefficient and the same density table (curvefit) is used both in data reduction in the experiment and in the simulation. In such cases, additional "correlated bias" terms must be included in Eq. (2). Approximation and inclusion of such terms are discussed in Coleman and Steele (1989, 1995), Coleman et al. (1995), and Brown et al. (1996) and will not be covered in further detail in this article.

Validation of a Single CFD Code. The validation uncertainty, U_V , sets the level at which validation can be achieved. If the objectives of a program require that validation be accomplished "within ± 2 percent," then $|E|$ must be less than U_V and U_V must be less than (roughly) $0.02 D$. If U_V is greater than $0.02 D$, the objectives of the program cannot be achieved until the sum of the terms on the right-hand-side of Eq. (5) is reduced to an acceptable level. When $|E|$ is greater than U_V , validation is not accomplished, and the magnitude and sign of E can be valuable in designing strategies to improve the mathematical modeling.

As one reviewer pointed out, consideration of Eq. (5) shows that (a) the more uncertain the data, and/or (b) the more inaccurate the code (greater U_{SN} and U_{SPD}), the easier it is to validate a code. That is true, since the greater the uncertainties in the data and the code predictions, the greater the "noise level" (U_V). If this value of U_V is greater than that designated as necessary in a research/design/development program, however, then the required level of validation could not be achieved without improvement in the quality of the data, the code, or both. Likewise, if U_{SN} and U_{SPD} are not estimated but $|E|$ is less than U_D , then validation has been achieved *but at an unknown level*. Obviously, if no uncertainties are estimated, no statements about validation can be made within the concept of the validation process as considered in this article.

In general, validation of a code's predictions of a number (N) of different variables is desired, and this means that in a particular validation effort there will be N different E 's and U_V 's and (perhaps) some successful validations and some unsuccessful. For each variable, a plot of the simulation prediction versus X compared with the (X_i, r_i) data points gives a traditional overview of the validation status, but the interpretation of the comparison is greatly affected by choice of the scale and the size of the symbols. A plot of $\pm U_V$ and E versus X for each variable is particularly useful in drawing conclusions, as demonstrated in Section 4, and the interpretation of the comparison is more insensitive to scale and symbol size choices.

Comparison of Multiple Codes and/or Models in a Validation Effort. When a validation effort involves multiple codes and/or models, the procedure discussed above—comparison of the E 's and U_V 's for the N variables—should be performed for each code/model.

Since each code/model may have a different U_V , some method to compare the different codes'/models' performance for each variable in the validation is useful. The range within which (95 times out of 100) the true value of E lies is $E \pm U_E$. From Eq. (5), when U_{SMA} is zero then $U_V = U_E$, so for that ideal condition the maximum absolute magnitude of the 95% confidence interval is given by $|E| + U_V$. Comparison of the $(|E| + U_V)$'s for the different codes/models then shows which has the smallest range of likely error assuming all U_{SMA} 's are zero. This allows appropriate comparisons of (low E)/(high U_V) with (high E /low U_V) codes/models.

Validation of Predictions of Trends. In some instances, the ability of a code or model to predict the trend of a variable may be the subject of a validation effort. An example would

be the difference in drag for two ship configurations tested at the same Froude number. The procedure discussed above—comparison of $|E|$ and U_V for the drag—should be performed for each configuration. The difference δ in drag for the two configurations should then be considered as the variable that is the subject of the validation. As discussed in detail in Coleman et al. (1995), because of correlated bias uncertainty effects in the experimental data the magnitude of the uncertainty in δ may be significantly less than the uncertainty in either of the two experimentally-determined drag values. This means that the value of U_V for δ may be significantly less than the U_V 's for the drag values, allowing for a more stringent validation criterion for the difference than for the absolute magnitudes of the variables.

It is probable that in some instances the U_{SMA} for the difference δ will be less than the U_{SMA} 's for the absolute magnitudes of the variables because of correlated systematic uncertainty effects in the modeling. This is an unexplored area at this time.

4 Results of Verification/Validation for a Single CFD Code and for a Comparison of Multiple Turbulence Models

Example results of verification/validation are presented both for a single CFD code and for a comparison of multiple turbulence models. In both cases, the magnitude of U_{SPD} was assumed negligible relative to the other uncertainties. The CFD code and verification procedures of Stern et al. (1996) are used for two applications for which numerical and experimental uncertainty analyses are available: marine-propulsor flow (Chen, 1996; Jessup, 1994) and two-dimensional turbulent flat-plate boundary-layer flow (Sreedhar and Stern, 1997; Longo et al., 1998). The former represents a practical geometry and is used for the single CFD code validation example, whereas the latter represents an idealized geometry and is used for the comparison of turbulence models example.

For the marine-propulsor geometry, Jessup (1989) provided an extensive data set (including circumferential-average, phase-average, and detailed blade boundary-layer, wake, and tip-vortex velocities) for the relatively simple marine propulsor P4119. This propeller-shaft configuration, shown viewed from upstream in Fig. 4, was tested in a 24 in. water tunnel with measurements made using a three-component laser-Doppler velocimeter (LDV) system. Detailed uncertainty estimates have also been reported (Jessup, 1994). An initial validation effort was

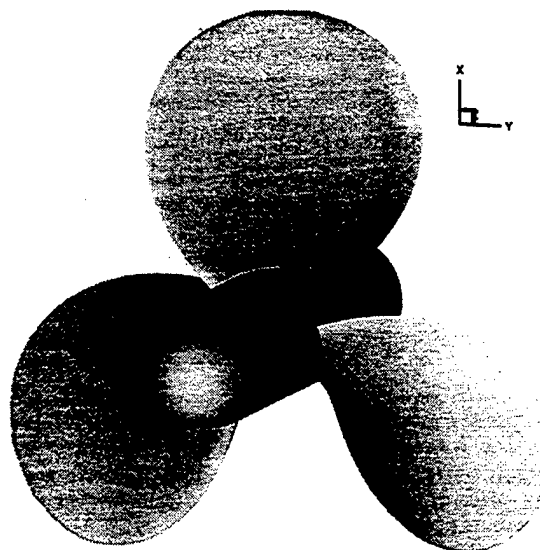


Fig. 4 Marine propulsor P4119

Table 1 Marine-propulsor flow: performance coefficients

	D	S	$E\%$	$U_v\%$	$U_D\%$	$U_r\%$	$U_{SN}\%$	$U_{SI}\%$	$U_{SG}\%$	U_{SN}/U_D
K_T	0.146	0.149	-2.1	3.2	2.0	2.0	2.5	1.0	2.3	1.3
$10K_Q$	0.280	0.276	1.9	3.4	2.0	2.0	2.7	1.0	2.5	1.4

% D .

reported by Stern et al. (1994). Documentation and verification are reported by Chen (1996) in conjunction with studies of design and off-design marine-propulsor performance.

For the two-dimensional turbulent flat-plate boundary-layer flow, Longo et al. (1996) provided data and uncertainty analysis in conjunction with their study of solid/free-surface juncture boundary layer and wake. A 1.2 m surface-piercing flat plate was tested in a $100 \times 3 \times 3$ m towing tank with measurements made using a two-component LDV system configured to obtain three mean velocities and five Reynolds stresses for both boundary layer and wake planes and regions deep and very close to the free surface. Sreedhar and Stern (1997) provided verification for multiple turbulence models for this application in conjunction with the development of nonlinear eddy-viscosity turbulence models, including both wall and free-surface effects.

The CFD method solves the unsteady incompressible RANS and continuity equations using either noninertial cylindrical or inertial cartesian coordinates and the Baldwin-Lomax turbulence model. The RANS equations are solved using finite-analytic spatial and first-order (steady flow) or second-order (unsteady flow) backward difference time discretization. The pressure equation is derived from a discretized form of the continuity equation and solved using second-order-central finite differences. The overall solution procedure is based on the two-step pressure-implicit-split-operator (PISO) algorithm. For steady flow, subiteration convergence is not required and time serves as an iteration parameter.

Verification Procedures. The verification procedures follow the approach of Stern et al. (1996). This approach is based on the editorial policy statement of the ASME (ASME, 1993). The ten issues of the statement are divided as documentation (1, 7, 8), verification (2-6), and validation (9, 10). Verification is comprised of grid-, iterative-, and time-convergence (4, 5, 6), artificial dissipation (3), and order-of-accuracy (2) studies. These studies are implemented using a five-step procedure: (i) grid design and identification of important parameters; (ii) convergence studies; (iii) determination of the effects of explicit artificial dissipation, if used; (iv) estimation of overall uncertainties for integral and point variables; and (v) order of accuracy and Richardson extrapolation.

Step (i) is self-explanatory. For steady flow, step (ii) consists of obtaining estimates for iterative and grid convergence

uncertainties (U_{SI} and U_{SG} , respectively) for integral and point variables.

The estimates for grid convergence uncertainty require a minimum of three grids and are based either on (a) the grid convergence metric

$$\epsilon = \frac{(\phi_1 - \phi_2)}{\phi_1} \quad (8)$$

where ϕ represents either an integral or point variable with subscripts 1 and 2 corresponding to the finer and coarser grids, respectively, or (b) the grid convergence index (Roache, 1997)

$$GCI = \frac{3\epsilon}{(r^p - 1)} \quad (9)$$

where r is the grid refinement ratio and p the order of accuracy such that for grid doubling and second-order methods $\epsilon = GCI$. For small grid refinement and/or order, the GCI is recommended since ϵ is arbitrarily small and inappropriate as a metric of grid convergence. Note that for small ϕ (including point variables with regions of small ϕ), ϵ should be normalized by the range of ϕ . Decreasing (increasing) ϵ/GCI indicates grid convergence (divergence) with uncertainty estimates based on ϵ for the finest grids. Oscillatory ϵ/GCI is indeterminate, with uncertainty estimated as roughly one-half the difference between the maximum and minimum values. For simple geometries and flows, negligible grid convergence uncertainty is attainable. For complex geometries and flows, convergence may be limited and oscillatory.

The estimates for iterative convergence uncertainty are based on evaluation of the iteration records for both integral and point variables. The level of iterative convergence is determined by the number of orders of magnitude reduction and magnitude in the residuals

$$\zeta = \phi^n - \phi^{n-1} \quad (10)$$

where n is the iteration number and ϕ can either be the solution variables or equation imbalances obtained by back substitution. Average (L_2 norms) or maximum values are used. For simple geometries and flows, sixteen orders of magnitude reduction of ζ to machine zero is possible such that the iterative convergence uncertainty is negligible. However, for practical geometries and flows, only a few orders of magnitude reduction in ζ to about

Table 2 Marine-propulsor flow: circumferential-average mean-velocity components (radial-magnitude average)

	$ E \%$	$U_v\%$	$U_D\%$	$U_r\%$	$\left(\frac{\partial r}{\partial x}\right)U_x\%$	$U_{SN}\%$	$U_{SI}\%$	$U_{SG}\%$	U_{SN}/U_D
U_1	1.2	1.3	1.2	1.2	0.02	0.8	0.4	0.7	0.7
V_1	2.6	1.3	1.2	1.2	0.01	0.7	0.2	0.7	0.6
W_1	1.7	1.3	1.2	1.2	0.02	0.6	0.4	0.5	0.5
U_2	2.3	3.2	3.1	3.1	0.02	0.9	0.5	0.8	0.3
V_2	2.1	3.1	3.1	3.1	0.01	0.7	0.3	0.6	0.2
W_2	2.7	3.2	3.1	3.1	0.02	0.9	0.5	0.7	0.3

¹ upstream.

² downstream.

% U_0 .

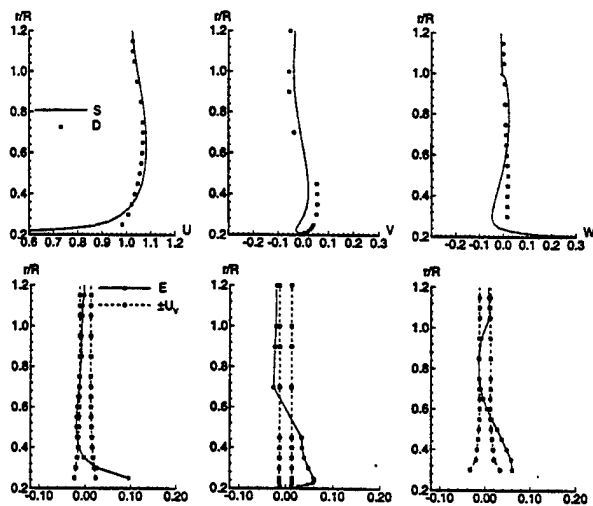


Fig. 5(a) Upstream ($x/R = -0.3$)

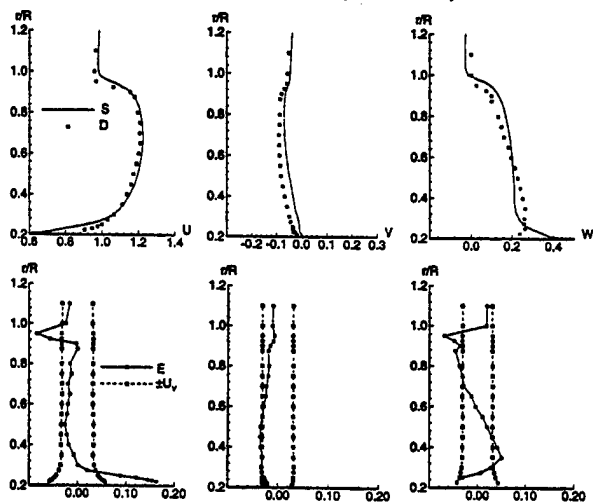


Fig. 5(b) Downstream ($x/R = 0.328$)

Fig. 5 Marine-propulsor flow: circumferentially-averaged mean velocity components; simulation prediction and experimental data; comparison error and validation uncertainty

10^{-4} may actually be attainable. In this case, the estimates for iterative convergence uncertainty are based on statistics of the iteration records of integral and point variables and are taken as roughly one-half the difference between the maximum and minimum values.

Step (iii) consists of determination of effects of explicit artificial dissipation through parametric studies with uncertainty estimates U_{SAD} based on a convergence metric similar to Eq. (8). Step (iv) combines the uncertainties (U_{SI} , U_{SG} , U_{SAD} , ...) using root sum square (in analogy with experimental uncertainty analysis and assumed for the present to be the appropriate form) to obtain overall estimates of the numerical uncertainty U_{SN} for both integral and point variables. Step (v) consists of

obtaining solutions on three grids in the asymptotic range (i.e., base, halved, and doubled grids with monotonically decreasing ϵ at rate r^p) and Taylor series expansions to determine the order of accuracy and Richardson extrapolated coarse grid order $3p$ benchmark.

Steps (i)–(iv) are required. Step (v) is useful in providing p and the $3p$ benchmark and desirable for guiding CFD development, but often difficult, especially in obtaining solutions in the asymptotic range for complex geometries. Note that p is required for evaluation of the GCI, that other evaluations (e.g., rate of iterative convergence) are also useful for guiding CFD development, and that additional uncertainty estimates may be required (e.g., local and global non-conservation of mass, momentum, energy, etc.).

Verification/Validation for a Single CFD Code. Variables chosen to illustrate the verification and validation results are the propulsor thrust and torque performance coefficients (K_T and K_Q , respectively); the radial average of the circumferential-average mean-velocity components in a plane upstream (U_1 , V_1 , W_1) and a plane downstream (U_2 , V_2 , W_2) of the propeller; and the radial profiles of the circumferential-average mean velocities in the same planes.

The results for the performance coefficients are shown in Table 1, where all percentages given are percentage of D . The verification results show that the uncertainty in grid convergence dominates the iteration convergence uncertainty, resulting in numerical uncertainties in the simulation, U_{SN} , of about 2.4 percent. The uncertainties, U_D , associated with the experimentally determined results are about 2.0 percent, leading to estimates of U_V of about 3.3 percent. This means that, for this flow condition, validation of the CFD code predictions cannot be achieved better than about 3.3 percent for the performance coefficients. Since the calculated comparison error $|E|$ is less than U_V , validation in this case is successful at the 3.3 percent level for both K_T and K_Q .

The results for the average velocities in the upstream and downstream planes are shown in Table 2, where all percentages given are percentage of the uniform inflow velocity U_0 . As for the performance coefficients, the uncertainty in grid convergence is always greater than the iteration convergence uncertainty, and the resulting numerical uncertainties in the simulation, U_{SN} , are 0.6–0.9 percent. The uncertainties, U_D , associated with the experimentally determined results are about 1.2 percent (upstream) and 3.2 percent (downstream), leading to estimates of U_V of about 1.3 percent (upstream) and 3.2 percent (downstream). The calculated comparison error $|E|$ is less than U_V for average velocities U_1 , U_2 , V_2 , and W_2 , indicating successful validation for those variables. Validation of the simulations of the average velocities V_1 and W_1 , however, is not achieved. It should also be noted that since

$$\left(\frac{\partial r}{\partial X_j} \right) (U_{X_j})_i < U_{r_i}$$

(where $r_i = (U, V, W)$ and $X_j = r/R$) the influence of the uncertainties in the X_j -locations of the measurement positions are negligible.

Table 3 Two-dimensional turbulent flat-plate boundary-layer flow: streamwise mean velocity (average magnitude across the boundary layer)

Turbulence model	$ E \%$	$U_V\%$	$U_D\%$	$U_r\%$	$\left(\frac{\partial r}{\partial x} \right) U_{X_j}\%$	$U_{SN}\%$	$U_{SI}\%$	$U_{SG}\%$	U_{SN}/U_D	$ E + U_V\%$
Baldwin Lomax (1978)	1.30	2.52	1.60	1.60	0.09	1.95	0.00	1.95	1.22	3.82
Chen and Patel (1988)	2.07	2.40	1.60	1.60	0.09	1.79	0.00	1.79	1.12	4.47
Myong and Kassagi (1990)	2.30	2.67	1.60	1.60	0.09	2.14	0.00	2.14	1.34	4.97

% U_r .

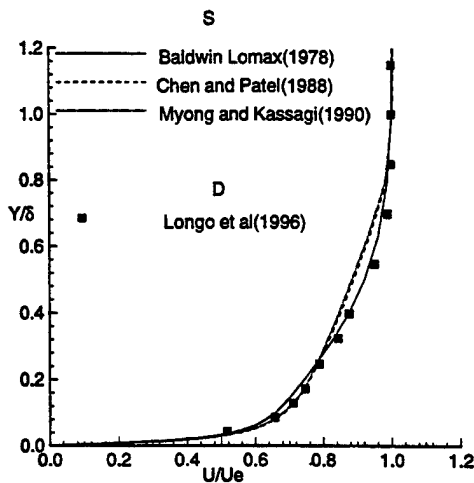


Fig. 6(a) Simulation prediction and experimental data

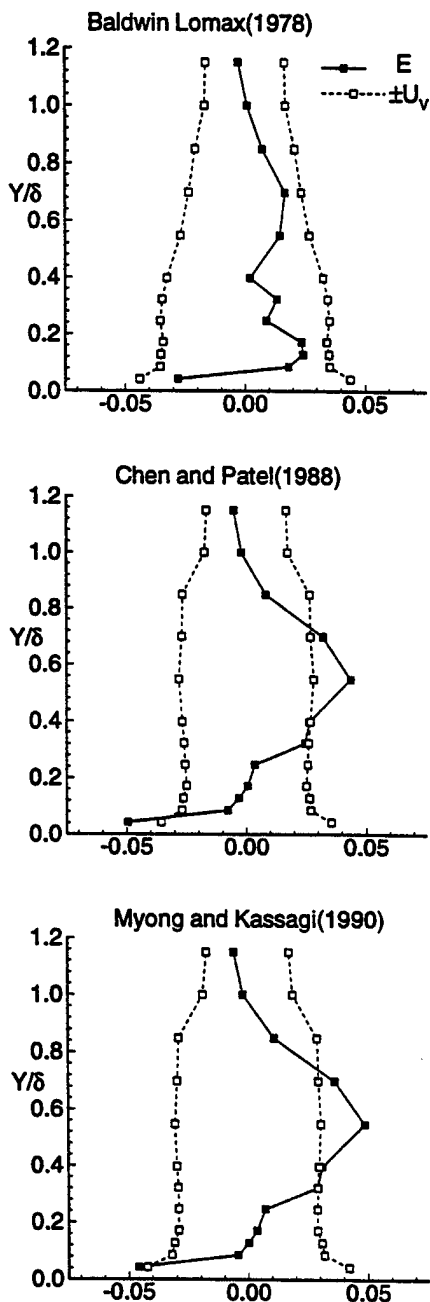


Fig. 6(b) Comparison error and validation uncertainty

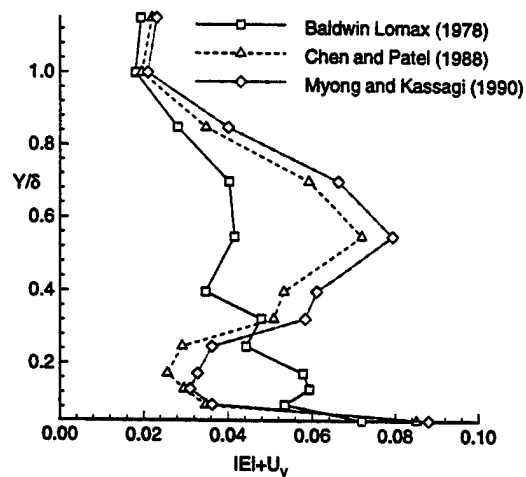


Fig. 6(c) $|E| + U_v$

Fig. 6 Two-dimensional turbulent flat plate boundary layer flow-streamwise mean velocity

The validation comparisons for the radial profiles of the circumferential-average velocity components are shown in Fig. 5(a) for the upstream plane and Fig. 5(b) for the downstream plane. In this presentation, R is the outer radius of the propeller, the outer radius of the shaft is at $r/R = 0.2$, and the three velocity components E and U_v are normalized by U_0 . The plots of U , V , and W versus r/R show the comparisons as they have traditionally been made in past validation efforts. The plots of E and $\pm U_v$ present the new validation view introduced in this article, and it is immediately obvious where validation has been achieved and where it has not. In this specific case presented, validation is achieved for some variables in some regions of the flow but not for all variables in all regions of the flow field. The largest errors are for the regions of the flow corresponding to the shaft/blade juncture and the blade tip regions, which is confirmed by the validation results using the complete data set (Chen and Stern, 1997).

Verification/Validation for Comparison of Multiple Turbulence Models. Variables chosen to illustrate the verification and validation are the average magnitude across the boundary layer of the streamwise mean velocity and the profile of the streamwise mean velocity. The comparisons are for three turbulence models of increasing complexity, i.e., the Baldwin and Lomax (1978) algebraic model (BL), the Chen and Patel (1988) $k-\epsilon$ and near-wall model (CP), and the Myong and Kassagi (1990) nonlinear $k-\epsilon$ model (MK). In the presentations, the velocity, comparison error, and validation uncertainty are normalized by the edge velocity U_e and the independent variable Y is normalized by the boundary-layer thickness δ .

The results for the average velocity are shown in Table 3. As for the previous example, the uncertainty in grid convergence dominates the iteration convergence uncertainty, resulting in numerical uncertainties U_{SN} for the three models ranging from about 1.8–2.1 percent. The data uncertainty U_D is 1.6 percent leading to validation uncertainties U_v of 2.5–2.7 percent. Here again, the contribution to U_D from uncertainties in the measurement locations (where $r_i = U/U_e$ and $X_i = Y/\delta$) is negligible. All three models are validated at the level $U_v = 2.5$ –2.7 percent. The estimates for $|E| + U_v$ range for increasing model complexity from 3.8–5 percent.

The validation comparisons for the streamwise mean velocity are shown in Figs. 6(a–c). The simulation prediction and data comparisons U/U_e vs. Y/δ [Fig. 6(a)] for the CP and MK models show relatively large underprediction in the mid-region of the boundary-layer, whereas the BL model

shows relatively small underprediction in the near-wall region. The plots of E and $\pm U_v$ show that the BL model is validated across the entire boundary layer, whereas the CP and MK models failure is confined to the mid-region of the boundary layer. The plots of the $|E| + U_v$ comparisons for the three models show that the BL model maximum values are less than 4 percent U_e , except for the near-wall region where the values increase to 7 percent U_e at the wall, whereas the CP and MK models have large values (8 percent U_e) at the wall and in the outer part and relatively small values (3 percent U_e) for the near-wall region.

5 Summary and Conclusions

A new approach to CFD validation is developed that gives proper consideration to both the experimental and simulation uncertainties. The comparison error E is defined as the difference between the data D (benchmark) and simulation prediction value S and thus includes the errors associated with the experimental data and the errors associated with the simulation. The validation uncertainty is defined as the combination of the uncertainties in the experimental data and the portion of the uncertainties in the CFD prediction that can be estimated. Estimates for U_{SN} , the simulation numerical uncertainty, are obtained through verification procedures involving parametric, convergence, and order-of-accuracy studies. The verification procedures are discussed in detail. U_D includes contributions from the independent and dependent variable uncertainties and is obtained using established uncertainty analysis procedures.

The validation uncertainty U_v sets the level at which the validation can be achieved. The criterion for validation is that $|E|$ must be less than U_v . The acceptable level of validation is set by program objectives. If $|E|$ is greater than U_v , than validation is not accomplished and the magnitude and sign of E can be valuable in designing strategies to improve the mathematical modeling. When a validation effort involves multiple codes and/or models, additionally the comparisons should include the quantity $|E| + U_v$. Validation of the prediction of trends involves reduction in uncertainties, at least for the experiments, through inclusion of correlated bias errors.

Example results of verification/validation are presented both for a single CFD code and for a comparison of multiple turbulence models. A RANS CFD code is used for two applications for which numerical and experimental uncertainty analyses are available: marine-propulsor flow and two-dimensional turbulent flat-plate boundary-layer flow. The former represents a practical geometry and is used for the single CFD code validation example, whereas the latter represents an idealized geometry and is used for the comparison of turbulence models example. The results demonstrate the usefulness of the proposed validation strategy.

The authors recommend the adoption of this approach for CFD code validation. It will be useful both in guiding future developments in CFD through validation studies and in the transition of CFD codes to design through establishment of credibility and ultimately certification once procedures for the latter are established. Realization of the full potential of the approach requires refinements through applications using various CFD methods and data sets (benchmarks), especially with regard to verification procedures. The authors also recommend that general verification procedures be established similar to those used here, but generalized to encompass broad categories of simulation methods and perhaps additional error sources in those methods.

Acknowledgments

This research was sponsored by the Office of Naval Research under grants N00014-96-1-0018 and N00014-97-1-

0014 under the administration of Dr. E. P. Rood. The authors gratefully acknowledge Dr. Rood and other colleagues who made significant contributions through many discussions. In particular, Prof. W. G. Steele's comments on an early draft led to some important modifications. Mr. B. Chen and Dr. M. Sreedhar generously provided the example results. The criticisms and suggestions of the six reviewers were invaluable and resulted in considerable improvements to the initial manuscript. The computations were performed using the NAVO Oceanographic Office supercomputers.

References

- American Institute of Aeronautics and Astronautics (AIAA), 1994, "Editorial Policy Statement on Numerical Accuracy and Experimental Uncertainty," *AIAA Journal*, Vol. 32, No. 1.
- American Institute of Aeronautics and Astronautics (AIAA), 1997, "Guide to the Assessment of Uncertainty in Computational Fluid Dynamics Simulations," AIAA G-077, Jan. 1997 draft of a recommended practices document.
- American Society of Mechanical Engineers (ASME), 1993, "Editorial Policy Statement on the Control of Numerical Accuracy," *ASME JOURNAL OF FLUIDS ENGINEERING*, Vol. 115, No. 3.
- Baldwin, B. S., and Lomax, H., 1978, "Thin Layer Approximation and Algebraic Model for Separated Turbulent Flows," *AIAA Paper AIAA 78-257*.
- Beard, R. M., and Landrum, D. B., 1996, "Effects of Kinetic Rate Uncertainty on the Predicted Performance of Small Hydrogen Thrusters," *AIAA Paper AIAA-96-2856*.
- Blottner, F. G., 1990, "Accurate Navier-Stokes Results for the Hypersonic Flow over a Spherical Nosedip," *Journal of Spacecraft and Rockets*, Vol. 27, No. 2.
- Brown, K. K., Coleman, H. W., and Butas, J. P., 1994, "Impact of Uncertainty on Modeling and Testing of the Space Shuttle Main Engine," *ASME FED-Vol. 205*.
- Brown, K. K., Coleman, H. W., Steele, W. G., and Taylor, R. P., 1996, "Evaluation of Correlated Bias Error Effects in Experimental Uncertainty Analysis," *AIAA Journal*, Vol. 34, No. 5.
- Celik, I., Chen, C. J., Roache, P. J., and Scheuerer, G., eds., 1993, *Quantification of Uncertainty in Computational Fluid Dynamics*, ASME FED-Vol. 158.
- Chen, H. C., and Patel, V. C., 1988, "Near-Wall Turbulence Models for Complex Flows Including Separation," *AIAA Journal*, Vol. 26, No. 6, pp. 641-648.
- Chen, B., 1996, "Computational Fluid Dynamics of Four-Quadrant Marine-Propulsor Flow," M.S. thesis, Dept. of Mechanical Engineering, University of Iowa.
- Chen, B., and Stern, F., 1997, "Computation of Marine-Propulsor Flow—Part 1: Design Condition," in preparation.
- Coleman, H. W., 1996, "Uncertainty Considerations in Validating CFD Codes with Experimental Data," *AIAA Paper AIAA-96-2027*.
- Coleman, H. W., and Steele, W. G., 1989, *Experimentation and Uncertainty Analysis for Engineers*, Wiley, New York.
- Coleman, H. W., and Steele, W. G., 1995, "Engineering Application of Uncertainty Analysis," *AIAA Journal*, Vol. 33, No. 10.
- Coleman, H. W., Steele, W. G., and Taylor, R. P., 1995, "Implications of Correlated Bias Uncertainties in Single and Comparative Tests," *ASME JOURNAL OF FLUIDS ENGINEERING*, Vol. 117, No. 4.
- Gresho, P. M., and Taylor, C., 1994, "Editorial," *International Journal of Numerical Methods in Fluids*, Vol. 19, No. 12.
- International Association of Hydraulic Research (IAHR), 1994, "Guidelines for Documenting the Validity of Computational Modeling Software."
- International Towing Tank Conference (ITTC), 1996, 21st ITTC Proceedings, Bergen, Norway.
- Jessup, S. D., 1989, "An Experimental Investigation of Viscous Aspects of Propeller Blade Flow," Ph.D. Dissertation, School of Engineering and Architecture, The Catholic University of America.
- Jessup, S. D., 1994, "Propeller Blade Flow Measurements Using LDV," *ASME Fluids Engineering Division Summer Meeting*, Lake Tahoe, NV.
- Longo, J., Huang, H. P., and Stern, F., 1998, "Solid-Fluid Junction Boundary Layer and Wake," to appear in *Experiments in Fluids*.
- Marvin, J. G., 1995, "Perspective on Computational Fluid Dynamics Validation," *AIAA Journal*, Vol. 33, No. 10.
- Mehta, U. B., 1996, "Guide to Credible Computational Fluid Dynamics Simulations," *Journal of Propulsion and Power*, Vol. 12, No. 5.
- Melnik, R. E., Siclari, M. J., Barber, T. J., and Verhoff, A., "A Process for Industry Certification of Physical Simulation Codes," *AIAA Paper 94-2235*.
- Myong, H. K., and Kasagi, N., 1991, "Prediction of Anisotropy of the Near-Wall Turbulence with an Anisotropic Low-Reynolds Number $k-\epsilon$ Model," *ASME JOURNAL OF FLUIDS ENGINEERING*, Vol. 112.
- Oberkampf, W. L., Blottner, F. G., and Aeschliman, D. P., 1995, "Methodology for Computational Fluid Dynamics Code Verification/Validation," *AIAA Paper AIAA-95-2226*.

Roache, P. J., 1997, "Quantification of Uncertainty in Computational Fluid Dynamics," *Annual Review of Fluid Mechanics*, Vol. 29, pp. 123-160.

Rood, E. P., 1996, "Validation Strategy for "RANS" Computational Ship Hydrodynamics," Second International Conference on Hydrodynamics, Hong Kong.

Sreedhar, M., and Stern, F., 1997, "Non-Linear Eddy-Viscosity Turbulence Model for Solid/Free-Surface Boundary Layer and Wake," 3rd Forum on Advances in Num. Modeling of Free Surface and Interface Fluid Dynamics, ASME FED Summer Meeting, Vancouver, Canada.

Stern, F., Zhang, D. H., Chen, B., Kim, H. T., and Jessup, S., 1994, "Computation of Viscous Marine Propulsor Blade and Wake Flow," *Proc. 20th ONR Symposium on Naval Hydro.*, Santa Barbara, CA.

Stern, F., Paterson, E. G., and Tahara, Y., 1996, "CFDSHIP-IOWA: Computational Fluid Dynamics Method for Surface-Ship Boundary Layers and Wakes and Wave Fields," Iowa Institute of Hydraulic Research, University of Iowa, IIHR Report No. 381.

Zingg, D. W., 1992, "Grid Studies for Thin-Layer Navier-Stokes Computations of Airfoil Flowfields," *AIAA Journal*, Vol. 30, No. 10.

Uncertainties and CFD Code Validation¹

Patrick J. Roache.² The paper by Coleman and Stern (1997) proposes a new approach to CFD code validation that gives consideration to both experimental and simulation uncertainties. It is a valuable and thought-provoking contribution. Two criticisms follow.

(1) Hypothetical data-simulation comparisons are given in Figure 1 (see also Coleman, 1996), without and with experimental uncertainty bars (parts a and b, respectively). The authors state that one might interpret part a to indicate that Model 1 is superior to Model 2 since it seems to "capture the trend of the data." In contrast, when the experimental uncertainty is considered in part b, "it is obvious that arguing for one method over another based on comparison with the experimental data is wasted effort since the predictions from both methods fall well within the data uncertainty."

This negative evaluation would be true if and only if the uncertainty distribution within the plotted range of experimental uncertainty (commonly called "error bars") was flat, i.e. a step function. (For example, if the "error bar" covered the data value D to $\pm 10\%$, this flat distribution would give equal probability that the true value was at $D + 1\%$, $D - 3\%$, $D + 9\%$, etc. or at D itself.) In such a case, our probabilistic knowledge is indifferent to any values within the range of the "error bar" and therefore to the relative merits of Model 1 and 2, and the authors' argument holds. Of course, we do not know what the appropriate probability distribution is, but most physical experiments have some preference for the data values reported, and the default model of probability is a Gaussian distribution. If, in the judgment of the reader, this is the more likely distribution, then there is probably a trend in the true values, and Model 1 does indeed "capture the trend of the data." One could readily express this quantitatively as a weighted integral over the assumed probability distributions within the "error bars," but qualitatively, I believe that the naive preference for Model 1 is justifiable.

(2) The principal thrust of the paper is that the validation uncertainty U_v should be the key metric in the validation process. They define the "validation uncertainty U_v as the combination of all uncertainties that we know how to estimate," which includes experimental and numerical uncertainties, the latter including lack of grid convergence. With the "comparison error" E defined as the difference between the experimental data set value the value produced by the simulation, they then interpret the condition $|E| < U_v$ to be the criteria for claiming that validation has been achieved at the U_v level.

The authors are well aware of a paradox inherent in this criterion, that increasing uncertainty of the experiments or the simulation (e.g., less convincing grid convergence tests) makes it easier to achieve validation. (The resolution of the paradox lies in the recognition that the validation level so achieved is less demanding, i.e. U_v is greater.) See more complete discussion in Coleman and Stern (1997) and in Roache (1998). However, besides the evident potential for misinterpretation in the use of U_v , a more basic problem exists with their proposal; it fails to account for an acceptable error tolerance in the Validation. This is easily demonstrated by the following "thought experiment."

Imagine a programmatic need for Validation with a 5% error tolerance (call it TOL_v). That is, the need is for a model/code that can predict physical reality to within 5%. Further imagine the limit of good experiments and calculations, i.e. vanishingly small experimental uncertainty and simulation uncertainty, so that their validation uncertainty U_v is also vanishingly small. Finally, imagine excellent agreement between experiment and simulation, say an observation error $|E| = 0.1$ percent. Then, their proposed criterion does not allow this to be considered a validation. No matter how good the agreement between experiment and simulation, nor how lax the programmatic needs, if the agreement is not as good as the combined uncertainties from experiment and simulation, it cannot be considered a validation, in this approach.

A modification of their validation criterion to include a programmatic validation tolerance TOL_v would avoid this difficulty.

$$|E| < U_v + TOL_v$$

However, the previously mentioned paradox remains, e.g. increasing experimental and/or numerical uncertainty still make it easier to achieve validation, at the level now defined by $U_v + TOL_v$. Further consideration by the simulation community will be required to determine whether or not this modification makes their proposal practical. See also further discussion in Roache (1998).

References

- Coleman, H. W., 1996, "Uncertainty Consideration in Validating CFD Codes with Experimental Data," AIAA Paper 96-2027, 27th AIAA Fluid Dynamics Conference, June 17-20, 1996, New Orleans, LA.
- Coleman, H. W., and Stern, F., 1997, "Uncertainties and CFD Code Validation," ASME JOURNAL OF FLUIDS ENGINEERING, Vol. 119, Dec., pp. 795-803.
- Roache, P. J., 1998, *Verification and Validation in Computational Science and Engineering*, Hermosa Publishers, P. O. Box 9229, Albuquerque, NM 87119, Chapter 10.

Authors' Closure

We appreciate the thoughtful comments by Dr. Roache and the many contributions he has made in this field.

We do not accept his first point for a general case. If, for instance, the uncertainty bands plotted included a significant

¹ By H. W. Coleman and F. Stern published in the December 1997 issue of the JOURNAL OF FLUIDS ENGINEERING, Vol. 119, No. 4, pp. 795-803.

² Consultant, P.O. Box 9229, Albuquerque, N. Mex. 87119.

random uncertainty component and the data points were single realizations, we would hesitate to bet that the trend (curvature) shown would be the same as that shown by a succeeding set of single realizations of if many data sets were obtained and the average values were plotted. On the other hand, in the very special case that (1) we knew each data point was affected by the same systematic uncertainty that did not vary with X and (2) the data points were averages of many readings so that the random component of uncertainty was negligible, we would believe the trend shown.

His comments on the second point are insightful and cover a case we did not consider or discuss in the article. His "error tolerance" corresponds to our "required level of validation" discussed in the article. Call this U_{reqd} since validation is required at that uncertainty level or below. The salient point raised by Roache is how should we interpret the case $U_v < |E| < U_{\text{reqd}}$? We believe that case should also be considered a successful validation since the comparison error is less than U_{reqd} and the noise level U_v allows discrimination.

From a general perspective, if we consider the three variables U_v , $|E|$ and U_{reqd} there are six combinations (assuming none of the three variables are equal):

1. $|E| < U_v < U_{\text{reqd}}$
2. $|E| < U_{\text{reqd}} < U_v$
3. $U_{\text{reqd}} < |E| < U_v$
4. $U_v < |E| < U_{\text{reqd}}$
5. $U_v < U_{\text{reqd}} < |E|$
6. $U_{\text{reqd}} < U_v < |E|$

In cases 1, 2, and 3, $|E| < U_v$; validation is achieved at the U_v level; and the comparison error is below the noise level, so attempting to decrease the error (E_{SMA}) due to the modeling assumptions in the simulation is not feasible from an uncertainty standpoint. In case 1 validation has been achieved at a level below U_{reqd} , so validation is successful from a programmatic standpoint.

In cases 4, 5, and 6, $U_v < |E|$, so the comparison error is above the noise level and attempting to decrease E_{SMA} is feasible from an uncertainty standpoint. In case 4 (the one pointed out by Roache), validation is successful at the $|E|$ level from a programmatic standpoint. Note that for $U_v \ll |E|$, E corresponds to E_{SMA} and the error from the modeling assumptions can be determined unambiguously.

We did not follow the logic in comparing $|E|$ with $(U_v + U_{\text{reqd}})$.

Appendix B

Stern, F., Longo, J., Penna, R., Olivieri, A., Ratcliffe, T., and Coleman, H.,
"International Collaboration on Benchmark CFD Validation Data for
Surface Combatant DTMB Model 5415," Proceedings of the 23rd
Symposium on Naval Hydrodynamics, Val de Reuil, France, September
17-22, 2000.

INTERNATIONAL COLLABORATION ON BENCHMARK CFD VALIDATION DATA FOR SURFACE COMBATANT DTMB MODEL 5415*

F. Stern¹, J. Longo¹, R. Penna², A. Olivieri², T. Ratcliffe³, H. Coleman⁴

(¹Iowa Institute of Hydraulic Research, The University of Iowa, Iowa City, IA, USA; ²Italian Ship Model Basin, Rome, Italy; ³David Taylor Model Basin, Bethesda, MD, USA; ⁴Propulsion Research Center, University of Alabama in Huntsville, Huntsville, AL, USA)

ABSTRACT

Results are presented from overlapping towing tank tests between three institutes for resistance, sinkage and trim, wave profiles and elevations, and nominal wake using the same model geometry and conditions, including rigorous application of standard uncertainty assessment procedures. Two of the institutes used 5.7 m models whereas the third institute used a smaller 3 m model. Comparison variables were defined for data-reduction equations and data differences and data-difference uncertainties. Detailed descriptions were provided of facilities, measurement systems, data-acquisition and reduction procedures, and uncertainty assessment. Results were discussed with regard to levels and causes of data differences and data-difference uncertainties and to estimate facility/model geometry and scale effect biases. For same size 5.7 m models, data differences were in general oscillatory, and in many cases, larger in magnitude than data-difference uncertainties, which indicates unaccounted for bias and precision limits and that current individual facility uncertainty estimates are often too optimistic. Scale effects for the 3 m model are only evident for resistance and trim tests at high Fr. Facility/model geometry and scale effect bias are estimated based on comparisons. Uncertainty estimates including such biases may provide better estimates, especially for use in CFD validation, which is the recommendation of the present study along with efforts towards improvement of individual institute uncertainty estimates. Use of standard models and current ITTC efforts in providing standard quality manual procedures for towing tank tests and uncertainty estimates will also be helpful in this regard.

INTRODUCTION

Towing tank testing is undergoing change from routine tests for global variables to detailed tests for local variables for model development and

computational fluid dynamics (CFD) validation, as design methodology changes from model testing and theory to simulation-based design. Such detailed testing requires that towing tanks utilize advanced modern instrumentation with complete documentation of test conditions, procedures, and uncertainty assessment. The requirements for levels of uncertainties are even more stringent than those required previously since they are a limiting factor in establishing the level of validation and credibility of simulation technology. Also, routine test data is more likely utilized in house, whereas detailed test data is more likely utilized internationally, which additionally requires use of standard procedures and establishment of benchmark levels of data uncertainties. Detailed testing offers new opportunities for towing tanks, as the amount and complexity of testing is increased. International collaborations are attractive from a resource perspective.

The benchmark database for CFD validation for resistance and propulsion is fairly extensive with current focus on modern hull forms and detailed tests as reported by the Resistance Committee of the 22nd International Towing Tank Conference (ITTC, 1999). Tanker (KVLCC2), container ship (KCS), and surface combatant (DTMB 5415) hull forms were recommended for use and are currently being used as test cases in the Gothenburg 2000 Workshop on CFD for Ship Hydrodynamics (Gothenburg 2000; <http://www.ihr.uiowa.edu/gothenburg2000/>). KVLCC2 and KCS were conceived by the Korean Institute of Ships & Ocean Engineering (KRISO) specifically as test cases for modern tanker and container ship hull forms for CFD validation for ship hydrodynamics ca. 1997. KVLCC2 and KCS have bulbous bows and bulbous cruiser and transom sterns, respectively. The KVLCC2 and KCS data were procured by KRISO (Van et al., 1997 and 1998a, b) in collaboration with Pohang University of Science and

* 23rd Symposium on Naval Hydrodynamics, 17-22 September 2000, Val de Reuil, France

Technology, Korea (Lee et al., 1998) and Ship Research Institute, Japan, respectively. DTMB 5415 was conceived by David Taylor Model Basin, USA Navy as a preliminary design for a surface combatant ca. 1980 with a sonar dome bow and transom stern. The DTMB 5415 data were procured by DTMB (Ratcliffe, 1995; <http://www50.dt.navy.mil/5415/>) in collaboration with Istituto Nazionale per Studi ed Esperienze di Architettura Navale (INSEAN), Italy (Avanzini et al., 1998, Avanzini et al., 2000, Olivieri and Penna, 1999, Olivieri and Penna, 2000), and Iowa Institute of Hydraulic Research, USA (Longo and Stern, 1998, Gui et al., 1999, Longo et al., 2000, Stern, 2000: <http://www.ihr.uiowa.edu/~towtank/>).

The present paper describes the international collaboration on DTMB model 5415 between DTMB, INSEAN, and IHR. The collaboration was done at DTMB using 5415 (5.72 m, 1/24.8 scale model), at INSEAN using INSEAN model 2340 and 2340A (exact geosyms of 5415), and at IHR using DTMB model 5512 (3.038 m, 1/46.6 scale geosym of 5415). Figure 1 shows models 5415, 2340A, and 5512. Between all three institutions many conditions and physics are under investigation. The conditions include bare hull without (all) and with appendages and propulsor (DTMB), and fixed and free model (all). The physics are comprehensive and include model size (IHR), facility biases (all), Reynolds number (Re) effects (all), boundary layer and wake (INSEAN), stern flow (all), Froude number (Fr) effects (all), bow and transom flow (DTMB), wave breaking (INSEAN), and turbulence and head waves (IHR). The uncertainty assessment procedures closely follow ITTC (1999) recommendations. Overlapping tests for resistance, sinkage and trim, wave profile, wave elevations, and nominal wake are included for evaluation between institutes of facilities; measurement systems; test procedures; uncertainty assessments; model size, offsets, and turbulence stimulation; and facility/model geometry and scale effect biases, through comparisons of both data and uncertainties.

The results of the overlapping tests build on information provided by the Cooperative Experimental Program of the Resistance Committees of the 17-19 ITTC and the cooperative uncertainty assessment example for resistance test of the Resistance Committee of the 22nd ITTC. The former provided comparison between up to 22 institutes of global (resistance, sinkage and trim, wave profile, wave cut, wake survey, form factor, and blockage) and local (surface pressure and boundary layer traverses) data for a standard geometry (Series 60) of different sizes (1.2-9.6 m), but did not consider uncertainty assessment. The latter built on the former in providing comparison between 7

institutes of resistance test uncertainties following standard uncertainty assessment methodology, but for different model geometries and sizes (Series 60, container ships, and 5415). Present work builds on both in providing comparisons between 3 institutes of both data and uncertainties for the same model geometry of 2 sizes (3 and 5.72 m). Such comparisons between facilities is apparently relatively uncommon in other fields such as aerospace and mechanical engineering, which may be due to increased complexity of routine ship model testing due to viscous and free surface effects in comparison to routine testing in other fields. The results are timely with regard to the Gothenburg 2000 Workshop on CFD for Ship Hydrodynamics and should be taken into consideration in reaching conclusions regarding levels of CFD validation.

The focus herein is on the overlapping tests; however, highlights are given of the overall test program. Sections describe, respectively: the overlapping test design, comparison variables, and conditions; facilities, measurement systems, and procedures; uncertainty assessments; CFD validation/complementary CFD; comparisons of results; highlights of the overall test program; and conclusions.

OVERLAPPING TEST DESIGN, COMPARISON VARIABLES, AND CONDITIONS

The most typical towing-tank tests were selected for the overlapping tests, i.e., resistance, sinkage and trim, wave profile, wave elevations, and nominal wake. Each institute followed their usual procedures; however, special consideration was given to integration of uncertainty assessment into all phases of the experimental process, CFD validation, and complementary CFD.

Comparison variables were defined for total C_T^{15deg} and residuary C_R resistance, sinkage σ and trim τ , wave profile and elevations ζ , and nominal wake mean velocity \bar{V} and pressure C_p , as given by the following data-reduction equations:

$$C_T^{15deg} = C_R + C_F^{15deg} (1+k) \quad (1a)$$

$$C_R = C_T^{Tm} - C_F^{Tm} (1+k) \quad (1b)$$

$$C_T^{Tm} = \frac{M_x^{Tm} g}{0.5 \rho U_c^2 S} \quad (1c)$$

$$C_F = \frac{0.075}{(\log_{10} Re - 2.0)^2} \quad (1d)$$

$$\sigma = \frac{(\Delta FP + \Delta AP)}{2L} \quad (2)$$

$$\tau = \frac{(\Delta AP - \Delta FP)}{2L} \quad (3)$$

$$\zeta = \frac{z}{L} \quad (4)$$

$$\bar{V} = \frac{(U, V, W)}{U_c} \quad (5)$$

$$C_p = \frac{2(p - p_{ref})}{\rho U_c^2} \quad (6)$$

C_T^{15deg} is selected as the comparison variable for resistance, since it calibrates all data to the same temperature $T=15^\circ\text{C}$; thereby, enabling quantitative comparisons for similar tests and models at different institutes, as recommended by ITTC Quality Manual Procedure 4.9-03-03-01.2 1978 ITTC Performance Prediction Method. k is the form factor and C_F is the flat-plate friction line. σ and τ are defined without Fr^2 in the denominator. ζ , \bar{V} , and C_p are normalized by model length L , carriage speed U_c , and dynamic pressure ρU_c^2 , respectively.

To facilitate the comparisons of data procured at the different institutes, data (A, B, C), data differences D_i , and data differences uncertainty U_{D_i} variables are defined as follows:

$$(A, B, C) = (C_T^{15deg}, \sigma, \tau, \zeta, \bar{V}, C_p)_i, \quad (7)$$

$$i = A(DTMB), B(INSEAN), C(IIHR)$$

$$D_{AB} = A - B \quad (8)$$

$$U_{DAB}^2 = U_A^2 + U_B^2 \quad (9)$$

$$D_{AC} = A - C \quad (10)$$

$$U_{DAC}^2 = U_A^2 + U_C^2 \quad (11)$$

$$D_{BC} = B - C \quad (12)$$

$$U_{DBC}^2 = U_B^2 + U_C^2 \quad (13)$$

Data differences D_i are attributed to differences in facility (size, water quality, carriage); model size (for C), offsets, and turbulence stimulation; and

measurement systems and procedures. Comparison of two institutes is relatively straightforward. For

$$|D_i| \leq U_{D_i}, i=AB, AC, BC \quad (14)$$

data between institutes agree at level U_{D_i} . Presumably, design sets the required level of agreement between institutes. Better agreement requires reduction of U_{D_i} and possibly D_i . For

$$|D_i| > U_{D_i}, i=AB, AC, BC \quad (15)$$

data disagreement is attributed to model size (for C) and unaccounted for bias $B_{(A,B,C)}$ and precision $P_{(A,B,C)}$ limits. Comparison of three institutes is not straight forward as there are many combinations of equation (14) and (15). Various combinations were considered such as $A=B-2C$, $A+C-2B$, and $B+C-2A$; however, it was difficult to draw conclusions from these results. Presentations of comparisons are therefore limited to (A, B, C), D_i , $U_{(A,B,C)}$, and U_{D_i} .

The conditions at each institute for the overlapping tests are summarized in Table 1. For each test, the measurement system, Fr , Re , average temperature T_{ave} , density, kinematic viscosity, surface tension, density of data, and model installation with displacements at bow (FP) and stern (AP), is indicated.

FACILITIES, MEASUREMENT SYSTEMS, AND PROCEDURES

Facilities. Experiments with 5415 are performed in basin no. 2 (575 m long, 15.5 m wide, 6.7 m deep). Basin no. 2 is equipped with an electro-hydraulically operated drive carriage and capable of speeds of 10.3 m/s. Sidewall and endwall beaches enable 20-minute intervals between carriage runs. Towing-tank water is supplied by the Washington Suburban Sanitation Commission. Experiments with 2340A are performed in towing tank no. 2 (220 m long, 9 m wide, 3.6 m deep). Towing tank no. 2 is equipped with a single drive carriage that is capable of speeds of 10 m/s. Sidewall and endwall beaches enable 20-minute intervals between carriage runs. Towing tank water is spring water. Experiments with 5512 are performed in the IIHR towing tank (100 m long and 3.048 m wide and deep). The IIHR tank is equipped with an electric-motor operated drive carriage that is cable driven by a 15-horsepower motor and capable of speeds of 3 m/s. Sidewall and endwall beaches enable twelve-minute intervals between carriage runs. Towing-tank water is supplied by the city of Iowa City.

Model geometry. 5415 was constructed at the DTMB model workshop in 1980 from a blank of laminated wood and a computerized numerical-cutting (CNC) machine. Turbulence stimulation is at $x=0.05$

with cylindrical studs having 3.2 mm diameter, 2.5 mm height, and spaced 5.0 mm. The geometry offset measurement system consists of twenty-five wooden templates.

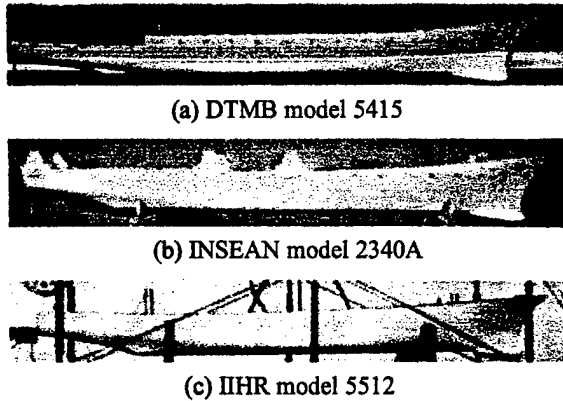


Fig. 1: Model geometries for the overlapping tests.

2340A was constructed in 1998 at the INSEAN model workshop from a blank of laminated wood and a CNC machine. Turbulence stimulation is at $x=0.01$ with cylindrical studs having 3.0 mm diameter, 3.0 mm height, and spaced 30.0 mm. The geometry offset measurement system consists of computer-aided design (CAD), hand-cut templates, level table, right angle, plumb, and rulers and feeler gauges. The data is reduced by computing crossplane and global average values for the error in the offsets for each coordinate and for S . 5512 was constructed in 1996 at the DTMB model workshop from molded fiber-reinforced Plexiglas. Turbulence stimulation is at $x=0.05$ with cylindrical studs having 3.2 mm diameter, 1.6 mm height, and 10.0 mm spacing. The measurement system and data-reduction procedures for determination of the errors in the geometry offsets and S are virtually the same as at INSEAN, however, the IIHR templates are CNC milled.

Carriage speed. At each facility, carriage speed U_c is measured with encoder-based measurement systems and PC data acquisition. The operating principle is integer pulse (n) counting at a wheel-mounted (diameter= D) encoder in known time intervals (Δt). The data-reduction equations are of the form

$$U_c = \frac{n\pi D}{a\Delta t} \quad (16)$$

where $a=(520, 1000, 8000)$, respectively for (A, B, C). Pulse count data is either passed to a PC directly as a frequency or through an analog-to-digital (AD) conversion. DTMB utilizes a 520-pulse, magnetic encoder carriage speed measurement system that is calibrated periodically to monitor its accuracy. Linear

resolution is 0.33 mm/pulse. Data acquisition is done through collection of 2000 discrete samples over 5 seconds at 400 Hz. Pulses are counted in Δt and entered into the PC as a frequency. Data reduction is completed through statistical analysis of the sample population (average, standard deviation, minimums, maximums, outliers). Outliers are identified and deleted using Chauvenet's criterion. INSEAN utilizes a 1000-window, optical encoder carriage speed measurement system. Linear resolution is 1 mm/window. Data acquisition is done through a 16-bit AD card by collection of 300 samples over 10 seconds at 30 Hz. Digital output from the encoder is converted to velocity prior to being recorded by the PC AD card and/or digital recorder (DAT). Data reduction is similar as for DTMB. IIHR utilizes an 8000-window, optical encoder carriage speed measurement system that is calibrated periodically at IIHR to determine its voltage-frequency relationship. Linear resolution is 0.15 mm/window. Data acquisition is done through collection of 2000 samples over 10 seconds at 200 Hz. Pulses undergo two conversions (DA and AD) before entering the PC. The data-reduction processes are similar as for DTMB and INSEAN.

For the resistance and sinkage and trim tests, the models are free to heave, pitch, and roll but restrained in surge, sway, and yaw. For all other tests, the models are restrained from heave, pitch, roll, surge, sway, and yaw but fixed at their dynamic sinkage and trim (Table 1).

Resistance. Resistance C_{TISC} is measured with loadcell-based measurement systems and PC data acquisition. The towing force in (kg) is converted to Newtons (N) by multiplication with g ($g_A=9.8009 \text{ m/s}^2$; $g_B=9.8033 \text{ m/s}^2$; $g_C=9.8031 \text{ m/s}^2$) based on the local latitude (Halliday and Resnick, 1981). Towing tank water temperature is measured daily at the model mid draft using a digital thermometer from which density ρ and kinematic viscosity ν are linearly interpolated using fresh water values as recommended by ITTC Quality Manual Procedure 4.9-03-01-03 Density and Viscosity of Water. The form factor $k=0.15$ is calculated using Prohaska's method, as recommended by ITTC Quality Manual Procedure 4.9-03-03-01.2 1978 ITTC Performance Prediction Method. Data-reduction processes are the same as for the carriage-speed tests. DTMB uses a variable reluctance, in-house manufactured loadcell, signal conditioner, and 16-bit AD card with carriage PC for the resistance tests. The loadcell, signal conditioner, and carriage PC AD card are statically calibrated on a DTMB test stand to determine the voltage-mass relationship. Data acquisition is done through collection of 2000 discrete samples over 5 seconds at 400 Hz. Data is filtered

through a 10 Hz low-pass filter. INSEAN uses a Hottinger Baldwin Messtechnik model U1, 50 kg loadcell, signal conditioner, and 16-bit AD card with PC for the resistance tests. The loadcell, signal conditioner, and carriage PC AD card are statically calibrated on a Kempf and Remmers precision test stand to determine the voltage-mass relationship. Data acquisition is done through collection of 300 discrete samples over 10 seconds at 30 Hz. Amplified analog voltages are converted to frequency (3000 ± 2500 Hz) for transmission to the AD card to reduce signal sensitivity to noise. Data is filtered through a 10 Hz low-pass filter. IIHR uses a Nisshio strain-gage type 20 kg loadcell, signal conditioner, and 12-bit AD card with PC for the resistance tests. The loadcell, signal conditioner, and carriage PC AD card are statically calibrated on an IIHR test stand to determine the voltage-mass relationship. Data acquisition is done through collection of 2000 discrete samples over 10 seconds at 200 Hz. Data is filtered through a 3 Hz low-pass filter.

Sinkage and trim. Sinkage σ and trim τ are measured with potentiometer-based measurement systems and PC data acquisition. The potentiometers sense displacements of the model at the FP and AP which are converted to σ and τ with equations (2) and (3). Data-reduction processes are the same as for the resistance tests. DTMB employs linear potentiometers, signal conditioners, and a 16-bit AD card with PC for the sinkage and trim tests. The potentiometers, signal conditioners, and carriage PC AD card are statically calibrated on a DTMB test stand to determine the voltage-displacement relationship. Data acquisition is done through collection of 500 discrete samples over 5 seconds at 100 Hz. Data is filtered through a 10 Hz low-pass filter. INSEAN employs rotative potentiometers, signal conditioners, and a 16-bit AD card with PC for the sinkage and trim tests. Displacement measurements are made by conversion of vertical to angular displacements through weight-balanced, mechanical parallelograms. The potentiometers, signal conditioners, and carriage PC AD card are statically calibrated on an INSEAN test stand to determine the voltage-displacement relationship. Data acquisition is done through collection of 300 discrete samples over 10 seconds at 30 Hz. Data is filtered through a 10 Hz low-pass filter. IIHR employs linear potentiometers and a 12-bit AD card with PC for the sinkage and trim tests. The potentiometers and carriage PC AD card are statically calibrated on an IIHR test stand to determine the voltage-displacement relationship. Data acquisition is done through collection of 2000 discrete samples over 10 seconds at 200 Hz. Data is not filtered.

Wave profile. Wave profiles ζ are measured with different measurement systems and normalized with model length L . DTMB utilizes a waterproof pencil and hull-based grid system for the wave profile tests. Wave profiles are marked on the model as it is towed through the basin. Vernier calipers are used to quantify the wave profile heights referenced to the full-load water line. INSEAN utilizes a photographic and digitizing measurement system with a hull-based grid system for the wave profile tests. Data acquisition is done by photographing the wave profile in sections ($20\% L$) and digitizing the negatives with a high-resolution scanner. Wave heights are quantified at x-stations on the model with CAD software. IIHR utilizes adhesive markers, flexible ruler, level table, height gauge, and hull-based grid system for the wave profile tests. Data acquisition is done by fixing the adhesive markers at the top of the wave profile at each x-station. The model is removed from the tank and a flexible ruler is used to measure the wave profile distance along the girth of the model from the calm waterline. The above two steps are repeated three times. The model is inverted and mounted on a level table and the average wave height values are remarked along the girth of the model from the calm waterline. The height gauge is used to measure the wave height z .

Far-field wave elevations. Far-field wave elevations ζ_{FF} are measured with either capacitance- or servo/acoustic-based measurement systems or PC data acquisition. A longitudinal-cut method is used to acquire the far-field data. Data-reduction is completed by conversion of longitudinal-cut time histories to a ship coordinate system and then normalizing elevations with model length. DTMB uses capacitance-wire probes suspended from an automated 2D traversing system, a 16-bit AD card, and shore-based PC for the far-field wave elevations tests. The probes and traversing system are cantilevered from the tank sidewall on a boom. The capacitance wires, 2D traversing system, and shore-based PC AD card are statically calibrated to determine their voltage-elevation relationships. Data acquisition is done through collection of 2000 and 3000 discrete samples over 20 and 30 seconds at 100 Hz for $Fr=0.28$ and 0.41 , respectively. Data is filtered at 10 Hz. Data was collected at two longitudinal positions: $y=0.097$ and 0.324 . INSEAN uses an array of four capacitance-wire probes, moveable slide, 12-bit AD card, and shore-based PC for the far-field wave elevation tests. The probes and traversing system are cantilevered from the tank sidewall on a boom. The capacitance wires, moveable slide, and shore-based PC AD card are statically calibrated to determine their voltage-elevation relationships. Data acquisition is done through

collection of 552 discrete samples over 12 seconds at 92 Hz. Data is filtered at 20 Hz. Data is collected at a total of 136 longitudinal cuts that are spaced at $\Delta y=0.0026$ between the maximum beam of the model and $y=0.433$. IIHR uses a Kenek servo-type wave probe and signal conditioner, a Keyence acoustic-type wave probe and signal conditioner, 2D traversing system, 12-bit AD card, and shore-based PC for the far-field wave elevation tests. The probes and traversing system are cantilevered from the tank sidewall on a 1.0 m boom. The servo and acoustic probes, signal conditioners, 2D traversing system, and shore-based PC AD card are statically calibrated to determine their voltage-elevation relationships. Data acquisition is done through collection of 2700 discrete samples over 13.3 seconds at 202.5 Hz. Data is not filtered. Data is collected at a total of 32 longitudinal cuts that are spaced at $\Delta y=0.01$ between the maximum beam of the model and the sidewall wave dampeners ($y=0.392$).

Near-field wave elevations. Near-field wave elevations ζ_{NF} are measured with servo-based measurement systems and PC data acquisition at DTMB and IIHR. A transverse-cut method is used to acquire the data at the bow, stern, and wake regions which are inaccessible with the longitudinal-cut method. Data-reduction processes are similar as for the carriage speed tests. DTMB employs four DTMB whisker probes, signal conditioners, 2D traversing system, 16-bit AD card and carriage PC for the near-field wave elevation tests. The whisker probes, signal conditioners, and carriage PC AD card are statically calibrated on the traverse system to determine its voltage-elevation relationships. Data acquisition is done at 100 Hz and the data is filtered at 10 Hz. Data is collected at a total of 20 transverse cuts that are spaced at $\Delta x=0.0088$ in bow and stern regions. Data is collected with a continuous traversing method in the y (transverse) coordinate with $\Delta y=0.0009$. IIHR employs a Kenek servo wave probe, signal conditioner, 2D traversing system, 12-bit AD card and carriage PC for the near-field wave elevation tests. The servo probe, signal conditioner, and carriage PC AD card are statically calibrated on the traverse system to determine its voltage-elevation relationship. Data acquisition is done through collection of 4096 discrete samples over 9 seconds at 455 Hz. Data is not filtered. Data is collected at a total of 46 transverse cuts that are spaced at $\Delta x=0.05$ in bow and stern/wake regions. Data is acquired with a point-to-point method with $\Delta y=0.005$ between measured points.

Nominal wake. Nominal wake data (U, V, W, C_p ; $x=0.935$) are measured with multihole probe/differential pressure transducer-based measurement systems and PC data acquisition. DTMB

utilizes a five-hole (3.2 mm tip), boundary layer pitot probe, pitot-static probe, five differential pressure transducers and signal conditioners, 16-bit AD card, and carriage PC for the nominal wake tests. The five-hole probe is calibrated before acquisition of the nominal wake data. Pitot tube calibration pressure coefficient matrices are determined from the calibration measurements, performed on a calibration rig towed in calm water with no ship model present. The calibration is expressed in coefficient form as: pitch angle (C_p pitch) versus yaw angles (C_p yaw), and axial velocity (C_p vel) versus yaw angle. Data acquisition for these experiments was done in a rectangular coordinate frame through collection of 500 samples over 5 seconds at 100 Hz. Data is collected at 358 points on 18 horizontal cuts with variable spacing in y and z . Data reduction is done with the calm-water calibration matrices. INSEAN utilizes a port-side, five-hole, boundary layer pitot probe (3.2 mm tip), pitot-static probe, five differential pressure transducers and signal conditioners, 16-bit AD card, and carriage PC for the nominal wake tests. Three calibrations are used for the nominal wake tests: (1) five-hole pitot probe is calibrated in the IIHR 1.07-m open throat wind tunnel. (2) differential pressure transducers and signal conditioners are statically calibrated with water head to establish the voltage-pressure relationships; and (3) calibration is made for the five-hole pitot probe preset angles (α_p, ϕ_p), by taking initial data at each x -station with the probe located at sufficient (y, z) that uniform-flow conditions prevail. Data acquisition is done through collection of 2000 samples over 2 seconds at 1000 Hz. Data is collected at a total of 32 horizontal cuts that are spaced $\Delta z=0.0025$. Transverse spacing of data is $\Delta y=0.0025$. Data reduction is done in five steps: (1) AD card output is statistically analyzed; (2) the average value is converted to mm H_2O using the voltage-pressure calibration with linear interpolation; (3) velocity vector angles (α, ϕ) and probe calibration coefficients (M, P) are obtained with local linear interpolation; (4) correction for five-hole pitot probe preset angle from calibration for (α_p, ϕ_p); and (5) U, V, W , and C_p are calculated. Density is calculated as described for the resistance test. IIHR utilizes the same equipment and procedures as INSEAN except: (1) IIHR uses a proportionately smaller five-hole pitot probe which has the same size probe tip; (2) IIHR measures starboard-side nominal wake data; and (3) IIHR collects 1500 samples over 12 seconds at 125 Hz with a 12-bit AD card.

UNCERTAINTY ASSESSMENT

All three institutes followed ITTC Quality Manual Procedures 4.9-03-01-01 Uncertainty Analysis

in EFD, Uncertainty Analysis Methodology; 4.9-03-01-02 Uncertainty Analysis in EFD, Guideline for Towing Tank Tests; and 4.9-03-01-01 Uncertainty Analysis, Example for Resistance Test. The Example for Resistance Test is based on results from most members of the 22nd ITTC Resistance Committee, including the present results from INSEAN and IIHR. Bias limits are estimated with consideration to significant elemental error sources for individual variables, whereas precision limits are estimated end-to-end for experimental results based on multiple tests at the same conditions. Total uncertainties are estimated with a root-sum-square (RSS) and normalization with the range of the result. Table 2 summarizes the uncertainty assessment results for the overlapping tests.

Model geometry. Precision limits are not considered in the analyses, thus, all of U_S is from the bias limit. For DTMB and INSEAN, 100% of the bias limit is associated with the errors in the model geometry offsets (x, y, z) which are averaged over 25 x -stations with templates. For IIHR, inaccuracies in loading the model to the correct draft account for 78% of U_S , and the remaining 22% are associated with the errors in the model geometry offsets which are averaged over 31 x -stations with templates. The error in the geometry offsets is small ($B_{x,y,z}=0.8$ mm), but U_S is relatively high because the model is comparatively small, having 3.5-times less wetted surface area than 5415 and 2340A.

Carriage speed. Uncertainty in U_c at DTMB is very small (0.03%) for low and medium Fr . Bias errors stemming from measurement of D and n are major contributors to the bias limit. Precision limits contribute moderately and increase with increasing Fr . Uncertainty in U_c at INSEAN is one order of magnitude larger than at DTMB and decreases with increasing Fr . As per DTMB, measurement uncertainty in D and n are significant and account for most of the bias limits. Precision limits are relatively low and not Fr -dependent which suggests that the drive motor for INSEAN towing tank no. 2 is stable at all speeds in the test matrix. Uncertainty in U_c at IIHR is somewhat higher than at INSEAN due to the lower range of speeds for the smaller model. U_{Uc} also decreases with increasing Fr as per INSEAN. For all Fr , bias limits dominate (82-94%) U_{Uc} and decrease with increasing Fr . Measurement of n occurs twice in the data stream and accounts for 95-100% of the bias limits. Contributions from measurement of D are 0.2-3.5% and errors in the AD timebase are negligible as per DTMB and INSEAN. P_{Uc} increases with increasing Fr indicate reduced ability of the drive motor to maintain constant U_c for increasing speeds, i.e., for increasing load on the motor.

Resistance. Uncertainty in C_T^{15deg} at DTMB is of same order as values presented by 22nd ITTC Resistance Committee, 4.9-03-01-01 Uncertainty Analysis, Example for Resistance Test. Uncertainty in the loadcell calibration weight standard produces high and moderate contributions of bias limit to total uncertainty for $Fr=0.10$ and 0.28 , respectively. Precision limit contributions are relatively high which is possibly due to residual tank motions between runs. Uncertainty in C_T^{15deg} at INSEAN is moderately higher than at DTMB and decreases with increasing Fr . Biases in the measurement of F_x contribute 70%-10% of B_{CT15} for increasing Fr and are attributed to the standardized calibration weights and scatter in the calibration data. Other significant factors in B_{CT15} are U_S which contributes 10%-65% for increasing Fr and U_{Uc} which contributes 5%-15% for increasing Fr . The uncertainties in the water temperature measurement are negligible for all Fr as per DTMB and IIHR. Precision limit contributions are relatively high as per DTMB which also may be possibly due to residual tank motions between runs. Uncertainty in C_T^{15deg} at IIHR is roughly similar as for INSEAN except for low Fr where IIHR is 46% lower than INSEAN. The bulk of U_{CT15} is bias related with U_{Uc} and U_S contributing 62%-29% to B_{CT15} for increasing Fr and 9%-71% to B_{CT15} for increasing Fr , respectively. Effects of scatter in loadcell calibration data account for 100% of B_{F_x} . Precision limit contributions are relatively low for all Fr which may be due to less residual tank motions between runs as compared with DTMB and INSEAN.

Sinkage and trim. Uncertainty in σ and τ at DTMB is somewhat large for $Fr=0.10$ but decreases significantly with increasing Fr as the range of the measurements increase, i.e., the potentiometers operate further from their limiting resolution for higher Fr . Bias limit contributions for both variables are mainly affected by the scatter in the potentiometer calibrations and decrease with increasing Fr . Conversely, precision limit contributions increase with increasing Fr which may indicate elevated carriage vibration for higher Fr and/or residual tank motions. Uncertainty in σ and τ at INSEAN is large for $Fr=0.10$ but decreases significantly to values comparable with DTMB with increasing Fr . Bias limits are negligible for both variables and all Fr due to dominance of precision limits whose elevated values are attributed to residual tank motions between carriage runs. Uncertainty in σ and τ at IIHR is somewhat large for $Fr=0.10$ but decreases significantly with increasing Fr as per DTMB and INSEAN. Bias limit contributions for σ are high to moderate for $Fr=0.10$ and $Fr=0.28/0.41$, respectively, with no Fr -dependence. Bias limit contributions for τ are high at $Fr=0.10$ and decrease with increasing Fr as

per DTMB. Bias limit magnitudes originate from scatter in the calibration data. Precision limit contributions are mostly high for both variables and all Fr and caused by residual tank motions and heave/pitch oscillations at the model mount as the model seeks its hydrodynamic equilibrium. This 'porpoising' of the model is likely present at all facilities.

Wave profile. Uncertainty in ζ is less than 5% for all facilities and both Fr and decreases with increasing Fr. For DTMB and both Fr, bias limits account for 64.5% of U_{ζ} and are composed of error estimates for marking the wave profile at the exact air-water interface (85%) and measuring the distance from draftline to measurement with a vernier caliper (15%). Precision limits account for 35.5% of U_{ζ} and are based on three measurements of the wave profiles and estimates of the contact-line unsteadiness. For INSEAN precision limits are not considered in the analysis. Contributions to the bias limits are associated with the uncertainties in the hull-gridline thickness (40%), optical distortion for the camera (50%), scanner resolution (5%), and interpolation error (5%). For IIHR and both Fr, bias and precision limit contributions to U_{ζ} are roughly 80% and 20%, respectively. Contributions to the bias limits are associated with uncertainties in the adhesive marker placement on the hull (50%), placement of the draft and x-station lines on the model (23%), reapplication of the wave profile marks on the hull after the test when the model is removed from the tank (23%), and height-gauge readings from draftline to measurement (4%). Precision limit contributions to U_{ζ} are relatively low and computed for N=3 multiple tests.

Far-field wave elevations. Uncertainty in ζ_{FF} at DTMB is better than 4% for Fr=0.28 and 0.41. A longitudinal cut at $y=0.082$ is chosen for detailed assessment of measurement uncertainty. For both Fr, bias limits are main contributor to $U_{\zeta_{FF}}$ and are composed mainly of scatter in the calibration data. Precision limits are estimated from N=9 multiple tests and increase with Fr which may be due to elevated levels of free-surface turbulence with increasing Fr and "snapshot"-like feature of the longitudinal-cut method. Uncertainty in ζ_{FF} at INSEAN is 3% or better for Fr=0.28 and 0.41. Longitudinal cuts at $y=0.082, 0.172, 0.259$, and 0.347 are chosen for detailed analysis of measurement uncertainty. The majority of $U_{\zeta_{FF}}$ is bias-limit related. The uncertainty in U_{ζ} accounts for 70% of $B_{\zeta_{FF}}$ with a 10%-15% contribution from the uncertainty in (x, y) probe position in the test region. Uncertainty in the distance measurement D between the wave probes and the FP of the model at $t=0$ accounts for 5% of $B_{\zeta_{FF}}$. Uncertainty in the time lag between switch engagement and data acquisition is negligible. Precision limits are estimated with N=10 multiple tests,

contribute moderately to $U_{\zeta_{FF}}$, and decrease with Fr in opposition to those at DTMB. Uncertainty in ζ_{FF} at IIHR is better than 3.5% for Fr=0.28. A longitudinal cut at $y=0.082$ is chosen for detailed analysis of measurement uncertainty. The majority of $U_{\zeta_{FF}}$ is bias-limit related. The uncertainty in carriage speed accounts for 79% of $B_{\zeta_{FF}}$ with 6%-8% contribution from the uncertainty in (x, y) probe positioning in the test region. Uncertainty in the distance measurement D between the wave probes and the FP of the model at $t=0$ accounts for 6% of $B_{\zeta_{FF}}$. Uncertainty in the time lag between switch engagement and data acquisition is negligible. Precision limits are estimated with N=10 multiple tests and contribute significantly to $U_{\zeta_{FF}}$ as per DTMB and INSEAN.

Near-field wave elevations. For DTMB, low-turbulence LTR and high-turbulence HTR (x, y) regions are identified for detailed analysis. In the HTR, precision limit contributions to $U_{\zeta_{NF}}$ are elevated (85.5%) from large fluctuations in the free surface and air entrainment into the flow. This produces comparatively high uncertainty in the near-field measurements. For the LTR, contributions of bias and precision limits are more balanced and the uncertainty is less than 5%. For this case, the scatter in the whisker probe calibration governs bias limit magnitude. For IIHR, LTR $(x, y=0.05, 0.07)$ and HTR $(x, y=1.075, 0)$ regions are identified in the wavefield for detailed analysis. Bias limits contribute (25-50%) to $U_{\zeta_{NF}}$ which is mainly (~100%) due to scatter in the servo-probe calibration data. Relatively high $P_{\zeta_{NF}}$ is due to free-surface turbulence at the multiple-test conditions. Note that $P_{\zeta_{NF}}$ is three-times greater in the HTR than the LTR.

Nominal wake. For DTMB, LTR $(x, y, z=0.9346, 0.04, -0.065)$ and HTR $(x, y, z=0.9346, 0.02, -0.02)$ regions are identified in the flowfield for detailed assessment of the measurement uncertainty. In both HTR and LTR, bias limit contributions to total uncertainties are dominant for U and C_p but somewhat evenly matched with precision limit contributions for V and W. Uncertainties in the five-hole calibration accounts for 23% of the bias limit with the remaining portion due to probe position uncertainty in the flowfield and pressure stabilization during a carriage run. Precision limits are estimated from N=10 multiple tests and are moderate for V, but 15-35% of the total uncertainty for U, W, and C_p which may be a result of high free-surface turbulence/probe vibration. For INSEAN, LTR $(x, y, z=0.9346, 0.06, -0.0602)$ and HTR $(x, y, z=0.9346, -0.0025, -0.0602)$ regions are identified in the flowfield for detailed assessment of the measurement uncertainty. Bias and precision limit contributions to total uncertainties of all variables are

evenly distributed in the LTR and HTR. B_U and B_{Cp} are influenced mostly by uncertainties in wind tunnel coefficients, M and P , respectively. For crossflow velocities, B_V and B_W are mainly affected by uncertainties in velocity vector pitch and yaw angles (α , ϕ). Contributions from uncertainties in U_c to all variables are less than 3.5%, and uncertainties in measurement of pressures at the probe tip are negligible, except for the center hole where roughly 12% and 2% contributions to B_U and B_{Cp} are computed. Precision limits are estimated from $N=10$ multiple tests and are moderate and high for U and V , respectively, but 10-30% for W and C_p which may be caused as per DTMB. For IIHR, LTR ($x, y, z=0.9346, 0.1, -0.01375$) and HTR ($x, y, z=0.9346, 0, -0.02125$) regions are identified in the flowfield for detailed assessment of the measurement uncertainty. Bias limit contributions to total uncertainties of all variables are dominant in the LTR and HTR. In the LTR, B_U and B_{Cp} are influenced mostly by uncertainties in wind tunnel coefficients, M and P , respectively. B_V and B_W are mainly affected by uncertainties in velocity vector pitch and yaw angles (α , ϕ). In the HTR, B_U , B_V , B_W , and B_{Cp} are mainly influenced by uncertainties in the measurement of water head at the five-hole probe tip since the size of the tip is large with respect to the shear-flow gradients. B_V and B_W are also still affected significantly by uncertainty in the pitch and yaw angles in the HTR. Precision limits are estimated from $N=10$ multiple tests and are very small in relation to the bias limits, which may be due to lack of free-surface turbulence/pitot-probe vibration.

CFD VALIDATION/COMPLEMENTARY CFD

The conditions and data locations and densities (Table 1) were selected with consideration to use of data for CFD validation. Cruise ($Fr=0.28$) and flank ($Fr=0.41$) speeds were selected for detailed validation with most extensive tests for former condition. No specific requirement was placed on experimental uncertainties U_D , but rather considered an important quantity to be estimated at each facility with final estimates based on collective results, as discussed below. Additionally, previous experience and complementary CFD was used for determining data densities.

COMPARISON OF RESULTS

The focus of the discussions is on the comparison between institutes of facilities, model geometry, and overlapping test results for evaluation of facility/model geometry and scale effect biases. Comparisons are made of measurement systems and procedures and data (A, B, C) [equation (7)], data differences D_i [equations (8), (10), (12)], data

uncertainties $U_{(A,B,C)}$ and data-difference uncertainties U_{D_i} [equations (9), (11), (13)]. Data differences for all variables are computed after interpolation of two data sets onto standard dependent variable values and subtraction. Average data differences are expressed as percentages by normalizing the average difference with the average range (all institutes) of the variable.

Facilities. Facility locations are different as manifest by latitude, climate, and zone. Yearly average high/low/dew point temperatures are $66.6^\circ/48.8^\circ/44.4^\circ$, $68.0^\circ/51.9^\circ/52.8^\circ$, and $59.8^\circ/39.7^\circ/39.5^\circ$, respectively, at A, B, C . A and B have similar mild yearly climates, whereas C experiences harsher climate, especially during the fall and winter months. Zones for A and B are on outskirts of large cities, whereas C is in the center of a small city. Such differences in ambient conditions are partially accounted for by using values of g and density and viscosity based on local values of latitude and water temperature, respectively. Water quality is also different at each facility. A and C use local tap water and B uses local spring water; however, no account is made for water quality since as already mentioned all institutes base values of density and viscosity on water temperature only and fresh water values from standard tables.

The tanks at each facility have different dimensions with the largest to smallest being A, B , and C , respectively, which affects both blockage and residual tank water motions between carriage runs. The blockage values (ratio of beam/draft product and tank cross-sectional area) at A, B , and C are 0.0017, 0.0042, and 0.0055, respectively, which are all nearly at or below the recommended maximum value of 0.005. It is also recommended that model length should not be greater than tank depth or more than half-as-long as tank width. Thus only A satisfies all three requirements and B and C each violate one. Effects of blockage are partially accounted for through correction to carriage speed. Tank size and side and end wall wave damping affect residual tank water motions (free and sub surface) and required time intervals between carriage runs. A and B require 20 minutes between carriage runs and C 12 minutes all based on visual observations. In spite of waiting times, low frequency motions are still evident especially in the larger tanks (as mentioned above with regard to large precision limits for sinkage and trim measurements).

Carriage speed affects all results, although not always included directly in data-reduction equations. Although each institute measures carriage speed with similar instrumentation (encoders and pulse counters), they have different resolutions. A has the lowest angular resolution in their magnetic encoder (520

pulses/rev) but the lowest uncertainty, while C has the highest resolution but the highest uncertainty. The uncertainty differences are due to the procedures for transferring pulse count into the data-acquisition PC (frequency for A and two AD conversions for C) and the speed range for the uncertainty assessment. Since A and B operate at nearly twice the carriage speed for a given Fr , and speed range is the normalizing factor for determination of U_{U_c} , A and B have less uncertainty in measured U_c . U_{U_c} can be further reduced through implementation of a closed-loop feedback system that constantly assesses and updates U_c with respect to a desired value. Currently, B is adopting this capability, however, none of the facilities had this capability during the overlapping tests. Carriage ride affects results through carriage vibration; however, such effects were not considered.

Model geometry. Model geometry offsets, bow details (leading-edge radius), turbulence stimulation, surface roughness, and installation also surely affect all results, although, here again, not always directly through data-reduction equations. For each institute, U_s is estimated to be 0.5% which is near the level of U_s reported by the participating members of the 22nd ITTC uncertainty assessment example for resistance test. The method for determination of the uncertainties in the offsets is crude as templates are used at a limited number of stations and error estimation is tedious, involving moderate and low accuracy at low- and high-points on the hull surface, respectively. Accounting for twisting or sagging of a model in the estimation of the offset errors is a very difficult, if not impossible task with templates. Also complicating the issue is changes to the model offsets over time with changes in ambient temperature and humidity or by long-term water-immersion. Leading-edge radius on each model is 3.2 mm for A and B and 1.6 mm for C. Turbulence stimulation is different at each facility in terms of tripping location, however, results in C_T^{15deg} suggest that the turbulence stimulation was effective for all three models. Model surfaces were finished using usual procedures at each facility and assumed hydraulically smooth. All models were installed according to draft line, which is presumed the best method for CFD validation purposes. However, it was noted by 22nd ITTC uncertainty assessment example for resistance test that installation according to ballast weight reduces uncertainty in surface area by partially accounting for inaccuracy of design offsets. Tow points are also different for each model, but have not yet been compared.

Resistance. For resistance tests, measurement systems, procedures, and data uncertainty estimates (Table 2) are similar for all three institutes. Figure 2

displays the results. Figure 2a compares the resistance data and Figures 2b, c, d compare the data difference and data-difference uncertainties between institutes AB, AC, and BC, respectively. Trends in Figure 2a for all three institutes are typical for high-speed combatant, i.e., limited humps and hollows for low and medium Fr and sharply increasing resistance for high Fr . For low and medium Fr results for A, B, and C are very consistent with C usually between A and B, whereas for high Fr C is consistently lower than A and B.

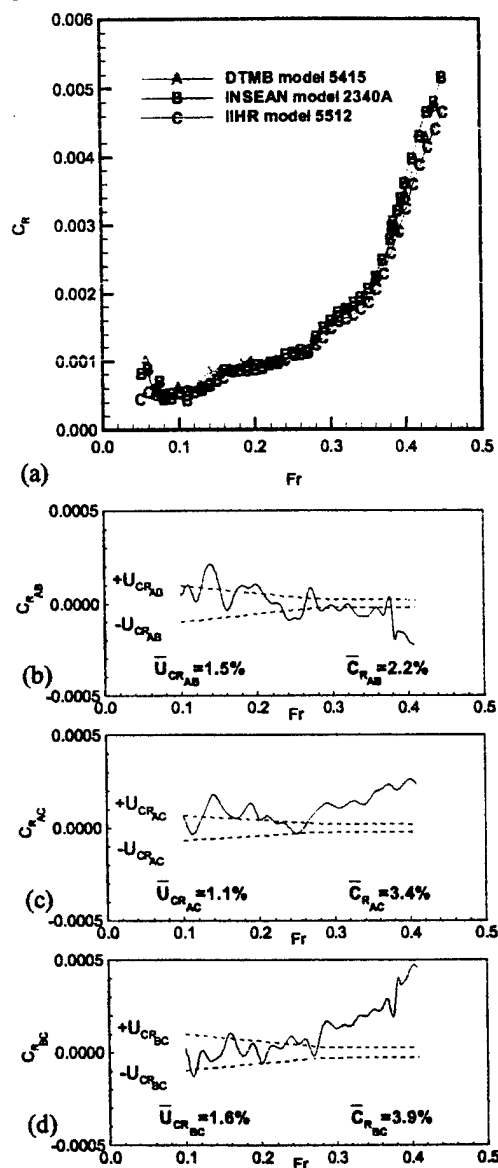


Fig. 2: Resistance results and data differences.

For AB (Figure 2b), data differences are oscillatory with Fr and intermittently greater/less than or within data-difference uncertainty, which suggests

unaccounted for bias and precision limits. Average data difference is 2.2%, whereas average data-difference uncertainty is only 1.5%.

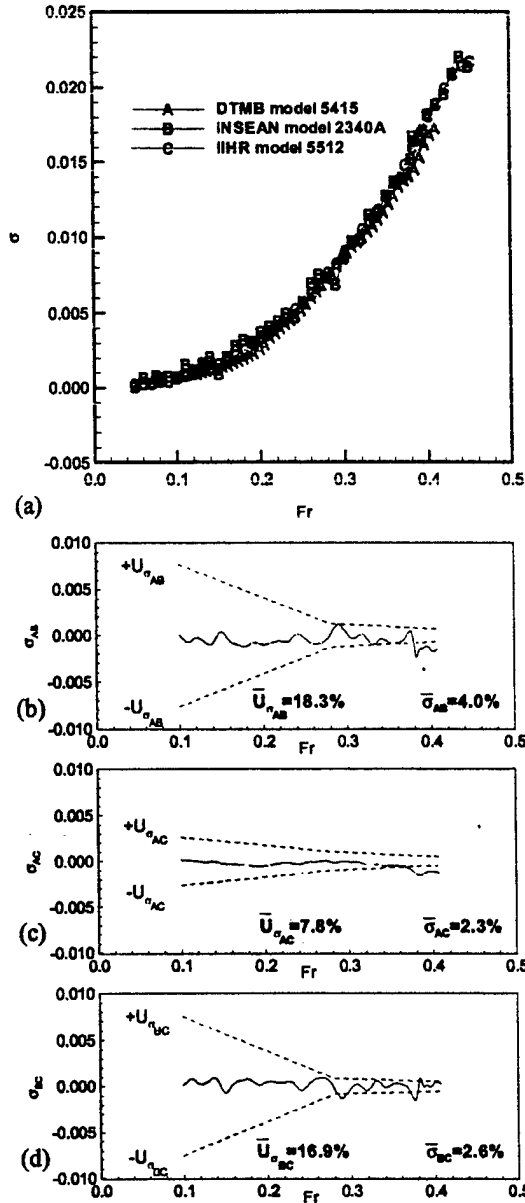


Fig. 3: Sinkage results and data differences.

For AC (Figure 2c) and low and medium Fr , trends are similar (i.e., data differences are oscillatory and intermittently greater/less than or within data-difference uncertainty), whereas for high Fr the trend is evident that data difference increases nearly linearly and is much greater than data-difference uncertainty. Average data difference and data-difference uncertainty are 3.4% and 1.1%, respectively. Former is

considerably larger than for AB and latter is somewhat smaller. Clearly the differences for AC compared to AB for larger Fr are due to scale effects. Trends for BC (Figure 2d) are very similar as for AC with average data differences and data-difference uncertainties of 3.9% and 1.6%, respectively.

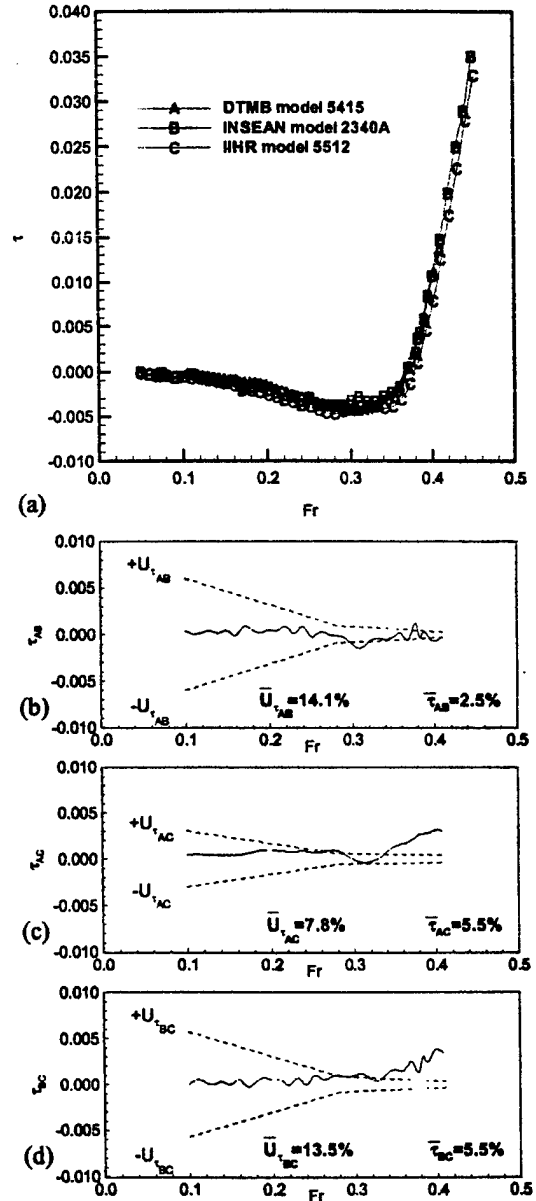


Fig. 4: Trim results and data differences.

Results are important in showing that for same size model (5.72 m) a better estimate for uncertainty in resistance test is 2.2%, which is considerably larger than individual facility estimates, especially for medium and high Fr . Results also show that scale

effects for 3 m model are significant for $Fr > 0.26$, which is likely due to differences in wave breaking as will be discussed later with regard to wave elevation measurements. For resistance, average facility/model geometry and scale effect ($Fr > 0.26$) biases are estimated as 0.5% and 5.8%, respectively, as summarized in Table 3. Note that averages are based on all three facilities and Fr ranges as given in Table 3, and that facility and model geometry biases are combined as they cannot be separated without use of a standard model.

Table 3: Summary of facility/model geometry and scale effect biases.

Result	Fac./model geometry ($U_{F/MG}$)			Scale (U_{SE})	
	AB	AC	BC	AC	BC
C_R	0.7%	0.9%†	0%†	4.9%?	6.7%?
σ	0%	0%	0%	0%	0%
τ	0%	0%‡	0%‡	11.6%?	12.7%?
$\zeta_{0.25}$	1.0%	0%	0%	0%	0%
$\zeta_{0.41}$	2.6%	1.9%	0%	0%	0%
ζ_{FF}	2.9%	1.1%	0%	0%	0%
U	0%	0%	0%	0%	0%
V	0.2%	0%	2.3%	0%	0%
W	13.0%	0%	11.7%	0%	0%

†: $Fr < 0.26$; ‡: $Fr < 0.33$; ?: $Fr > 0.26$; *: $Fr > 0.33$

Sinkage and trim. For sinkage and trim tests, measurement systems and procedures are similar for all three institutes. However, data uncertainties are fairly large and show some differences (Table 2). Uncertainties for B at low Fr are very large. Figures 3 and 4 display the results. Figures 3a and 4a compare the sinkage and trim data and Figures 3b, c, d and 4b, c, d compares the data difference and data-difference uncertainties between institutes AB, AC, and BC, respectively. Trends in Figures 3a and 4a for all three institutes are also typical for high-speed combatant, i.e., increasing sinkage and bow down than up trim for increasing Fr . In general, results between institutes are consistent, however, for trim and high Fr , C is consistently lower than A and B.

For AB (Figures 3b and 4b), data differences are oscillatory and mostly within the data-difference uncertainties. Average data differences are 4% and 2.5%, whereas average data-difference uncertainties are 14.1% and 18.3%, respectively, for sinkage and trim. In this case, data differences are fairly small but with large data-difference uncertainties. For AC (Figures 3c and 4c), trend for sinkage is similar as AB although percentage values are lower, whereas trend for trim is different for high Fr wherein as with resistance test data difference increases nearly linearly and is much greater than data-difference uncertainty. Average data difference and data-difference uncertainty are 5.5% and

7.8%, respectively. Former is larger than for AB and latter is smaller. Clearly for trim test, as with resistance test, the differences for AC compared to AB for larger Fr are due to scale effects. Trends for BC (Figures 3d and 4d) are very similar as for AC with average data differences and data-difference uncertainties of 2.6% and 16.9% and 5.5% and 13.5%, respectively, for sinkage and trim.

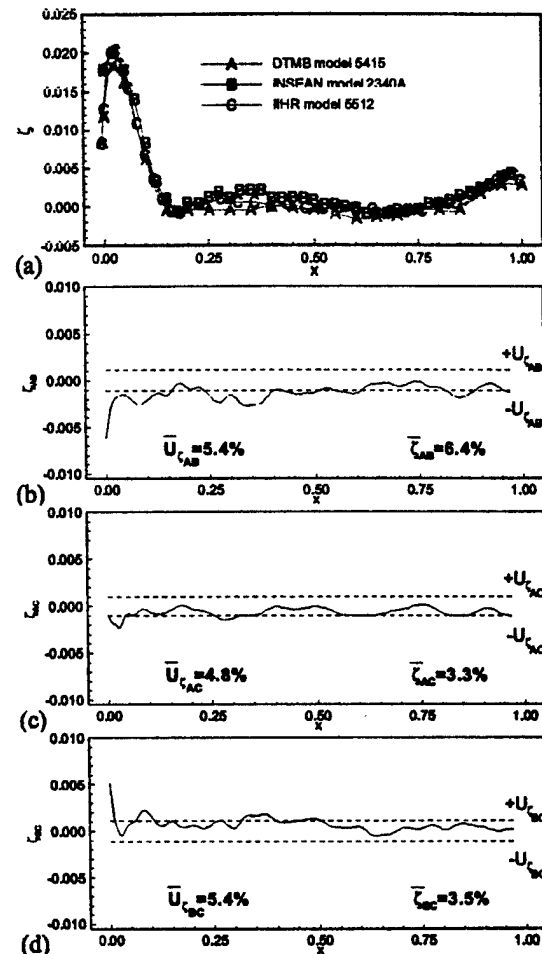


Fig. 5: Wave profile results and data differences ($Fr = 0.28$).

Results are important in showing that for same size model (5.72 m) data differences are fairly small (i.e., similar level as resistance test) and for low Fr considerably less than data-difference uncertainties. All institutes (especially B) need to reduce uncertainties for low Fr . Results also show that scale effects for 3 m model are significant for trim and $Fr > 0.33$. Facility/model geometry biases are not evident for both sinkage and trim. Scale effect biases are not evident for sinkage and estimated as 12.2% for trim (Table 3).

Wave profile. For wave profile tests, measurement systems and test procedures are very different between institutes. However, data uncertainties have similar values (Table 2). Figures 5 and 6 display the results. Figures 5a and 6a compare the wave profile data for $Fr = 0.28$ and 0.41 and Figures 5b, c, d and 6b, c, d compare the data difference and data-difference uncertainties between institutes AB, AC, and BC, respectively. Trends in Figures 5a and 6a for all three institutes are also typical for high-speed combatant for medium and high Fr , i.e., display bow, shoulder and stern waves and increasing transverse wavelength with increasing Fr .

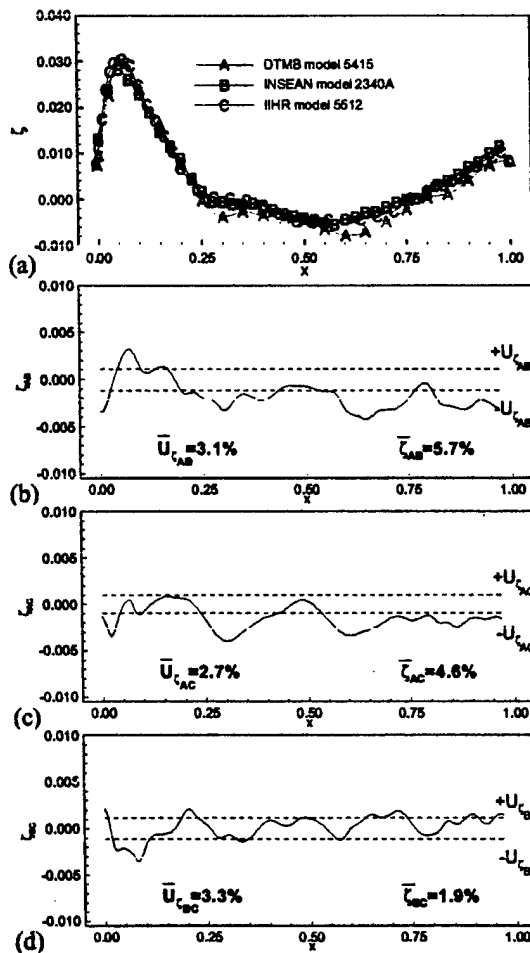


Fig. 6: Wave profile results and data differences ($Fr=0.41$).

Results between institutes are fairly consistent, although A seems to show consistently smaller values especially for shoulder and stern waves.

For AB (Figures 5b and 6b), data differences are oscillatory and mostly less than data-difference

uncertainties. Average data differences are 6.4% and 5.7%, whereas average data-difference uncertainties are 5.4% and 3.1%, respectively for $Fr=0.28$ and 0.41. Results for AC (Figures 5c and 6c) and BC (Figures 5d and 6d) are fairly similar; however, in these cases data differences are mostly within data-difference uncertainties.

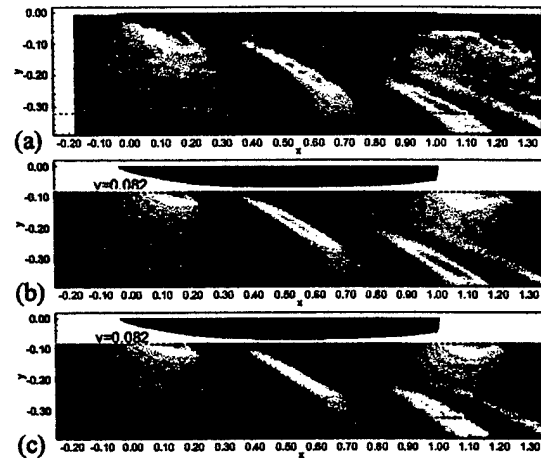


Fig. 7: Far-field wave elevation results at $Fr=0.28$: (a) DTMB 5415; (b) INSEAN 2340A; (c) IIHR 5512.

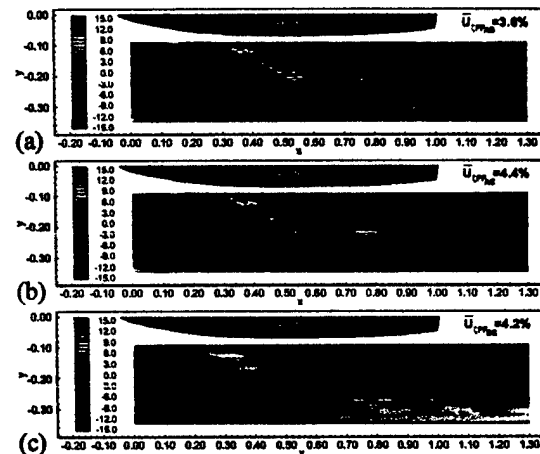


Fig. 8: Far-field wave elevation differences at $Fr=0.28$: (a) DTMB-INSEAN; (b) DTMB-IIHR; (c) INSEAN-IIHR.

Results are important in showing that a better estimate for uncertainty in wave profile test is about 5-6%, which is larger than individual facility estimates, especially for high Fr . Results also show that scale effects for the 3 m model are insignificant. Average facility/model geometry and scale effect biases are estimated as 0.9% and not evident, respectively (Table 3).

Wave elevations. For wave elevation tests, measurement systems and test procedures are different between institutes. However, data uncertainties have similar values (Table 2). Figures 7-10 display the results for the far field tests for $Fr=0.28$. Comparisons for the near field tests are not included. Figure 7 and 8 compare the wave pattern data and data differences, respectively. Figures 9 and 10 compare the data and data differences for two cuts $y=0.324$ and 0.082 , respectively. Figures 8a, b, c and 9b, c, d are for AB, AC, and BC, respectively. Figure 10b is for BC. Trends in wave patterns for all three institutes are typical for high-speed combatant, i.e., show diverging and transverse wave systems originating from bow, shoulder, and stern. Overall patterns for all three institutes are very similar, although resolution for A appears less than that for B and C. Figure 9a shows fairly large differences between A, B, and C at this distance from the hull, whereas Figure 10a shows small differences between B and C close to the hull.

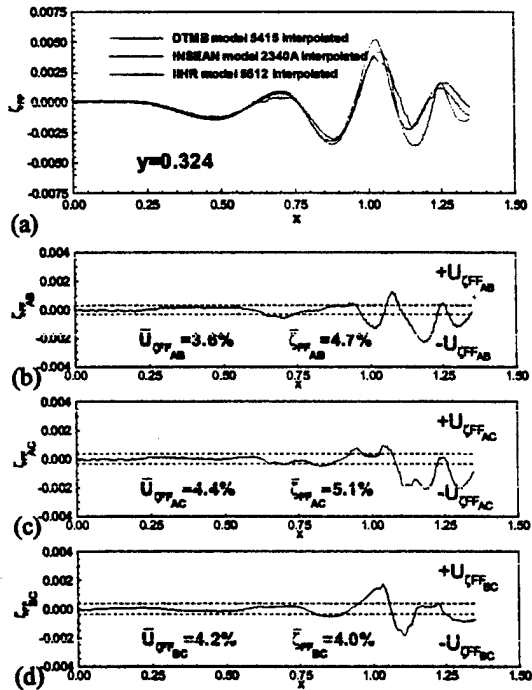


Fig. 9: Far-field wave cut data and differences at $y=0.324$, $Fr=0.28$: (a) interpolated wave cuts; (b) DTMB-INSEAN; (c) DTMB-IIHR; (d) INSEAN-IIHR.

Data differences (Figure 8) are largest for the diverging waves at crests and troughs. For AB, AC, and BC average data differences are 6.5%, 5.5%, and 2.5%, respectively, whereas average data-difference uncertainties for AB, AC, and BC are about 4%.

Detailed comparisons at $y=0.324$ show that data differences are oscillatory and average data differences of about 4-5% and data-difference uncertainties of about 4% for AB, AC, and BC. Here again, largest differences are at crests and troughs. Trends are similar at $y=0.082$, except average data difference is only 0.6% and data-difference uncertainty is 2.8%. In this case uncertainty estimates include dependency on x.

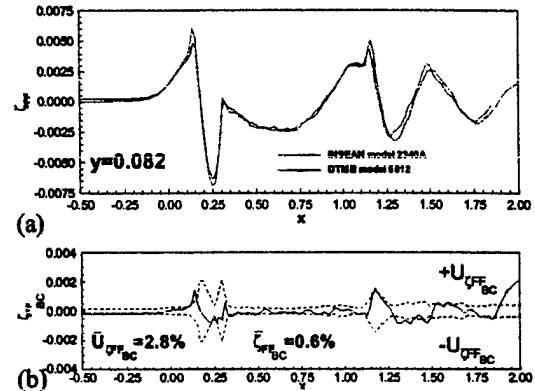


Fig. 10: Far-field wave cut data and differences at $y=0.082$, $Fr=0.28$: (a) data; (b) INSEAN-IIHR.

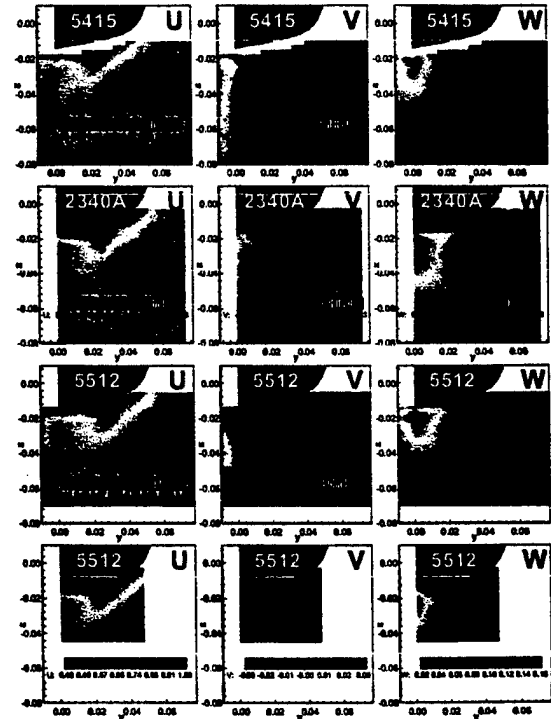


Fig. 11: Nominal wake results at $Fr=0.28$.

Results are important in showing that wave elevation differences are fairly small and close to the

uncertainty estimates. Also, scale effects are not evident. However, visual observation of wave patterns especially for higher Fr shows differences in wave breaking, i.e., wave breaking is considerably reduced for the 3 m model in comparison to the 5.7 m models presumably due to differences in Weber number and also some differences between wave breaking patterns for larger models presumably due to water quality differences between facilities A and B. Average facility/model geometry and scale effect biases are estimated as 1.3% and not evident, respectively (Table 3).

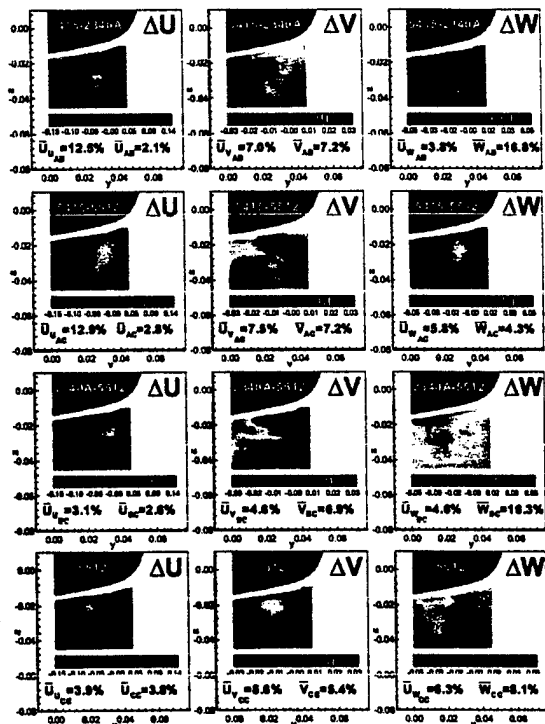


Fig. 12: Nominal wake data differences at $Fr=0.28$.

Nominal wake. For the nominal wake tests, measurement systems and test procedures are similar between facilities. However, data uncertainties are fairly large and show some differences (Table 2). Figures 11 and 12 display the results for the mean velocity components (U , V , W) data and data differences, respectively, for $Fr=0.28$. Trends for nominal wake for all three institutes are typical for high-speed combatant, i.e., relatively thin boundary layer near keel and free surface and thick boundary layer near mid girth due to effects of sonar dome vortex. V and W show influences of sonar some vortex and upward/inward stern flow. Flow patterns for all three institutes are similar, although differences in

resolution are apparent. For C , scale effects are not obvious.

For AB , data differences are less than data difference uncertainties for U , whereas they are larger for V and W . However, data-difference uncertainties (and data differences, except U) are fairly large. Interestingly, results for AC and BC are similar, i.e., scale effects are mostly lost in noise, although pattern for data differences for both AC and BC are nearly same, which may be an indication of scale effects.

Results are important in showing that the data differences and data uncertainty are reasonable close albeit with fairly large values. All institutes need to reduce uncertainties. Average facility/model geometry and scale effect biases are estimated for (U , V , W) as (0%, 0.8%, 8.2%) and 0%, respectively (Table 3).

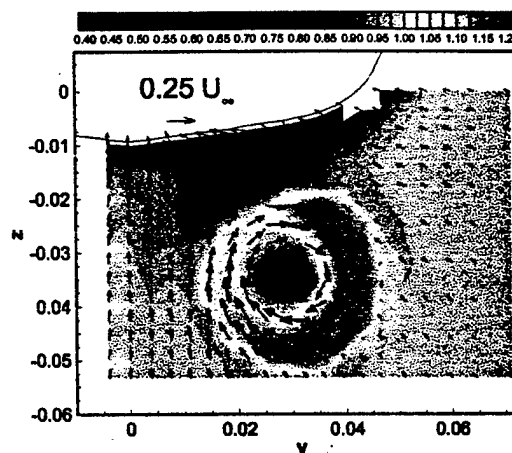


Fig. 13: DTMB 5415 axial velocity (U) contours and crossflow vectors for the w/propeller condition: $Fr=0.28$, $x=0.9603$, 436 rpm.

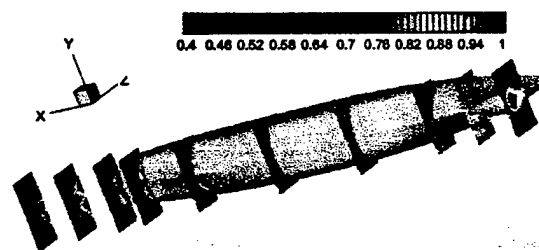


Fig. 14: INSEAN 2340A flow mapping at $Fr=0.28$.

HIGHLIGHTS OF OVERALL TEST PROGRAM

Although the emphasis herein has been on the overlapping tests, the collaborative effort also consists of focus studies at each institute. These studies were

designed to address a variety of important physics and expand the surface-ship database with quality datasets and uncertainty assessment. At A, model 5415 was used in a series of propeller-hull interaction tests. Shafts and struts were added to the model and data was obtained with and without the propellers operating. The measurements include free surface topographies of the transom wave field, longitudinal wave cuts (Ratcliffe, 2000), and velocity measurements in the nominal wake plane and both upstream and downstream of the operating propulsors. The velocity measurements were obtained with three-component laser-doppler velocimetry (LDV). Fig. 13 is a sample of results for the latter. At B, model 2340A was used for a comprehensive flow mapping of the boundary layer and wake flow at eleven cross planes with multi-hole probes and pressure transducers. The axial velocity results are plotted in Fig. 14. Results from this study as well as the overlapping tests and the near field bow and stern wave elevations from A will be used at the Gothenburg 2000 workshop on CFD in ship hydrodynamics. At C, model 5512 is currently being used for unsteady-flow testing in regular head waves. Measurements include unsteady forces and moment with a load cell, far- and near-field wave elevations (Fig. 15) with servo and acoustic probes, and mean and turbulent flow field with a towed particle-image velocimetry (PIV) system. The latter measurements are ongoing and will be archived with the rest of the unsteady data at <http://www.ihr.uiowa.edu/~towtank>. Figures 11 and 12 also include comparisons of nominal wake data for 5512 and pitot and PIV measurement systems. Data differences are similar to data-difference uncertainties.

CONCLUSIONS

Results are presented from overlapping towing tank tests between three institutes for resistance, sinkage and trim, wave profiles and elevations, and nominal wake using the same model geometry and conditions, including rigorous application of standard uncertainty assessment procedures as per the 1999 ITTC Quality Manual. Two of the institutes used 5.7 m models whereas the third institute used a smaller 3 m model. Comparison variables were defined for data-reduction equations and data differences and data-difference uncertainties. Detailed descriptions were provided of facilities, measurement systems, data-acquisition and reduction procedures, and uncertainty assessment. Results were discussed with regard to levels and causes of data differences and data-difference uncertainties and to estimate facility/model geometry and scale effect biases.

For same size 5.7 m models, data differences were in general oscillatory, and in many cases, larger in magnitude than data-difference uncertainties, which indicates unaccounted for bias and precision limits and that current individual facility uncertainty estimates are often too optimistic. Scale effects for the 3 m model are only evident for resistance and trim tests for $Fr > 0.26$ and $Fr > 0.33$, respectively. Facility/model geometry and scale effect bias are estimated based on comparisons, as summarized in Table 3. Uncertainty estimates including such biases may provide better estimates, especially for use in CFD validation, which is the recommendation of the present study along with efforts towards improvement of individual institute uncertainty estimates. Use of standard models and current ITTC efforts in providing standard quality manual procedures for towing tank tests and uncertainty estimates will also be helpful in this regard.

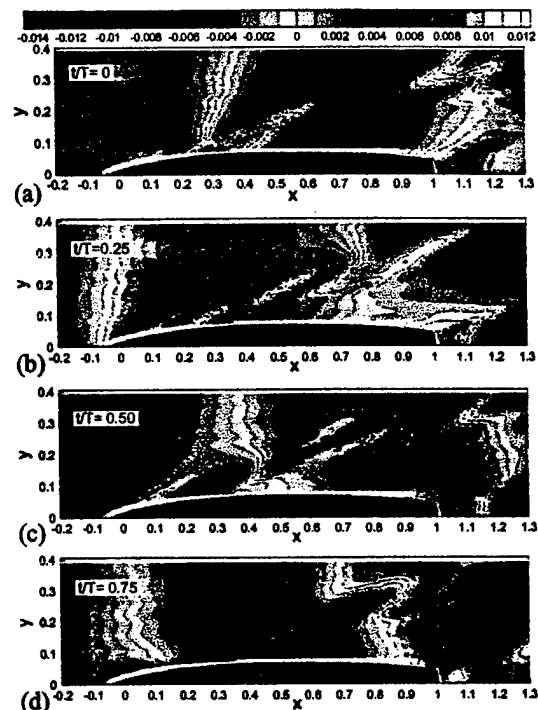


Fig. 15: IIHR 5512 unsteady wave field at four instances in the encounter period: $Fr=0.28$, $Ak=0.025$, $\lambda=4.572$ m.

ACKNOWLEDGEMENTS

The research at IIHR and a portion of the research at INSEAN and at UAH were sponsored by the Office of Naval Research under Grants N00014-98-1-0156 and N00014-97-1-0014, respectively, under the administration of Dr. E.P. Rood. The research at

DTMB was sponsored by the Office of Naval Research with 6.2 Funding, administered by Dr. E.P. Rood. The research at INSEAN was also sponsored by the Italian Ministry of Transportation and Navigation in the frame of Research Plan 1997-1999.

REFERENCES

- Avanzini, G., Bennedetti, and Penna, R., 1998, "Experimental Evaluation of Ship Resistance for RANS Code Validation," ISOPE '98, Montreal, Canada, May.
- Avanzini, G., Benedetti, and Penna, R., 2000, "Experimental Evaluation of Ship Resistance for RANS Code Validation," Journal of Offshore and Polar Engineering, Vol. 10, No. 1, March 2000 (pp.10-18).
- G2K, 2000, <http://www.ihr.uiowa.edu/gothenburg2000>
- Gui, L., Longo, J., and Stern, F., 1999, "Towing Tank PIV Measurement System and Data and Uncertainty Assessment for DTMB Model 5512," 3rd International Workshop on PIV, Santa Barbara, CA, 16-18 September.
- Haliday, D. and Resnick, R., 1981, "Fundamentals of Physics", John Wiley and Sons, New York, 816 pp.
- ITTC, 1999, "Report of the Resistance Committee," Proceedings International Towing Tank Conference, Seoul, Korea & Shanghai, China, 5-11 September.
- Lee, J., Lee, S.J., and Van, S.H., 1998, "Wind Tunnel Test on a Double Deck Shaped Ship Model," 3rd International Conference on Hydrodynamics, Seoul, Korea.
- Longo, L., Gui, L., Metcalf, B., and Stern, F., 2000, "Naval Surface Combatant in Regular Head Waves," abstract submitted 23rd ONR Symposium on Naval Hydrodynamics, Val de Reuil, France, 17-22 September.
- Longo, J. and Stern, F., 1998, "Resistance, Sinkage and Trim, Wave Profile, and Nominal Wake and Uncertainty Assessment for DTMB Model 5512," Proc. 25th ATTC, Iowa City, IA, 24-25 September.
- Olivieri, A. and Penna, R., 1999, "Uncertainty Assessment in Wave Elevation Measurements," ISOPE '99, Brest, France, June.
- Olivieri, A. and Penna, R., 2000, "Detailed measurements of wave-pattern and nominal wake of a fast displacement ship model", AFM Conference, Montreal, May 2000.
- Principles of Naval Architecture, 1967, The Society of Naval Architects and Marine Engineers, New York, N.Y., 827 pp.
- Ratcliffe, T., 1995, <http://www50.dt.navy.mil/5415/>
- Ratcliffe, T., 2000, "An Experimental and Computational Study of the Effects of Propulsion on the Free-Surface Flow Astern of Model 5415," 23rd ONR Symposium on Naval Hydrodynamics, Val de Reuil, France, 17-22 September.
- Stern, F., 2000, <http://www.ihr.uiowa.edu/~towtank/>
- Van, S.H., Yim, G.T., Kim, W.J., Kim, D.H., Yoon, H.S., and Eom, J.Y., 1997, "Measurement of Flows Around a 3600TEU Container Ship Model," *Proceedings of the Annual Autumn Meeting*, SNAK, Seoul, pp. 300-304 (in Korean).
- Van, S.H., Kim W.J., Kim, D.H., Yim, G.T., Lee, C.J., and Eom, J.Y., 1998a, "Flow Measurement Around a 300K VLCC Model," *Proceedings of the Annual Spring Meeting*, SNAK, Ulsan, pp. 185-188.
- Van, S.H., Kim, W.J., Yim, G.T., Kim, D.H., and Lee, C.J., 1998b, "Experimental Investigation of the Flow Characteristics Around Practical Hull Forms," *Proceedings 3rd Osaka Colloquium on Advanced CFD Applications to Ship Flow and Hull Form Design*, Osaka, Japan.

Table 1: Summary of overlapping test conditions for DTMB, INSEAN, and IIHR.

EXPERIMENT	DTMB (A)	INSEAN (B)	IIHR (C)
MODEL GEOMETRY	<i>Templates</i>	<i>Templates</i>	<i>Templates</i>
CARRIAGE SPEED	<i>Magnetic encoder</i>	<i>Optical encoder</i>	<i>Optical encoder</i>
RESISTANCE	<i>Loadcell</i>	<i>Loadcell</i>	<i>Loadcell</i>
Fr	0.05-0.44	0.05-0.45	0.05-0.45
Re	0.21-1.92e07	0.21-1.92e07	0.93-8.41e06
T _∞ (°C)	17.8	22.1	25.1
ρ (kg/m ³)	998.6960	997.7200	997.0720
v (m/s)	1.0638e-06	0.9547e-06	0.8925e-06
σ (N/m)	0.0738	0.0732	0.0727
Data density	ΔFr=0.013	ΔFr=0.01	ΔFr=0.01
Model installation	free	free	free
ΔFP, ΔAP	-	-	-
SINKAGE/TRIM	<i>Linear pots</i>	<i>Rotative pots</i>	<i>Linear pots</i>
Fr	0.05-0.44	0.05-0.45	0.05-0.45
Re	0.21-1.92e07	0.21-1.92e07	0.86-7.72e-06
T _∞ (°C)	17.8	22.1	21.5
ρ (kg/m ³)	998.6960	997.7200	997.9400
v (m/s)	1.0638e-06	0.9547e-06	0.9708e-06
σ (N/m)	0.0738	0.0732	0.0733
Data density	ΔFr=0.013	ΔFr=0.01	ΔFr=0.01
Model installation	free	free	free
ΔFP, ΔAP	-	-	-
WAVE PROFILE	<i>Wax pencil</i>	<i>Photography</i>	<i>Adhesive marker</i>
Fr	0.28, 0.41	0.28, 0.41	0.28, 0.41
Re	1.19, 1.75e07	1.19, 1.75e07	4.47, 6.54e06
T _∞ (°C)	20.6	22.1	18.5
ρ (kg/m ³)	998.1560	997.7200	998.5700
v (m/s)	0.9907e-06	0.9547e-06	1.0448e-06
σ (N/m)	0.0735	0.0732	0.0733
Data density	23pts, 25pts	41 pts	40 pts
Model installation	fixed	fixed	fixed
ΔFP, ΔAP	(-0.0027L, -0.00086L), (-0.00054L, -0.0083L)	(-0.0027L, -0.00086L), (-0.00054L, -0.0083L)	(-0.0031L, -0.00079L), (-0.0015L, -0.0079L)
NEAR-FIELD WAVES	<i>Whisker probe</i>		<i>Servo probe</i>
Fr	0.28, 0.41		0.28
Re	1.19, 1.75e07		3.81e06
T _∞ (°C)	20.6		12.5
ρ (kg/m ³)	998.1560		999.5000
v (m/s)	0.9907e-06		1.224e-06
σ (N/m)	0.0735		0.0745
Data density	20 cuts, Δx=0.09L, Δy=0.0009L		46 cuts, Δx=0.05, Δy=0.005
Model installation	fixed		fixed
ΔFP, ΔAP	(-0.0027L, -0.00086L), (-0.00054L, -0.0083L)		(-0.0031L, -0.00079L)
FAR-FIELD WAVES	<i>Capacitance probes</i>	<i>Capacitance probes</i>	<i>Servo/acoustic probes</i>
Fr	0.28, 0.41	0.28, 0.41	0.28
Re	1.19, 1.75e07	1.19, 1.75e07	4.48e06
T _∞ (°C)	20.6	13.3	18.6
ρ (kg/m ³)	998.1560	999.4000	998.5520
v (m/s)	0.9907e-06	1.1923e-06	1.0421e-06
σ (N/m)	0.0735	0.0743	0.0737
Data density	2 cuts at y=0.097L and 0.324L	136 cuts, Δx=0.016, Δy=0.003	32 cuts, Δx=0.001, Δy=0.01
Model installation	fixed	fixed	fixed
ΔFP, ΔAP	(-0.0027L, -0.00086L), (-0.00054L, -0.0083L)	(-0.0027L, -0.00086L), (-0.00054L, -0.0083L)	(-0.0031L, -0.00079L)
NOMINAL WAKE	<i>S-hole probe</i>	<i>S-hole probe</i>	<i>S-hole probe</i>
Fr	0.28, 0.41	0.28	0.28, 0.41
Re	1.19, 1.75e07	1.19e07	3.83, 5.61e-06
T _∞ (°C)	20.6	11.0	12.7
ρ (kg/m ³)	998.1560	999.6800	998.7140
v (m/s)	0.9907e-06	1.2692e-06	1.2173e-06
σ (N/m)	0.0735	0.0744	0.0744
Data density	18 cuts, 358 points, variable	32 cuts, Δy=Δz=0.0025	27 cuts, Δy=Δz=0.0025
Model installation	fixed	fixed	fixed
ΔFP, ΔAP	(-0.0027L, -0.00086L), (-0.00054L, -0.0083L)	(-0.0027L, -0.00086L), (-0.00054L, -0.0083L)	(-0.0031L, -0.00079L), (-0.0015L, -0.0079L)

Table 2: Summary of uncertainties for DTMB, INSEAN, and IIHR overlapping tests.

RESULT		DTMB (A)			INSEAN (B)			IIHR (C)		
	Fr	B	P	U	B	P	U	B	P	U
S	All Fr	100%	0%	1.2%	100 %	0%	0.5%	100%	0%	0.5%
U _c	0.10	78.0%	22.0%	0.03%	99.1%	0.9%	0.18%	94.2%	5.8%	0.66%
U _c	0.28	68.2%	31.8%	0.03%	93.7%	6.3%	0.13%	85.9%	14.1%	0.25%
U _c	0.41	NA	NA	NA	99.5%	0.5%	0.12%	82.3%	17.7%	0.18%
C _{TIS} /C _R	0.10	76.3%	23.7%	1.49%	69.4%	30.6%	2.68%	87.6%	12.4%	1.46%
C _{TIS} /C _R	0.28	45.5%	54.5%	0.33%	80.0%	20.0%	0.64%	89.2%	10.8%	0.63%
C _{TIS} /C _R	0.41	NA	NA	NA	66.3%	33.7%	0.61%	80.5%	19.5%	0.60%
σ	0.10	75.6%	24.4%	12.2%	0%	100%	42%	82.2%	17.8%	8.72%
σ	0.28	68.4%	32.6%	5.6%	0%	100%	4.71%	30.4%	69.6%	1.40%
σ	0.41	56.3%	44.7%	2.5%	0%	100%	2.93%	42.8%	57.2%	0.61%
τ	0.10	64.5%	35.5%	14.4%	0%	100%	32%	50.8%	49.2%	10.22%
τ	0.28	54.7%	46.3%	2.8%	0%	100%	4.70%	36.1%	63.9%	1.83%
τ	0.41	38.1%	61.9%	1.5%	0%	100%	0.87%	4.1%	95.9%	1.76%
ζ	0.28	64.5%	35.5%	3.52%	100%	0%	4.18%	83.7%	16.3%	3.43%
ζ	0.41	64.5%	35.5%	1.84%	100%	0%	2.59%	81.6%	18.4%	2.00%
ζ _{NP} ^{HTR}	0.28	14.5%	85.5%	14.6%	NA	NA	NA	25.2%	74.8%	3.38%
ζ _{NP} ^{LTR}	0.28	56.7%	44.3%	4.6%	NA	NA	NA	52.6%	47.4%	4.75%
ζ _{NP}	0.41	32.4%	67.6%	2.9%	NA	NA	NA	NA	NA	NA
ζ _{FF}	0.28	76.5%	23.4%	2.73%	64.9%	35.1%	2.40%	59.0%	41.0%	3.42%
ζ _{FF}	0.41	66.4%	33.6%	3.54%	78.5%	21.5%	3.00%	NA	NA	NA
U ^{HTR}	0.28	74.5%	26.5%	12.5%	60.4%	39.6%	0.38%	99.2%	0.8%	3.11%
V	P	43.5%	56.5%	6.5%	15.9%	84.1%	2.71%	93.3%	6.7%	3.76%
W	I	44.6%	35.4%	3.7%	87.9%	12.1%	0.86%	99.2%	0.8%	4.48%
C _p	T	84.5%	15.5%	2.4%	81.8%	18.2%	9.03%	100%	0%	36.21%
U ^{LTR}	O	65.4%	34.4%	1.6%	47.8%	52.2%	0.42%	99.8%	0.2%	1.20%
V	T	54.3%	46.7%	2.9%	21.2%	78.8%	1.87%	99.7%	0.3%	5.54%
W		65.3%	34.7%	6.5%	79.1%	20.9%	0.95%	99.9%	0.1%	4.08%
C _p		88.7%	21.3%	1.2%	70.2%	29.8%	9.11%	100%	0%	29.29%
U	0.28							42.1%	57.9%	2.35%
V	P							72.4%	27.6%	7.73%
W	I							62.4%	37.6%	4.37%
u	V							20.8%	79.2%	4.72%
v								34.9%	65.1%	4.31%
w								37.3%	62.7%	4.99%
uv								13.0%	87.0%	4.09%
uw								30.1%	69.9%	5.80%

Appendix C

Coleman, H. W., Stern, F., Di Mascio, A., and Campana, E. "The Problem With Oscillatory Behavior in Grid Convergence Studies," ***J. Fluids Engineering***, Vol. 123, No. 2, p438-439, June 2001.

out of the same magnetoelastic material, which has reaction times in the order of a few micro-seconds. The response time of such a design will be primarily limited by the inductance of the magnetic coil.

References

- [1] Van Lintel, H. T. G., Van de Pol, F. C. M., and Bouwstra, S., 1988, "A piezoelectric micropump based on micromachining of silicon," *Sens. Actuators*, **15**, pp. 153–167.
- [2] Esashi, M., Shoji, S., and Nakano, A., 1989, "Normally closed microvalve fabricated on a silicon wafer," *Sens. Actuators*, **20**, pp. 163–169.
- [3] Smits, J. G., 1990, "Piezoelectric micropump with three valves working peristaltically," *Sens. Actuators A*, **21–23**, pp. 203–206.
- [4] Sen, M., Wajerski, D., and Gad el Hak, M., 1996, "A novel pump for MEMS applications," *ASME J. Fluids Eng.*, **118**, pp. 624–627.
- [5] Beskok A., and Warburton T. C., 2001, "An unstructured h/p finite element scheme for fluid flow and heat transfer in moving domains," Submitted to *Journal of Computational Physics*.
- [6] Karniadakis, G. E., and Sherwin, S. J., 1999, *Spectral/hp Element Methods for CFD*, Oxford University Press.
- [7] Papavasiliou, A. P., Liepmann D., and Pisano, A. P., 1999, "Fabrication of a free floating silicon gate valve," *Proceedings of ASME IMECE Meeting, MEMS*, Vol. 1, pp. 265–274.

The Problem With Oscillatory Behavior in Grid Convergence Studies

Hugh W. Coleman

Fellow ASME, Propulsion Research Center, Department of Mechanical and Aerospace Engineering, University of Alabama in Huntsville, Huntsville, AL 35899

Fred Stern

Fellow ASME, Iowa Institute for Hydraulic Research, Department of Mechanical Engineering, University of Iowa, Iowa City, IA 52242

Andrea Di Mascio and Emilio Campana

Istituto Nazionale Per Studi Ed Esperienze Di Architettura Navale (INSEAN), Rome, Italy

[DOI: 10.1115/1.1362672]

Discussion of the Problem

The possibility of oscillatory behavior of the value of a computed variable as grid size is refined in a simulation raises questions in the interpretation of grid convergence studies that have, to the authors' knowledge, never been addressed. Such oscillatory behavior has been observed by the authors, for example, in variables such as wave profiles along the hull and wave elevations in the stern flow in simulations of flows about ships with complex geometries. Roache [1], in his comprehensive presentation and critique of work up to that time in the area of verification and validation of simulations, points out that "behavior far away from asymptotic convergence can be non-monotone" and "the additional assumption of monotone truncation error convergence in the mesh spacing . . . may not be valid for coarse grids, or possibly other conditions."

Contributed by the Fluids Engineering Division of THE AMERICAN SOCIETY OF MECHANICAL ENGINEERS. Manuscript received by the Fluids Engineering Division September 1, 1999; revised manuscript received February 8, 2001. Associate Editor: V. Ghia.

Typically (see Stern, et al. [2], for instance), the behavior of a variable is categorized as monotonically convergent, oscillatory, or divergent based on its behavior as the grid used in a simulation is refined. Consider the values of a computed variable y as a simulation is run using a coarse grid (y_C), a medium grid (y_M), and a fine grid (y_F). The ratio

$$R = \frac{y_M - y_F}{y_C - y_M} = \frac{\Delta y_{M-F}}{\Delta y_{C-M}}$$

has been used to categorize the behavior of y as grid size is decreased as: (1) monotonically convergent when $0 < R < 1$; (2) oscillatory when $R < 0$; and (3) divergent when $R > 1$. If the behavior really is monotonically convergent, then (1) holds. If the behavior really is divergent, then (3) holds. The problem that has not been previously recognized and discussed is the ambiguity that arises when the behavior really is oscillatory.

Consider the results from a simulation in which the computed value of variable y is truly an oscillatory function of grid size Δx , as shown in Fig. 1. When a grid size is chosen in a simulation, its value is of course arbitrary relative to the unknown periods of any oscillations of the computed variables, so each of the following cases in this example must be considered equally likely. Three cases are investigated, with a different initial grid size in each. In each case, three simulations are run with grid doubling used twice, resulting in coarse (C), medium (M), and fine (F) grid simulation values of the variable y .

The computed values of y are shown in Table 1 and plotted in Fig. 1. For Case 1, Δy_{C-M} is -1.0 and Δy_{M-F} is $+0.3$, a situation that would be assessed as oscillatory since $R < 0$. For Case 2, Δy_{C-M} is $+0.36$ and Δy_{M-F} is $+0.28$, a situation that would be concluded as being monotonically convergent since $0 < R < 1$. Finally, for Case 3, Δy_{C-M} is $+0.14$ and Δy_{M-F} is $+0.36$, a situation that would be concluded as divergent since $R > 1$. Thus, for the same (true) oscillatory behavior any of three conclusions can be supported, depending on the relationship of the chosen grid size to the unknown period(s) of the oscillation(s).

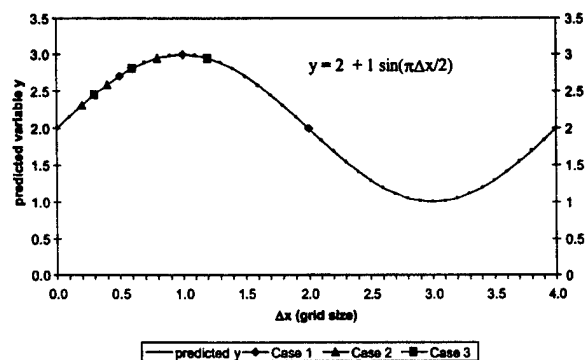


Fig. 1 Illustration of results of grid convergence studies using three grids when the true behavior is oscillatory convergence

Table 1 Results from grid convergence studies

Case	Grid Sizes (Δx 's)	y Coarse	y Medium	y Fine	Δy_{C-M}	Δy_{M-F}	Behavior Indication
1	2.0, 1.0, 0.5	2.00	3.00	2.70	-1.00	0.30	$R = -0.3$ Oscillatory
2	0.8, 0.4, 0.2	2.95	2.59	2.31	0.36	0.28	$R = +0.8$ Converging
3	1.2, 0.6, 0.3	2.95	2.81	2.45	0.14	0.36	$R = +2.6$ Diverging

Note that in real cases (with results from three grids, say), the true behavior of y with Δx is unknown, so the only information one has is the three computed values of y . If the true but unknown behavior is oscillatory, then depending on the choices of initial grid size and the grid refinement ratio those three values can produce any value of R (including a value indicating asymptotic convergence). Also note that whether the Δx in one's finest grid corresponds to a value of 1, 2, 3, or 100 on a scale such as that shown in Fig. 1 is unknown.

Conclusion

Although the example presented is somewhat contrived, the dilemma one faces in interpreting results of grid convergence studies is not. If there is the possibility of oscillatory behavior of the value of a computed variable as grid size is refined in a simulation, then interpretation of the results of grid convergence studies seems impossible to achieve unambiguously.

Acknowledgment

The authors gratefully acknowledge the sponsorship of this research by the Office of Naval Research under Grants N00014-97-1-0014 and N00014-97-1-0151 under the administration of Dr. E. P. Rood.

References

- [1] Roache, P. J., 1998, *Verification and Validation in Computational Science and Engineering*, Hermosa Publishers, Albuquerque, NM.
- [2] Stern, F., Wilson, R. V., Coleman, H. W., and Paterson, E. G., 1999, "Verification and Validation of CFD Simulations," Iowa Institute of Hydraulic Research, The University of Iowa, IIHR Report No. 407.

Prediction of Fully Developed Pressure Drops in Regular Polygonal Ducts

SuiFei Nan

Professor, Department of Chemical Engineering, Zhejiang University, HangZhou, 310027, P. R. China

Introduction

Many researchers have investigated the Fanning factors in circular ducts and proposed many correlating equations to calculate the Fanning factors. As to various noncircular ducts, the frictional pressure drops have rarely been investigated. So it has been common practice in the field of fluid mechanics to use the hydraulic or equivalent diameter in the Reynolds number in predicting turbulent pressure drops along duct lengths having noncircular cross section.

But, there is usually large deviation from the circular tube line by using the hydraulic diameter in the Reynolds number. And, therefore, some researchers have proposed various modifying methods to predict friction factors. In the case of rectangular ducts, for example, Jones [1] uses a "laminar equivalent diameter" to form the Reynolds number, which is in turn used in any circular tube correlation for friction factors. And in case of annuli, Brighton and Jones [2] modify the constant C in the Blasius equation on the basis of the experimental data. As to triangular ducts, Nan and Dou [3] use an area equivalent round diameter in the Reynolds number.

Contributed by the Fluids Engineering Division of THE AMERICAN SOCIETY OF MECHANICAL ENGINEERS. Manuscript received by the Fluids Engineering Division September 14, 2000; revised manuscript received February 9, 2001. Associate Editor: D. R. Williams.

In the case of regular polygonal ducts, there were no experimental data reported in the literature except equilateral-triangular [4] and square [5] ducts. Therefore, the purpose of the investigation reported here was to obtain friction factors for isothermal, fully developed, laminar, and turbulent flow in smooth equilateral-triangular, square, pentagonal, hexagonal, heptagonal, and octagonal ducts, respectively. Moreover, an area equivalent round diameter is proposed to use in Reynolds number in predicting Fanning factor of turbulent flow in a duct having regular (n -sided) polygonal cross section.

Apparatus

The regular polygonal ducts were made of plate glass. Take a hexagonal duct for example. First cut six slabs of plate glass (width 8.10 mm, thickness 3.0 mm). Then precisely work pattern plates of the hexagonal polygon. Put the slabs of glass into the pattern plates. Finally seal the seams between the adjacent slabs with silica gel, as shown in Fig. 1. The ducts made of plate glass, therefore, are hydraulically smooth.

The sketch of the experimental procedure used to obtain pressure drop data is illustrated in Fig. 2 and Fig. 3. In the setup used, water was pumped from the water pool into the elevated tank that had an overflow pipe to maintain a fixed water level, then flowed through a duct and past an abrupt entrance and into the hydrodynamic entrance section where it became fully developed. It then entered the test section that consisted of four identical test sections in series. These multiple section served to check on the reproducibility of the measurements and to insure that the flow was fully developed. In the test section, the pressure drop readings were

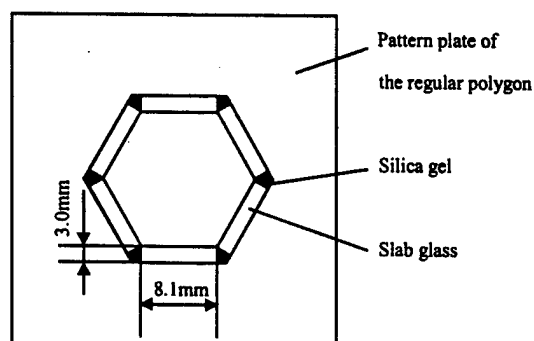


Fig. 1 Structure of the hexagonal polygonal duct

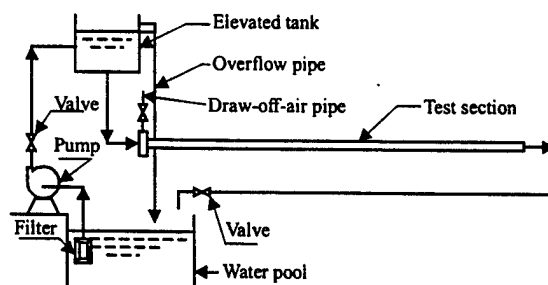


Fig. 2 Sketch of the experimental procedure

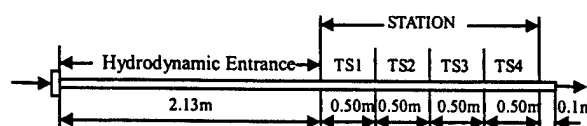


Fig. 3 Sketch of the positions of the pressure holes distributed over the test sections (TS)

Appendix D

Stern, F., Wilson, R. V., Coleman, H. W., and Paterson, E. G.,
"Comprehensive Approach to Verification and Validation of CFD
Simulations – Part 1: Methodology and Procedures," *J. Fluids
Engineering*, Vol. 123, No. 4, December 2001.

Fred Stern
Professor Mechanical Engineering and
Research Engineer
Fellow ASME

Robert V. Wilson
Assistant Research Engineer
Mem. ASME

Iowa Institute Hydraulic Research,
The University of Iowa,
Iowa City, IA 52242

Hugh W. Coleman
Eminent Scholar in Propulsion,
Professor of Mechanical Engineering,
Propulsion Research Center,
Mechanical and Aerospace Engineering
Department,
University of Alabama in Huntsville,
Huntsville, AL 35899
Fellow ASME

Eric G. Paterson
Associate Research Engineer,
Iowa Institute Hydraulic Research,
The University of Iowa,
Iowa City, IA 52242
Mem. ASME

Comprehensive Approach to Verification and Validation of CFD Simulations—Part 1: Methodology and Procedures

Part 1 of this two-part paper presents a comprehensive approach to verification and validation methodology and procedures for CFD simulations from an already developed CFD code applied without requiring availability of the source code for specified objectives, geometry, conditions, and available benchmark information. Concepts, definitions, and equations derived for simulation errors and uncertainties provide the overall mathematical framework. Verification is defined as a process for assessing simulation numerical uncertainty and, when conditions permit, estimating the sign and magnitude of the numerical error itself and the uncertainty in that error estimate. The approach for estimating errors and uncertainties includes (1) the option of treating the numerical error as deterministic or stochastic, (2) the use of generalized Richardson extrapolation for J input parameters, and (3) the concept of correction factors based on analytical benchmarks, which provides a quantitative metric to determine proximity of the solutions to the asymptotic range, accounts for the effects of higher-order terms, and are used for defining and estimating errors and uncertainties. Validation is defined as a process for assessing simulation modeling uncertainty by using benchmark experimental data and, when conditions permit, estimating the sign and magnitude of the modeling error itself. The approach properly takes into account the uncertainties in both the simulation and experimental data in assessing the level of validation. Interpretation of results of validation efforts both where the numerical error is treated as deterministic and stochastic are discussed. Part 2 provides an example for RANS simulations for a cargo/container ship where issues with regard to practical application of the methodology and procedures and interpretation of verification and validation results are discussed.

[DOI: 10.1115/1.1412235]

1 Introduction

Discussion and methodology for estimating errors and uncertainties in computational fluid dynamics (CFD) simulations have reached a certain level of maturity with recognition of importance through editorial policies (Freitas [1]), increased attention and recent progress on common terminology (AIAA, [2]), advocacy and detailed methodology (Roache [3]), and numerous case studies (e.g. [4]). Progress has been accelerated in response to the urgent need for achieving consensus on concepts, definitions, and useful methodology and procedures, as CFD is applied to increasingly complex geometry and physics and integrated into the engineering design process. Such consensus is required to realize the goals of simulation-based design and other uses of CFD such as simulating flows for which experiments are difficult (e.g., full-scale Reynolds numbers, hypersonic flows, off-design conditions). In spite of the progress and urgency, the various viewpoints have not converged and current approaches fall short of providing practical methodology and procedures for estimating errors and uncertainties in CFD simulations.

The present work provides a pragmatic approach for estimating errors and uncertainties in CFD simulations. Previous work on verification (Stern et al. [5]) is extended and put on a more rigorous foundation and combined with subsequent work on validation (Coleman and Stern [6]) thereby providing a comprehensive framework for overall procedures and methodology. The philosophy

is strongly influenced by experimental fluid dynamics (EFD) uncertainty analysis (Coleman and Steele [7]), which has been standardized. Hopefully, CFD verification and validation procedures and methodology can reach a similar level of maturity and user variability can reach similar low levels, as for EFD. The work is part of a larger program (Rood [8]) for developing and implementing a strategy for verification and validation of Reynolds-averaged Navier-Stokes (RANS) ship hydrodynamics CFD codes. The program includes complementary CFD and EFD towing-tank investigations and considers errors and uncertainties in both the simulations and the data in assessing the success of the verification and validation efforts. The work also benefited from collaboration with the 21st and 22nd International Towing Tank Resistance Committees (ITTC [9,10]). The procedures proposed in this paper were adopted on an interim basis by the 22nd ITTC and also were recommended and used at the recent Gothenburg 2000 Workshop on CFD in Ship Hydrodynamics (Larsson et al. [11]).

The focus is on verification and validation methodology and procedures for CFD simulations with an already developed CFD code applied without requiring availability of the source code for specified objectives, geometry, conditions, and available benchmark information. The methodology and procedures were developed considering RANS CFD codes, but should be applicable to a fairly broad range of codes such as boundary-element methods and certain aspects of large-eddy and direct numerical simulations. The present work differs in many respects from recent literature. The presentation is relatively succinct with intention for use for practical applications (i.e., industrial CFD) for which numerical errors and uncertainties cannot be considered negligible or overlooked.

Contributed by the Fluids Engineering Division for publication in the JOURNAL OF FLUIDS ENGINEERING. Manuscript received by the Fluids Engineering Division November 4, 1999; revised manuscript received July 10, 2001. Associate Editor: P. E. Raad.

The definitions of errors and uncertainties and verification and validation that are used in any approach need to be clearly stated. The present and Roache [3] definitions for errors and uncertainties are consistent with those used for EFD. The AIAA [2] definitions are from an information theory perspective and differ from those used in EFD, but are not contradictory to the present definitions. The present concepts and definitions for verification and validation are closely tied to the present definitions of errors and uncertainties and equations derived for simulation errors and uncertainties thereby providing the overall mathematical framework. The Roache [3] and AIAA [2] definitions are broader, but not contradictory to the present definitions. The present approach includes both the situations (1) of estimating errors and the uncertainty of those estimates and (2) of estimating uncertainties only. Richardson extrapolation (RE) is used for verification, which is not new; however, the present generalizations for J input parameters and concept of correction factors based on analytical benchmarks, which provides a quantitative metric to determine proximity of the solutions to the asymptotic range, accounts for the effects of higher-order terms, and are used for defining and estimating errors and uncertainties constitute a new approach. The use of quantitative estimates for errors and the use of uncertainties for those estimates also constitute a new approach in verification and validation.

Part 1 of this two-part paper presents the verification and validation methodology and procedures. In Section 2, the overall verification and validation methodology is presented by providing concepts, definitions, and equations for the simulation numerical and modeling errors and uncertainties. In Section 3, detailed verification procedures for estimation of various sub-components of the simulation numerical error and uncertainty are given. In Section 4, validation procedures are given including a discussion of the interpretation of validation results and use of corrected simulation results. Finally, conclusions are provided in Section 5. Part 2 provides an example for RANS simulations for a cargo/container ship where issues with regard to practical application of the methodology and procedures and interpretation of verification and validation results are discussed (Wilson et al. [12]). Present papers are based on Stern et al. [13], which is sometimes referenced for additional details. However, presentation and expanded discussions of verification procedures and implementation were improved based on nearly two years experience with present approach, especially through ITTC community and Gothenburg 2000 Workshop on CFD in Ship Hydrodynamics.

2 Overall Verification and Validation Methodology

In Section 2.1, the overall verification and validation methodology is presented by providing key concepts, definitions, and derivation of equations for the simulation error and uncertainty, as sum and root-sum-square (RSS) of simulation numerical and modeling errors and uncertainties, respectively. The verification and validation equations are derived in Sections 2.2 and 2.3, respectively, where subcomponents of the simulation numerical error are identified and an approach for assessing the simulation modeling uncertainty is presented.

2.1 Concepts and Definitions. Accuracy indicates the closeness of agreement between a simulation/experimental value of a quantity and its true value. Error δ is the difference between a simulation value or an experimental value and the truth. Accuracy increases as error approaches zero. The true values of simulation/experimental quantities are rarely known. Thus, errors must be estimated. An uncertainty U is an estimate of an error such that the interval $\pm U$ contains the true value of δ 95 times out of 100. An uncertainty interval thus indicates the range of likely magnitudes of δ but no information about its sign.

For simulations, under certain conditions, errors can be estimated including both sign and magnitude (referred to as an error estimate δ^*). Then, the uncertainty considered is that correspond-

ing to the error in δ^* . When δ^* is estimated, it can be used to obtain a corrected value of the variable of interest.

Sources of errors and uncertainties in results from simulations can be divided into two distinct sources: modeling and numerical. Modeling errors and uncertainties are due to assumptions and approximations in the mathematical representation of the physical problem (such as geometry, mathematical equation, coordinate transformation, boundary conditions, turbulence models, etc.) and incorporation of previous data (such as fluid properties) into the model. Numerical errors and uncertainties are due to numerical solution of the mathematical equations (such as discretization, artificial dissipation, incomplete iterative and grid convergence, lack of conservation of mass, momentum, and energy, internal and external boundary noncontinuity, computer round-off, etc.). The present work assumes that all correlations among errors are zero, which is doubtless not true in all cases, but the effects are assumed negligible for the present analyses.

The simulation error δ_S is defined as the difference between a simulation result S and the truth T . In considering the development and execution of a CFD code, it can be postulated that δ_S is comprised of the addition of modeling and numerical errors

$$\delta_S = S - T = \delta_{SM} + \delta_{SN} \quad (1)$$

Support for this postulation is provided by using the model value M in definitions for modeling and numerical errors. The simulation modeling error $\delta_{SM} = M - T$ is defined as the difference between the true T and model M values while the simulation numerical error $\delta_{SN} = S - M$ is defined as the difference between the simulation S and model M values. The simulation S and model M values are obtained by numerical and exact solutions of the continuous equations used to model the truth, respectively. Since exact solution of nonlinear equations is seldom possible, approximations are used to replace the continuous modeled equations with discrete ones that are solved algebraically with a CFD code to yield the simulation value S .

The uncertainty equation corresponding to error equation (1) is

$$U_S^2 = U_{SM}^2 + U_{SN}^2 \quad (2)$$

where U_S is the uncertainty in the simulation and U_{SM} and U_{SN} are the simulation modeling and numerical uncertainties.

For certain conditions, the numerical error δ_{SN} can be considered as

$$\delta_{SN} = \delta_{SN}^* + \epsilon_{SN} \quad (3)$$

where δ_{SN}^* is an estimate of the sign and magnitude of δ_{SN} and ϵ_{SN} is the error in that estimate (and is estimated as an uncertainty since only a range bounding its magnitude and not its sign can be estimated). The corrected simulation value S_C is defined by

$$S_C = S - \delta_{SN}^* \quad (4)$$

with error equation

$$\delta_{S_C} = S_C - T = \delta_{SM} + \epsilon_{SN} \quad (5)$$

The uncertainty equation corresponding to error equation (5) is

$$U_{S_C}^2 = U_{SM}^2 + U_{\epsilon_{SN}}^2 \quad (6)$$

where U_{S_C} is the uncertainty in the corrected simulation and $U_{\epsilon_{SN}}$ is the uncertainty estimate for ϵ_{SN} .

Debate on verification and validation has included discussion on whether errors such as δ_{SN} are deterministic or stochastic, and thus how they should be treated in uncertainty analysis was unclear. In the "corrected" approach given by Eqs. (3)–(6), a deterministic estimate δ_{SN}^* of δ_{SN} and consideration of the error ϵ_{SN} in that estimate are used. The approach is analogous to that in EFD when an asymmetric systematic uncertainty is "zero-centered" by inclusion of a model for the systematic error in the data reduction equation and then the uncertainty considered is that associated with the model (Coleman and Steele [7]). In the "uncorrected"

The overall CFD verification and validation procedures can be conveniently grouped in four consecutive steps. The first step is preparation, which involves selection of the CFD code and specification of objectives, geometry, conditions, and available benchmark information. The objectives might be prediction of certain variables at certain levels of validation (e.g., programmatic validation requirements U_{reqd}). The variables can either be integral (e.g., resistance) or point (e.g., mean velocities and turbulent Reynolds stresses) values and the programmatic validation requirements may be different for each variable. The second and third steps are verification and validation, which are described in Sections 2.2 and 2.3. The fourth step is documentation, which is detailed presentation of the CFD code (equations, initial and boundary conditions, modeling, and numerical methods), objectives, geometry, conditions, verification, validation, and analysis.

The errors due to specification of input parameters are decomposed into error contributions from iteration number δ_i , grid size δ_G , time step δ_T , and other parameters δ_p , which gives the following expressions for the simulation numerical error and uncertainty

$$\delta_{SN} = \delta_I + \delta_G + \delta_T + \delta_P = \delta_I + \sum_{j=1}^J \delta_j \quad (7)$$

$$U_{SN}^2 = U_I^2 + U_G^2 + U_T^2 + U_P^2 = U_I^2 + \sum_{j=1}^J U_j^2 \quad (8)$$

$$\delta_{SN}^* = \delta_i^* + \sum_{j=1}^J \delta_j^* \quad (9)$$
$$S_C = S - \left(\delta_I^* + \sum_{j=1}^J \delta_j^* \right) = T + \delta_{SM} + \varepsilon_{SN} \quad (10)$$

$$U_{S_C N}^2 = U_{I_C}^2 + \sum_{j=1}^J U_{j_C}^2 \quad (11)$$

$$S = S_C + \left(\delta_I^* + \sum_{j=1}^J \delta_j^* \right) \quad (12)$$

mark since it is equal, as shown by Eq. (10), to the truth plus simulation modeling error and presumable small error ε_{SN} in the estimate of the numerical error δ_{SN}^* .

The validation methodology of Coleman and Stern [6] which properly takes into account the uncertainties in both the simulation and the experimental data is discussed in this section for both approaches of treating the numerical error as stochastic and as deterministic.

$$D - \delta_D = S - \delta_S \quad (13)$$
$$E = D - S = \delta_D - \delta_S = \delta_D - (\delta_{SMA} + \delta_{SPD} + \delta_{SN}) \quad (14)$$

If (X_i, r_i) , and S share no common error sources, then the uncertainty U_F in the comparison error can be expressed as

$$U_E^2 = \left(\frac{\partial E}{\partial D} \right)^2 U_D^2 + \left(\frac{\partial E}{\partial S} \right)^2 U_S^2 = U_D^2 + U_S^2 \quad (15)$$

or

$$U_F^2 = U_D^2 + U_{SMA}^2 + U_{SPD}^2 + U_{SN}^2 \quad (16)$$

DECEMBER 2001, Vol. 123 / 795

validation test as the practical alternative. If the validation uncertainty U_V is defined as the combination of all uncertainties that we know how to estimate (i.e., all but U_{SMA}), then

$$U_V^2 = U_E^2 - U_{SMA}^2 = U_D^2 + U_{STE}^2 \quad (17)$$

where $U_{STE}^2 = U_{SPD}^2 + U_{SN}^2$ is the total estimated simulation uncertainty, as shown in Fig. 1.

If $|E|$ is less than the validation uncertainty U_V , the combination of all the errors in D and S is smaller than the estimated validation uncertainty and validation has been achieved at the U_V level. U_V is the key metric in the validation process. U_V is the validation "noise level" imposed by the uncertainties inherent in the data, the numerical solution, and the previous experimental data used in the simulation model. It can be argued that one cannot discriminate once $|E|$ is less than this; that is, as long as $|E|$ is less than this, one cannot evaluate the effectiveness of proposed model "improvements." On the other hand, if $|E| \gg U_V$ one could argue that probably $E \approx \delta_{SMA}$.

Oberkamp and Trucano [14] have criticized Coleman and Stern [6] for fact that U_V excludes U_{SMA} . As already acknowledged, there is no known way for directly estimating U_{SMA} . However, the present approach does provide a more stringent validation metric U_V which sets the level that validation can be achieved as the root sum square of the experimental U_D and the total estimated simulation U_{STE} uncertainties. Additionally, under certain conditions, the simulation modeling error δ_{SMA} itself can be estimated, as further discussed in Section 4. Consideration of Eq. (17) shows that (1) the more uncertain the data (greater U_D) and/or (2) the more inaccurate the code (greater U_{STE}), the easier it is to validate a code, since the greater the uncertainties in the data and code predictions, the greater the noise level U_V . Both Roache [3] and Oberkamp and Trucano [14] have criticized Coleman and Stern [6] for this fact. However, if the value of U_V is greater than that designated as necessary in a research/design/development program, the required level of validation could not be achieved without improvement in the quality of the data, the code, or both. Also, if U_{SN} and U_{SPD} are not estimated, but $|E|$ is less than U_D , then a type of validation can be argued to have been achieved, but clearly as shown by the present methodology, at an unknown level.

If the "corrected" approach of Eqs. (3)–(6) is used, then the equations, equivalent to Eqs. (14) and (17) are

$$E_C = D - S_C = \delta_D - (\delta_{SMA} + \delta_{SPD} + \delta_{SN}) \quad (18)$$

for the corrected comparison error and

$$U_{V_C}^2 = U_{E_C}^2 - U_{SMA}^2 = U_D^2 = U_D^2 + U_{S_CTE}^2 \quad (19)$$

for the corrected validation uncertainty where $U_{S_CTE}^2 = U_{SPD}^2 + U_{S_CN}^2$ is the total estimated corrected simulation uncertainty, also shown in Fig. 1. Note that S_C and E_C can be either larger or smaller than their counterparts S and E , but U_{E_C} and U_{V_C} should be smaller than U_E and U_V , respectively, since U_{S_CN} should be smaller than U_{SN} .

If there is a programmatic validation requirement, there is another uncertainty U_{reqd} that must be considered since validation is required at that uncertainty level or below. Interpretation of the meaning of the relative magnitudes of E (or E_C), U_{reqd} and U_V (or U_{V_C}) and of the implications on the possibility of estimating δ_{SMA} are discussed in Section 4. Additional discussion is provided in Coleman and Stern [6] on: estimating U_{SPD} ; estimating U_D for the data point (X_i, r_i) , including both the experimental uncertainty in r_i and the additional uncertainties in r_i arising from the experimental uncertainties in the measurements of the n independent variables $(X_i)_i$ in X_i ; and for validation of a CFD code, multiple codes and/or models, and prediction of trends.

3 Verification Procedures

In Section 2, the simulation numerical error and uncertainty were decomposed into contributions from iteration number, grid size, time step, and other parameters in Eqs. (7) and (8). In this section, detailed verification procedures are given for estimation of these contributions through convergence studies (Section 3.1). Iterative (Section 3.2) and parameter (Sections 3.3–3.5) convergence studies are conducted using multiple solutions with systematic parameter refinement to estimate numerical errors and uncertainties. Three convergence conditions are possible: (i) monotonic convergence; (ii) oscillatory convergence; and (iii) divergence and are described in Sections 3.3, 3.4, and 3.5, respectively. For condition (i), as already mentioned, errors and uncertainties are estimated using generalized RE. For condition (ii), uncertainties are estimated simply by attempting to bound error based on oscillation maximums and minimums. For condition (iii), errors and uncertainties cannot be estimated. As discussed below and later in Section 5, there are many issues in estimating errors and uncertainties for practical applications.

3.1 Convergence Studies. Iterative and parameter convergence studies are conducted using multiple (m) solutions and systematic parameter refinement by varying the k th input parameter Δx_k while holding all other parameters constant. The present work assumes input parameters can be expressed such that the finest resolution corresponds to the limit of infinitely small parameter values. Many common input parameters are of this form, e.g., grid spacing, time step, and artificial dissipation. Additionally, a uniform parameter refinement ratio $r_k = \Delta x_{k_2} / \Delta x_{k_1} = \Delta x_{k_3} / \Delta x_{k_2} = \Delta x_{k_m} / \Delta x_{k_{m-1}}$ between solutions is assumed for presentation purposes, but not required as discussed later.

Careful consideration should be given to selection of uniform parameter refinement ratio. The most appropriate values for industrial CFD are not yet fully established. Small values (i.e., very close to one) are undesirable since solution changes will be small and sensitivity to input parameter may be difficult to identify compared to iterative errors. Large values alleviate this problem; however, they also may be undesirable since the finest step size may be prohibitively small (i.e., require many steps) if the coarsest step size is designed for sufficient resolution such that similar physics are resolved for all m solutions. Also, similarly as for small values, solution changes for the finest step size may be difficult to identify compared to iterative errors since iterative convergence is more difficult for small step size. Another issue is that for parameter refinement ratio other than $r_k = 2$, interpolation to a common location is required to compute solution changes, which introduces interpolation errors. Roache [3] discusses methods for evaluating interpolation errors. However, for industrial CFD, $r_k = 2$ may often be too large. A good alternative may be $r_k = \sqrt{2}$, as it provides fairly large parameter refinement ratio and at least enables prolongation of the coarse-parameter solution as an initial guess for the fine-parameter solution.

Equation (12) is written for the k th parameter and m th solution as

$$S_{k_m} = S_C + \delta_{i_{k_m}}^* + \delta_{k_m}^* + \sum_{j=1, j \neq k}^f \delta_{j_m}^* \quad (20)$$

Iterative convergence must be assessed and S_{k_m} corrected for iterative errors prior to evaluation of parameter convergence since the level of iterative convergence may not be the same for all m solutions used in the parameter convergence studies. Equation (20) shows that iterative errors $\delta_{i_{k_m}}^*$ must be accurately estimated or negligible in comparison to $\delta_{k_m}^*$ for accurate convergence studies and that they should be considered within the context of convergence studies for each input parameter. Methods for estimating U_i or $\delta_{i_{k_m}}^*$ and U_{i_C} are described in Section 3.2.2.

With $\delta_{i_{k_m}}^*$ evaluated, S_{k_m} is corrected for iterative errors as

$$\hat{S}_{k_m} = S_{k_m} - \delta_{k_m}^* = S_C + \delta_{k_m}^* + \sum_{j=1, j \neq k}^J \delta_{j_m}^* \quad (21)$$

\hat{S}_{k_m} can be calculated for both integral (e.g., resistance coefficients) and point (e.g., surface pressure, wall-shear stress, and velocity) variables. \hat{S}_{k_m} can be presented as an absolute quantity (i.e., non-normalized) or normalized with the solution as a percentage change; however, if the solution value is small, a more appropriate normalization may be the range of the solution.

Convergence studies require a minimum of $m=3$ solutions to evaluate convergence with respect to input parameter. Note that $m=2$ is inadequate, as it only indicates sensitivity and not convergence, and that $m>3$ may be required. Consider the situation for 3 solutions corresponding to fine \hat{S}_{k_1} , medium \hat{S}_{k_2} , and coarse \hat{S}_{k_3} values for the k th input parameter. Solution changes ε for medium-fine and coarse-medium solutions and their ratio R_k are defined by

$$\begin{aligned} \varepsilon_{k_{21}} &= \hat{S}_{k_2} - \hat{S}_{k_1} \\ \varepsilon_{k_{32}} &= \hat{S}_{k_3} - \hat{S}_{k_2} \\ R_k &= \varepsilon_{k_{21}} / \varepsilon_{k_{32}} \end{aligned} \quad (22)$$

Three convergence conditions are possible:

- (i) Monotonic convergence: $0 < R_k < 1$
- (ii) Oscillatory convergence: $R_k < 0^1$
- (iii) Divergence: $R_k > 1$

For monotonic convergence (i), generalized RE is used to estimate U_k or δ_k^* and U_{k_c} . Methods for estimating errors and uncertainties for condition (i) are described in Section 3.3.

For oscillatory convergence (ii), the solutions exhibit oscillations, which may be erroneously identified as condition (i) or (iii). This is apparent if one considers evaluating convergence condition from three points on a sinusoidal curve (Coleman et al. [15]). Depending on where the three points fall on the curve, the condition could be incorrectly diagnosed as either monotonic convergence or divergence. Methods discussed here for estimating uncertainties U_k for condition (ii) require more than $m=3$ solutions and are described in Section 3.4.

For divergence (iii), the solutions diverge and errors and uncertainties cannot be estimated. Additional remarks are given in Section 3.5.

Determination of the convergence ratio R_k for point variables can be problematic since solution changes $\varepsilon_{k_{21}}$ and $\varepsilon_{k_{32}}$ can both go to zero (e.g., in regions where the solution contains an inflection point). In this case, the ratio becomes ill conditioned. However, the convergence ratio can be used in regions where the solution changes are both non-zero (e.g., local solution maximums or minimums). Another approach is to use a global convergence ratio R_k , which overcomes ill conditioning, based on the L2 norm of the solution changes, i.e., $\langle R_k \rangle = \|\varepsilon_{k_{21}}\|_2 / \|\varepsilon_{k_{32}}\|_2$. $\langle \rangle$ is used to denote an averaged value and $\|\varepsilon\|_2 = [\sum_{i=1}^N \varepsilon_i^2]^{1/2}$ denotes the L2 norm of solution change over the N points in the region of interest. Caution should be exercised when defining the convergence ratio from the ratio of the L2 norm of solution changes because the oscillatory condition ($R_k < 1$) cannot be diagnosed since $\langle R_k \rangle$ will always be greater than zero. Local values of R_k at solution maximums or minimums should also be examined to confirm the convergence condition based on an L2 norm definition. An alternate approach suggested by Hoekstra et al. [16] is to transform the spatial profile to wave number space and to perform a conver-

gence study on the amplitude distribution of the Fourier modes. In principle, this approach would remove the problem of ill-conditioning of the convergence ratio, R_k .

3.2 Iterative Convergence. The number of order magnitude drop and final level of solution residual (or residual imbalance) can be used to determine stopping criteria for iterative solution techniques. Iterative convergence to machine zero is desirable, but for complex geometry and conditions it is often not possible. Three or four orders of magnitude drop in solution residual to a level of 10^{-4} is more likely for these cases. Methods for estimation of iterative errors and uncertainties can be based on graphical, as discussed below, or theoretical approaches and are dependent on the type of iterative convergence: (a) oscillatory; (b) convergent; or (c) mixed oscillatory/convergent.

For oscillatory iterative convergence (a), the deviation of the variable from its mean value provides estimates of the iterative uncertainty based on the range of the maximum S_U and minimum S_L values

$$U_I = \left| \frac{1}{2} (S_U - S_L) \right| \quad (24)$$

For convergent iterative convergence (b), a curve-fit of an exponential function can be used to estimate U_I or δ_I^* and U_{I_c} as the difference between the value and the exponential function from a curve fit for large iteration number CF_∞

$$\begin{aligned} U_I &= |S - CF_\infty| \\ \delta_{I_m}^* &= S - CF_\infty, U_{I_c} = 0 \end{aligned} \quad (25)$$

For mixed convergent/oscillatory iterative convergence (c), the amplitude of the solution envelope decreases as the iteration number increases, the solution envelope is used to define the maximum S_U and minimum S_L values in the I th iteration, and to estimate U_I or δ_I^* and U_{I_c}

$$\begin{aligned} U_I &= \left| \frac{1}{2} (S_U - S_L) \right| \\ \delta_{I_m}^* &= S - \frac{1}{2} (S_U - S_L), U_{I_c} = 0 \end{aligned} \quad (26)$$

An increase in the amplitude of the solution envelope as the iteration number increases indicates that the solution is divergent.

Estimates of the iterative error based on theoretical approaches are presented in Ferziger and Peric [17] and involve estimation of the principal eigenvalue of the iteration matrix. The approach is relatively straightforward when the eigenvalue is real and the solution is convergent. For cases in which the principal eigenvalue is complex and the solution is oscillatory or mixed, the estimation is not as straightforward and additional assumptions are required.

3.3 Monotonic Convergence: Generalized Richardson Extrapolation. For monotonic convergence, i.e., condition (i) in Eq. (23), generalized RE is used to estimate U_k or δ_k^* and U_{k_c} . RE is generalized for J input parameters and concept of correction factors based on analytical benchmarks is introduced. More detailed derivations are provided by Stern et al. [13].

As already mentioned, since Stern et al. [13] there has been nearly two years experience with present approach, especially through ITTC community and Gothenburg 2000 Workshop on CFD in Ship Hydrodynamics. In particular, detailed verification procedures have been the focus of attention (Eca and Hoekstra [18]; Ebert and Gorski [19]). After some background for generalized RE is given, two approaches for estimating errors and uncertainties are presented and are based on (i) correction factors proposed in the current paper and (ii) factor of safety approach proposed by Roache (1998). Finally, a discussion of fundamental and practical issues for verification is provided.

¹As discussed in the text that follows, $0 < R_k < 1$ and $R_k > 1$ may also occur for the oscillatory condition.

Background for Generalized RE. Generalized RE begins with Eq. (21). The error terms on the right-hand side of Eq. (21) are of known form (i.e., power series expansion with integer powers of Δx_k) based on analysis of the modified and numerical error equations which is written below as a finite sum (i.e., error estimate) and for the k th parameter and m th solution

$$\delta_{k_m}^* = \sum_{i=1}^n (\Delta x_{k_m})^{p_k^{(i)}} g_k^{(i)} \quad (27)$$

n = number of terms retained in the power series, powers $p_k^{(i)}$ correspond to order of accuracy (for the i th term), and $g_k^{(i)}$ are referred to as "grid" functions which are a function of various orders and combinations of derivatives of S with respect to x_k . It is assumed that the power series in Eq. (27) is convergent (i.e., the finite sum convergence to the infinite series value as more terms are included). Substituting Eq. (27) into Eq. (21) results in

$$\hat{S}_{k_m} = S_C + \sum_{i=1}^n (\Delta x_{k_m})^{p_k^{(i)}} g_k^{(i)} + \sum_{j=1, j \neq k}^J \delta_{j_m}^* \quad (28)$$

Subtraction of multiple solutions where input parameter Δx_k is uniformly refined eliminates the $\delta_{j_m}^*$ terms in Eq. (28) since $\delta_{j_m}^*$ is independent of Δx_k and provides equations for S_C , $p_k^{(i)}$, and $g_k^{(i)}$. This assumes $p_k^{(i)}$ and $g_k^{(i)}$ are also independent of Δx_k . Since each term (i) contains 2 unknowns, $m = 2n + 1$ solutions are required to estimate the numerical benchmark S_C and the first n terms in the expansion in Eq. (28) (i.e., for $n = 1$, $m = 3$ and for $n = 2$, $m = 5$, etc). The accuracy of the estimates depends on how many terms are retained in Eq. (27), the magnitude (importance) of the higher-order terms, and the validity of the assumption that $p_k^{(i)}$ and $g_k^{(i)}$ are independent of Δx_k . For sufficiently small Δx_k , the solutions are in the asymptotic range such that higher-order terms are negligible and the assumption that $p_k^{(i)}$ and $g_k^{(i)}$ are independent of Δx_k is valid. However, achieving the asymptotic range for practical geometry and conditions is usually not possible and $m > 3$ is undesirable from a resources point of view; therefore, methods are needed to account for effects of higher-order terms for practical application of RE. Additionally, methods may be needed to account for possible dependence of $p_k^{(i)}$ and $g_k^{(i)}$ on Δx_k , although not addressed herein. Usually δ_k^* is estimated for the finest value of the input parameter, i.e., $\delta_k^* = \delta_{k_1}^*$ corresponding to the finest solution S_{k_1} .

With three solutions ($m = 3$), only the leading-order term of Eq. (27) can be estimated. Solution of the three equations for S_C , $p_k^{(i)}$, and $g_k^{(i)}$ yields estimates for the error $\delta_{k_1}^*$ and order-of-accuracy p_k

$$\delta_{k_1}^* = \delta_{RE_{k_1}}^* = \frac{\varepsilon_{k_{21}}}{r_{k_1}^{p_k - 1}} \quad (29)$$

$$p_k = \frac{\ln(\varepsilon_{k_{32}}/\varepsilon_{k_{21}})}{\ln(r_{k_1})} \quad (30)$$

Solving for the first-order term is relatively easy since evaluation of Eqs. (29) and (30) only requires that the $m = 3$ solutions are monotonically convergent, even if the solutions are far from the asymptotic range and Eqs. (29) and (30) are inaccurate. With solutions from five systematically refined input parameters ($m = 5$), more complicated expressions can be derived to estimate the first two terms of the power series expansion. However, their range of applicability is more restrictive since all five solutions must be both monotonically convergent and sufficiently close to the asymptotic range for the expressions to be used.

As previously mentioned, solutions from three values of input parameter where the refinement ratio between the medium and fine input parameters $r_{k_{21}}$ is not equal to that between coarse and

medium input parameters $r_{k_{32}}$ can be used to estimate $\delta_{k_1}^*$ from Eq. (29), provided that Eq. (30) for estimating order of accuracy is modified as

$$p_k = \frac{\ln(\varepsilon_{k_{32}}/\varepsilon_{k_{21}})}{\ln(r_{k_{21}})} + \frac{1}{\ln(r_{k_{21}})} [\ln(r_{k_{32}}^{p_k} - 1) - \ln(r_{k_{21}}^{p_k} - 1)] \quad (31)$$

For situations when $r_{k_{21}} \neq r_{k_{32}}$, Eq. (31) is a transcendental equation implicitly defining p_k and must be solved iteratively. If $r_{k_{21}} = r_{k_{32}}$, Eq. (31) degenerates to Eq. (30).

Estimating Errors and Uncertainties Using Generalized RE With Correction Factors. Results from the numerical solution of the one-dimensional (1D) wave and two-dimensional (2D) Laplace equation analytical benchmarks show that Eq. (29) has the correct form, but the order of accuracy is poorly estimated by Eq. (30) except in the asymptotic range. Analysis of the results suggests the concept of correction factors, which provide a quantitative metric to determine proximity of the solutions to the asymptotic range, account for the effects of higher-order terms, and are used for defining and estimating errors and uncertainties. Details are provided in Appendix A.

Multiplication of Eq. (29) by a correction factor C_k provides an estimate for $\delta_{k_1}^*$ accounting for the effects of higher-order terms

$$\delta_{k_1}^* = C_k \delta_{RE_{k_1}}^* = C_k \left(\frac{\varepsilon_{k_{21}}}{r_{k_1}^{p_k - 1}} \right) \quad (32)$$

If solutions are in the asymptotic range, correction of Eq. (29) is not required [i.e., $C_k = 1$ so that Eqs. (29) and (32) are equivalent]. For solutions outside the asymptotic range, $C_k < 1$ or $C_k > 1$ indicates that the leading-order term over predicts (higher-order terms net negative) or under predicts (higher-order terms net positive) the error, respectively. The estimate given by Eq. (32) includes both sign and magnitude and is used to estimate U_k or δ_k^* and U_{k_c} depending on how close the solutions are to the asymptotic range (i.e., how close C_k is to 1) and one's confidence in Eq. (32). There are many reasons for lack of confidence, especially for complex three-dimensional flows.

For C_k sufficiently less than or greater than 1 and lacking confidence, U_k is estimated, but not δ_k^* and U_{k_c} . Equation (32) is used to estimate the uncertainty by bounding the error δ_k^* by the sum of the absolute value of the corrected estimate from RE and the absolute value of the amount of the correction

$$U_k = |C_k \delta_{RE_{k_1}}^*| + |(1 - C_k) \delta_{RE_{k_1}}^*| \quad (33)$$

For C_k sufficiently close to 1 and having confidence, δ_k^* and U_{k_c} are estimated. Equation (32) is used to estimate the error δ_k^* , which can then also be used in the calculation of S_C [in Eq. (10)]. The uncertainty in the error estimate is based on the amount of the correction

$$U_{k_c} = |(1 - C_k) \delta_{RE_{k_1}}^*| \quad (34)$$

Note that in the limit of the asymptotic range, $C_k = 1$, $\delta_k^* = \delta_{k_1}^*$, $= \delta_{RE_{k_1}}^*$, and $U_{k_c} = 0$.

Two definitions for the correction factor were developed. The first is based on solution of Eq. (32) for C_k with $\delta_{RE_{k_1}}^*$ based on Eq. (29) but replacing p_k with the improved estimate $p_{k_{est}}$

$$C_k = \frac{r_{k_1}^{p_k - 1}}{r_{k_1}^{p_{k_{est}} - 1}} \quad (35)$$

Similarly, the second is based on a two-term estimate of the power series which is used to estimate $\delta_{RE_k}^*$ where p_k and q_k are replaced with $p_{k_{est}}$ and $q_{k_{est}}$

$$C_k = \frac{(\varepsilon_{k_{23}}/\varepsilon_{k_{12}} - r_k^{q_{k_{est}}})(r_k^{p_k} - 1)}{(r_k^{p_{k_{est}}} - r_k^{q_{k_{est}}})(r_k^{p_{k_{est}}} - 1)} + \frac{(\varepsilon_{k_{23}}/\varepsilon_{k_{12}} - r_k^{p_{k_{est}}})(r_k^{q_k} - 1)}{(r_k^{p_{k_{est}}} - r_k^{q_{k_{est}}})(r_k^{q_{k_{est}}} - 1)} \quad (36)$$

$p_{k_{est}}$ and $q_{k_{est}}$ are estimates for limiting orders of accuracy of the first and second terms of the error expansion equation (27) as spacing size goes to zero and the asymptotic range is reached. Equation (35) roughly accounts for the effects of higher-order terms by replacing p_k with $p_{k_{est}}$ thereby providing an improved single-term estimate. Equation (36) more rigorously accounts for higher-order terms since it is derived from the two-term estimate with first and second term order of accuracy $p_k^{(1)}$ and $p_k^{(2)}$ replaced by $p_{k_{est}}$ and $q_{k_{est}}$. Equation (36) simplifies to Eq. (35) in the limit of the asymptotic range. Both correction factors only require solutions for three parameter values. The estimated values $p_{k_{est}}$ and $q_{k_{est}}$ can be based either on the assumed theoretical order of accuracy $p_{k_{th}}$ and $q_{k_{th}}$ or solutions for simplified geometry and conditions. In either case, preferably including the effects of grid stretching.

In Appendix A, exact (A) and numerical (S) solutions are used to compare the true simulation error (A-S) to (i) an uncorrected three-grid error estimate using Eq. (29) and (ii) corrected estimates based on Eq. (32) with correction factor defined by Eq. (35) or (36). Correction of error estimates with both definitions of C_k results in improved error estimates. Also, uncertainty estimates using Eq. (33) with correction factor defined by Eq. (35) or (36) are shown to bound the true simulation error (A-S), while uncertainty estimates using Eq. (34) are shown to bound the difference between the corrected solution and the truth (S_c-T). Additional testing of expressions for C_k given by Eqs. (35) and (36) is needed and development of improved expressions within the proposed general framework is certainly possible.

Estimating Uncertainties Using Generalized RE With Factors of Safety. In Roache [3], a GCI approach is proposed where a standard three-grid error estimate from RE is multiplied by a factor of safety F_S to bound the simulation error

$$U_k = F_S |\delta_{RE_k}^*| \quad (37)$$

Note that Eq. (37) with factor of safety differs significantly from Eq. (34). Herein $C_k = C_k(\varepsilon, r_k, p_k, p_{k_{est}}, q_{k_{est}})$, in contrast to Eq. (37) where C_k is a constant referred to as a factor of safety F_S . The exact value for factor of safety is somewhat ambiguous and Roache [3] recommends 1.25 for careful grid studies and 3 for cases in which only two grids are used.

Although not proposed in Roache [3], the factor of safety approach can be used for situations where the solution is corrected with an error estimate from RE. Equation (29) is used to estimate δ_k^* and the uncertainty in that error estimate is given by

$$U_{k_c} = (F_S - 1) |\delta_{RE_k}^*| \quad (38)$$

With this approach, a fixed percentage of a three-grid error estimate (e.g., 25% $\delta_{RE_k}^*$ for $F_S = 1.25$) is used to define the uncertainty of the error estimate regardless of how close solutions are to the asymptotic range.

Discussion of Fundamental and Practical Issues. Fundamental and practical issues for verification are discussed in this section. Fundamental issues include convergence of power series equation (27), assumptions that $p_k^{(i)}$ and $g_k^{(i)}$ are independent of Δx_k , and estimating $p_{k_{est}}$. Solution of analytical benchmarks has

been used to address some of these fundamental issues while others need further research. Although both correction factor and factor of safety approaches were presented, the authors advocate the use of former. Results from the numerical solution of analytic benchmarks show that the factor of safety approach is overly conservative, especially when the solutions approach the asymptotic range (Appendix A). This is in contrast to the variable correction factor approach proposed in Eqs. (33) and (34), where the uncertainty in the error estimate correctly goes to zero as the asymptotic range is approached because $C_k \rightarrow 1$. Admittedly, others have recommended the factor of safety approach, e.g., Eca and Hoekstra [18], although examination of their results as with our own analysis indicates that such estimates are overly conservative.

For practical applications, especially complex flows with relatively coarse grids, solutions may be far from asymptotic range such that some variables are convergent while others are oscillatory or even divergent. Order of accuracy and therefore correction factors and factors of safety may display large variability indicating the need for finer grids. Clearly, more than 3 grids are required to estimate errors and uncertainties for such cases. Eca and Hoekstra [18] suggest a least-squares approach to estimate the error by computing the three unknown parameters from RE when more than three solutions are available. The behavior of the asymptotic range was successfully demonstrated for simpler analytical benchmarks in Appendix A. However, the existence and behavior of the asymptotic range for practical problems has not been demonstrated due to lack of sufficiently refined grids, number of solutions to assess variability, and available resources, among other issues. Another practical issue involves selecting and maintaining appropriate parameter refinement ratio and resources for obtaining solutions with sufficient parameter refinement as well as number of solutions. Lastly, interpretation of results is an issue since, as already mentioned, there is limited experience and no known solutions for practical applications in the asymptotic range for guidance.

The present verification procedures represent the most rational approach presently known. However, alternative strategies for including effects of higher-order terms may be just as viable, e.g., treatment of the power series exponents as known integers as proposed by Oberkampf and investigated by Eca and Hoekstra [18]. Once available, improved verification procedures can be easily incorporated into the present overall verification and validation methodology. These issues are discussed further in Section 5 Conclusions and Recommendations and in Part 2 (Wilson et al. [12]).

3.4 Oscillatory Convergence. For oscillatory convergence, i.e., condition (ii) in Eq. (23), uncertainties can be estimated, but not the signs and magnitudes of the errors. Uncertainties are estimated based on determination of the upper (S_U) and lower (S_L) bounds of solution oscillation, which requires more than $m=3$ solutions. The estimate of uncertainty is based on half the solution range

$$U_k = \frac{1}{2} (S_U - S_L) \quad (39)$$

3.5 Divergence. For divergence, i.e., condition (iii) in Eq. (23), errors and or uncertainties can not be estimated. The preparation and verification steps must be reconsidered. Improvements in iterative convergence, parameter specification (e.g., grid quality), and/or CFD code may be required to achieve converging or oscillatory conditions.

4 Validation Procedures

In Section 2, an approach for assessing the simulation modeling uncertainty was presented where for successful validation, the comparison error, E is less than the validation uncertainty, U_v given by Eqs. (17) and (19) for uncorrected and corrected solutions, respectively. In this section, validation procedures are presented through discussions in Section 4.1 on interpretation of

validation results and in Section 4.2 on use of corrected simulation results. As previously mentioned, Coleman and Stern [6] provide additional discussion on validation procedures.

4.1 Interpretation of the Results of a Validation Effort.

First, consider the approach in which the simulation numerical error is taken to be stochastic and thus the uncertainty U_{SN} is estimated. From a general perspective, if we consider the three variables U_V , $|E|$, and U_{reqd} there are six combinations (assuming none of the three variables are equal):

1. $|E| < U_V < U_{reqd}$
2. $|E| < U_{reqd} < U_V$
3. $U_{reqd} < |E| < U_V$
4. $U_V < |E| < U_{reqd}$
5. $U_V < U_{reqd} < |E|$
6. $U_{reqd} < U_V < |E|$

(40)

In cases 1, 2, and 3, $|E| < U_V$; validation is achieved at the U_V level; and the comparison error is below the noise level, so attempting to estimate δ_{SMA} is not feasible from an uncertainty standpoint. In case 1, validation has been achieved at a level below U_{reqd} , so validation is successful from a programmatic standpoint.

In cases 4, 5, and 6, $U_V < |E|$, so the comparison error is above the noise level and using the sign and magnitude of E to estimate δ_{SMA} is feasible from an uncertainty standpoint. If $U_V \ll |E|$, then E corresponds to δ_{SMA} and the error from the modeling assumptions can be determined unambiguously. In case 4, validation is successful at the $|E|$ level from a programmatic standpoint.

Now consider the approach in which the simulation numerical error is taken to be deterministic and thus δ_{SN}^* and the uncertainty U_{VC} are estimated. A similar set of comparisons as those in Eq. (40) can be constructed using $|E_C|$, U_{VC} , and U_{reqd} . Since E_C can be larger or smaller than E , but U_{VC} should always be less than U_V , the results for a given corrected case are not necessarily analogous to those for the corresponding uncorrected case. That is, a variable can be validated in the corrected but not in the uncorrected case, or vice versa. For cases 4, 5, and 6 in which $U_{VC} < |E_C|$, one can argue that E_C is a better indicator of δ_{SMA} than is E , assuming that one's confidence in using the estimate δ_{SN}^* is not misplaced.

4.2. Use of Corrected Versus Uncorrected Simulation Results. As previously stated in Section 3.3, the requirements for correcting the solution are that the correction factor be close to one and that confidence in solutions exist. Since the variability of the order of accuracy cannot be determined from solutions on three grids, confidence is difficult to establish in this case. As a result, caution should be exercised when correcting solutions using information from only three grids.

If a validation using the corrected approach is successful at a set condition, then if one chooses to associate that validation uncertainty level with the simulation's prediction at a neighboring condition that prediction must also be corrected. That means enough runs are required at the new condition to allow estimation of the numerical errors and uncertainties. If this is not done, then the comparison error E and validation uncertainty U_V corresponding to the use of the uncorrected S and its associated (larger) U_{SN} should be the ones considered in the validation with which one wants to associate the prediction at a new condition. (Whether to and how to associate an uncertainty level at a validated condition with a prediction at a neighboring condition is very much unresolved and is justifiably the subject of much debate at this time.)

5 Conclusions

The present comprehensive approach to verification and validation methodology and procedures sets forth concepts, definitions, and equations derived for simulation errors and uncertainties, which provide a well-founded mathematical framework. The approach should have applicability to a fairly broad range of CFD codes, including RANS, Navier-Stokes, Euler, boundary-element methods, and others. However, clearly much more work is needed for other CFD codes (such as large-eddy simulations), additional error sources, and alternative error and uncertainty estimation methods, e.g., single-grid methods and both results for additional analytical benchmarks (especially for nonlinear equations and using stretched grids) for improved definitions of correction factors and estimates of orders of accuracy, and alternative strategies to account for the effects of higher-order terms in RE. Improved verification procedures once available can be easily incorporated into the present overall verification and validation methodology. Furthermore, more experience is needed through application for different codes and geometry and conditions, especially for practical applications.

As mentioned in the Introduction, present verification and validation methodology and procedures were recommended and used at the recent Gothenburg 2000 Workshop on CFD in Ship Hydrodynamics (Larsson et al. [11]). 22 participating research groups from 12 countries and 19 different RANS codes were used for simulations of 3 test cases representing tanker, container, and surface combatant hull forms. Most groups implemented the recommended procedures, but lack of familiarity with the procedures and use of coarse grids led to difficulties. Coarser grid solutions are far from the asymptotic range and show variability such that not all variables display monotonic convergence and oscillatory convergence and even divergence is evident. For monotonic convergence, variability in the estimated order of accuracy was observed for some cases. The current 1 million point grids are clearly insufficient for more complex hull forms such as the tanker and an order of magnitude increase in points may be required to remove variability and achieve monotonic convergence for most variables. In spite of difficulties, the effort was beneficial in enabling quantitative evaluation of levels of verification and validation, increasing familiarity with verification and validation procedures, interpretation of results, and identification of grid requirements for decreasing levels of errors and uncertainties. Careful examination of verification results even for relatively coarse grid solutions provides a road map towards achieving acceptable levels of verification.

Verification and validation methodology and procedures should be helpful in guiding future developments in CFD through documentation, verification, and validation studies and in transition of CFD codes to design through establishment of credibility. Presumably, with a sufficient number of documented, verified, and validated solutions along with selected verification studies, a CFD code can be accredited for a certain range of applications. The contribution of the present work is in providing methodology and procedures for the former, which hopefully will help lead to the latter.

Part 2 provides an example for RANS simulations for a cargo/container ship where issues with regard to practical application of the methodology and procedures and interpretation of verification and validation results are discussed (Wilson et al. [12]).

Acknowledgments

This research was sponsored by the Office of Naval Research under Grants N00014-96-1-0018, N00014-97-1-0014, and N00014-97-1-0151 under the administration of Dr. E. P. Rood. The authors gratefully acknowledge Dr. Rood and other colleagues, especially Prof. W. G. Steele and Dr. H. Raven, who made significant contributions through insightful discussions and comments on early drafts. The recent Masters and Ph.D. theses of

Dr. B. Chen, Mr. G. Dolphin and Dr. S. H. Rhee, all at The University of Iowa, Department of Mechanical Engineering, were helpful both in the development and testing of the present verification and validation methodology and procedures.

Nomenclature

- C_k = correction factor
 D = benchmark data
 E, E_C = comparison error, corrected
 p_k = order of accuracy
 R_k = parameter refinement ratio
 S, S_C = simulation result, corrected
 T = truth
 U = uncertainty estimate
 U_D = data uncertainty
 U_E, U_{EC} = comparison error uncertainty, corrected
 U_I = iteration uncertainty
 U_P, U_{PC} = parameter uncertainty (e.g., grid size G and time step T), corrected
 U_{reqd} = programmatic validation requirement
 U_S, U_{SC} = simulation uncertainty, corrected
 U_{SM} = simulation modeling uncertainty
 U_{SMA} = simulation modeling assumption uncertainty
 U_{SPD} = simulation uncertainty due to use of previous data
 U_{STE}, U_{SCTE} = simulation total estimated numerical uncertainty
 U_{SN}, U_{SCN} = simulation numerical uncertainty, corrected
 U_V, U_{VC} = validation uncertainty, corrected
 Δx_k = increment in k th input parameter (e.g., grid size G and time step T)
 δ = error
 δ^* = error estimate with sign and magnitude
 δ_I, δ_I^* = iteration error, estimate
 δ_P, δ_P^* = parameter error, estimate
 δ_S, δ_{SC} = simulation error, corrected
 δ_{SN} = simulation numerical error
 δ_{SMA} = simulation modeling assumption error
 ε = solution change
 ε_{SN} = error in δ^*

Appendix A. Analytical Benchmarks

The use of analytical benchmarks for development of the concept of correction factors as discussed in Section 3.3 is presented in this Appendix. For analytical benchmarks, the modeling error is zero such that the simulation error is solely due to numerical error. Results are obtained for two analytical benchmarks one-dimensional (1D) wave and two-dimensional (2D) Laplace equations. The results for the 2D Laplace equation were qualitatively similar to those for the 1D wave equation, which are presented. Exact solutions from analytical benchmarks are used to determine the exact simulation numerical error which is compared to estimates from RE, including use of correction factors. More details are provided in Stern et al. [13], including single grid error estimates.

Verification of Analytical Benchmarks. For verification using an analytical benchmark, the simulation error and uncertainty are given by $\delta_S = S - A = \delta_{SN}$ and $U_S^2 = U_{SN}^2$, while the corrected simulation error and uncertainty are given by $\delta_{SC} = S_C - A = \varepsilon_{SN}$ and $U_{SC}^2 = U_{SCN}^2$. Simulations are verified if $|E| = |A - S| < U_{SN}$ and corrected simulations are verified if $|E_C| = |A - S_C| < U_{SCN}$.

The first-order, linear 1D wave equation models the behavior of a more complicated (nonlinear) partial differential equation. The initial condition is prescribed by a Gaussian function centered at $x = 0.0$. Two discretization techniques were studied: (i) first-order (Euler) explicit method with first-order upwind spatial discretiza-

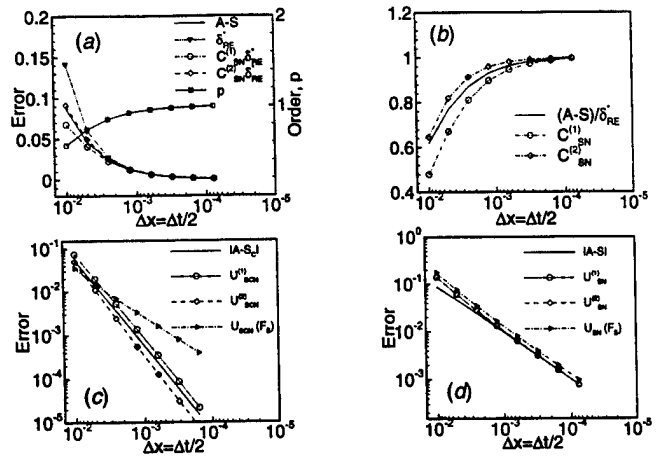


Fig. 2 Verification results for first-order numerical solution of 1D wave equation. (a) Comparison of true error $A-S$ to estimates from RE, (b) comparison of $|A-S|$ and U_{SCN} , and (d) comparison of $|A-S|$ and U_{SN} .

tion; and (ii) a second-order implicit method with second-order central spatial discretization. Since trends from both schemes are similar, only the results from the first-order scheme are presented.

A combined grid size and time step study was performed where ten solutions were obtained by successively doubling both the grid and time step such that $\Delta t/\Delta x = 0.5$ for all solutions. With this approach, solutions changes are used to estimate total (temporal and spatial) simulation errors and uncertainties. Accordingly, the generic subscript ' k ' appearing in expressions for errors and uncertainties in Section 3.3 is replaced with ' SN ' in this section where appropriate.

Errors, Uncertainties, and Correction Factors. The concept of a multiplication correction factor was introduced in Section 3.3. The correction factor C_k was used to define the numerical uncertainty in Eq. (33) or when conditions permit to improve error estimates in Eq. (32) and to define the uncertainty in that error estimate in Eq. (34). Error and uncertainty estimates given by Eqs. (32)–(34) are tested by numerical solution of analytical benchmarks as well as development of expressions for correction factor.

Figure 2(a) compares the true simulation error E to the three-grid error estimate $\delta_{RE_k}^*$ from Eq. (29) versus step size at one spatial location ($x = 1$ since maximums of numerical error occur there). The three-grid estimate accurately estimates the true error E for smaller step sizes, but over predicts E for larger step sizes. Closer examination reveals that Eq. (29) over estimates the error because Eq. (30) under estimates the order of accuracy, as also shown in Fig. 2(a).

Two definitions for C_k were investigated. The first is based on solving equation (32) for C_k with $\delta_{RE_k}^*$ defined in Eq. (29) but replacing p_k with the improved estimate $p_{k_{est}}$, which is provided by Eq. (35) where $p_{k_{est}}$ is an estimate of the limiting order of accuracy of the first term of the error expansion equation (27). Similarly, the second definition of correction factor is based on estimating $\delta_{RE_k}^*$ using the first two terms of the powers series and replacing p_k and q_k with improved estimates $p_{k_{est}}$ and $q_{k_{est}}$, which is provided by Eq. (36) where $p_{k_{est}}$ and $q_{k_{est}}$ are estimates for limiting orders of accuracy of the first and second terms of the error expansion equation (27) as spacing size goes to zero and the asymptotic range is reached. With this definition, correction factors approach one in the limit of zero spacing size. The estimated values $p_{k_{est}}$ and $q_{k_{est}}$ can be based either on the assumed theoret-

ical order of accuracy $p_{k,h}$ and $q_{k,h}$ or solutions for simplified geometry and conditions. In either case, preferably including the effects of grid stretching.

Figure 2(a) also compares the true error E to (i) an uncorrected three-grid error estimate using Eq. (29) and (ii) corrected estimates based on Eq. (32) with correction factor defined by Eq. (35) or (36). Both estimates are closer to E than the uncorrected three grid estimate $\delta_{RE_1}^*$, but for coarser grids $C_k^{(1)}$ is somewhat too small and $C_k^{(2)}$ is slightly too large. Figure 2(b) shows the same trends, but directly compares the exact correction factor E/δ_{RE}^* to Eqs. (35) and (36). In this case, $C_k < 1$ indicates that the leading-order term over predicts (higher-order terms net negative) the error. However, for the general case, C_k is equally likely to be < 1 or > 1 depending whether the order of accuracy is approached from below or above, respectively. $C_k > 1$ indicates that the leading-order term under predicts (higher-order terms net positive) the error. Thus, for the general case the correction to the leading-term error estimate is equally likely to be positive or negative and can be used to define the simulation numerical uncertainty.

For C_k sufficiently close to 1 and having confidence, δ_k^* and U_{k_c} are estimated. Correction factors $C_k^{(1)}$ and $C_k^{(2)}$ are used to estimate the error δ_k^* in Eq. (32) which can then also be used in the calculation of S_C [in Eq. (10)] and uncertainty U_{k_c} in Eq. (34). Figure 2(c) shows a comparison of $|A - S_C|$ and three uncertainty estimates: (i) $U_{S_{CN}}^{(1)}$ defined using $C_k^{(1)}$; (ii) $U_{S_{CN}}^{(2)}$ defined using $C_k^{(2)}$; and (iii) $U_{S_{CN}}$ from a factor of safety approach given by Eq. (38) with $F_S = 1.25$. The results show that the uncertainty estimate $U_{S_{CN}}^{(1)}$ successfully bounds $|A - S_C|$ over the entire range of step sizes and that $U_{S_{CN}}^{(2)}$ is not conservative enough since $U_{S_{CN}}^{(2)} < |A - S_C|$. The uncertainty estimate based on the factor of safety approach is not conservative enough for the coarsest two grids and is overly conservative by an order of magnitude for the four finest grids (i.e., when solutions are in the asymptotic range). For C_k sufficiently less than or greater than 1 and lacking confidence, U_k is estimated, but not δ_k^* and U_{k_c} . Correction factors $C_k^{(1)}$ and $C_k^{(2)}$ are used to estimate the uncertainty in Eq. (33) which is compared to factor of safety approach given by Eq. (37). Figure 2(d) shows that all three uncertainty estimates successfully bound the true error $|A - S|$ although the factor of safety approach is overly conservative for all grids.

Uncertainty estimates enable a quantitative measure of verification for analytical benchmarks. Figure 2(c, d) indicates that the present solutions are verified over the chosen range of grid size and time step. As expected, the largest levels of uncertainty are for the coarsest grid size and time step where levels are $(U_k, U_{k_c}) = (15\%, 7.5\%)$.

Eca and Hoekstra [18] also perform verification for the 2D

Laplace equation analytical benchmark. Their results are consistent with our own in showing that uncertainty estimates using Eq. (33) always bounded the true error. Unlike our own results, their results indicate that the uncertainty estimate from Eq. (34) failed to bound the difference in the truth and numerical benchmark for some grid triplets when the apparent order of accuracy was estimated to be larger than the theoretical value.

References

- [1] Freitas, C. J., 1993, "Editorial Policy Statement on the Control of Numerical Accuracy," *ASME J. Fluids Eng.*, **115**, pp. 339–340.
- [2] AIAA, 1998, *Guide for the Verification and Validation of Computational Fluid Dynamics Simulations*, G-077-1998.
- [3] Roache, P. J., 1998, *Verification and Validation in Computational Science and Engineering*, Hermosa Publishers, Albuquerque, New Mexico.
- [4] Mehta, U. B., 1998, "Credible Computational Fluids Dynamics Simulations," *AIAA J.*, **36**, pp. 665–667.
- [5] Stern, F., Paterson, E. G., and Tahara, Y., 1996, "CFDShip-IOWA: Computational Fluid Dynamics Method for Surface-Ship Boundary Layers and Wakes and Wave Fields," Iowa Institute of Hydraulic Research, The University of Iowa, IHR Report No. 381.
- [6] Coleman, H. W., and Stern, F., 1997, "Uncertainties in CFD Code Validation," *ASME J. Fluids Eng.*, **119**, pp. 795–803. (Also see "Authors' Closure," *ASME J. Fluids Eng.*, Vol. 120, Sept. 1998, pp. 635–636.)
- [7] Coleman, H. W., and Steele, W. G., 1999, *Experimentation and Uncertainty Analysis for Engineers*, 2nd Edition, Wiley, New York, NY.
- [8] Rood, E. P., 1996, "Validation Strategy for RANS Computational Ship Hydrodynamics," 2nd International Conference on Hydrodynamics, Hong Kong.
- [9] ITTC, 1996, 21st ITTC Proceedings, "Report of the Resistance Committee," Bergen/Trondheim, Norway, September.
- [10] ITTC, 1999, 22nd ITTC Proceedings, "Report of the Resistance Committee," Seoul, Korea/Shanghai, China, Sept.
- [11] Larsson, L., Stern, F., Bertram, V., 2000, "Gothenburg 2000 A Workshop on Numerical Ship Hydrodynamics," Chalmers University of Technology, Gothenburg, Sweden, Sept.
- [12] Wilson, R. V., Stern, F., Coleman, H., and Paterson, E., 2001, "Comprehensive Approach to Verification and Validation of CFD Simulations—Part 2: Applications for RANS Simulation of A Cargo Container Ship," *ASME J. Fluids Eng.*, **123**, published in the issue, pp. 803–810.
- [13] Stern, F., Wilson, R. V., Coleman, H., and Paterson, E., 1999, "Verification and Validation of CFD Simulations," Iowa Institute of Hydraulic Research, The University of Iowa, IHR Report No. 407.
- [14] Oberkampf, W. L., and Trucano, T. G., 2000, "Validation Methodology in Computational Fluid Dynamics," *AIAA Fluids 2000*, Paper No. 2549, Denver, CO.
- [15] Coleman, H. W., Stern, F., Mascio, A. Di, and Campana, E., 2001, "The Problem with Oscillatory Behavior in Grid Convergence Studies," *ASME J. Fluids Eng.*, **123**, No. 2, pp. 438–439.
- [16] Hoekstra, M., Eca, L., Windt, J., and Raven, H., 2000, "Viscous Flow Calculations for KVLCC2 AND KCS Models Using the PARNASSOS Code," Proceedings Gothenburg 2000 A Workshop on Numerical Ship Hydrodynamics, Gothenburg, Sweden.
- [17] Ferziger, J. H., and Peric, M., 1996, *Computational Methods for Fluid Dynamics*, Springer-Verlag, New York.
- [18] Eca, L., and Hoekstra, M., 2000, "On the Application of Verification Procedures in Computational Fluid Dynamics," 2nd MARNET Workshop.
- [19] Ebert, M. P., and Gorski, J. J., 2001, "A Verification and Validation Procedure for Computational Fluid Dynamics Solutions," NSWCCD-50-TR-2001/0006, Hydromechanics Directorate Report, NSWCCD, Carderock Division, West Bethesda MD 20817-5700.

Appendix E

Wilson, R. V., Stern, F., Coleman, H. W., and Paterson, E. G.,
"Comprehensive Approach to Verification and Validation of CFD
Simulations – Part 2: Application for RANS Simulation of a
Cargo/Container Ship," *J. Fluids Engineering*, Vol. 123, No. 4, December
2001.

Robert V. Wilson
Assistant Research Engineer,
Mem. ASME

Fred Stern
Professor Mechanical Engineering and
Research Engineer,
Fellow ASME

Iowa Institute Hydraulic Research,
Department Mechanical Engineering,
The University of Iowa,
Iowa City, IA 52242

Hugh W. Coleman
Eminent Scholar in Propulsion,
Professor of Mechanical Engineering,
Propulsion Research Center,
Mechanical and Aerospace Engineering
Department,
University of Alabama in Huntsville,
Huntsville, AL 35899
Fellow ASME

Eric G. Paterson
Associate Research Engineer,
Iowa Institute Hydraulic Research,
The University of Iowa,
Iowa City, IA 52242
Mem. ASME

Comprehensive Approach to Verification and Validation of CFD Simulations—Part 2: Application for Rans Simulation of a Cargo/Container Ship

Part 2 of this two-part paper provides an example case study following the recently developed comprehensive verification and validation approach presented in Part 1. The case study is for a RANS simulation of an established benchmark for ship hydrodynamics using a ship hydrodynamics CFD code. Verification of the resistance (integral variable) and wave profile (point variable) indicates iterative uncertainties much less than grid uncertainties and simulation numerical uncertainties of about 2% S_1 (S_1 is the simulation value for the finest grid). Validation of the resistance and wave profile shows modeling errors of about 8%D (D is the measured resistance) and 6% ζ_{\max} (ζ_{\max} is the maximum wave elevation), which should be addressed for possible validation at the 3%D and 4% ζ_{\max} levels. Reducing the level of validation primarily requires reduction in experimental uncertainties. The reduction of both modeling errors and experimental uncertainties will produce verified and validated solutions at low levels for this application using the present CFD code. Although there are many issues for practical applications, the methodology and procedures are shown to be successful for assessing levels of verification and validation and identifying modeling errors in some cases. For practical applications, solutions are far from the asymptotic range; therefore, analysis and interpretation of the results are shown to be important in assessing variability for order of accuracy, levels of verification, and strategies for reducing numerical and modeling errors and uncertainties. [DOI: 10.1115/1.1412236]

1 Introduction

Computational fluid dynamics (CFD) is fast becoming an integral tool in the engineering design process as it is applied to increasing complex geometry and physics. As with the use of experimental fluid dynamics (EFD) in making design decisions, assessment of quality of results is imperative, which has accelerated progress on development of verification and validation (V&V) methodology and procedures for estimating numerical and modeling errors and uncertainties in CFD simulations. However, in spite of the progress, the various viewpoints have not yet fully converged and current methodology and procedures are not yet standardized. Case studies are important for evaluating various current V&V approaches and achieving standardization. Mehta [1] provides several case studies following different approaches for a variety of applications. In some cases, large differences in approaches, use of different test cases, and incomplete documentation makes evaluation difficult.

Part 2 of the present two-part paper provides an example case study following the recently developed comprehensive V&V approach presented in Part 1 (Stern et al. [2]). The case study is for a RANS simulation of an established benchmark for ship hydrodynamics using a current ship hydrodynamics CFD code. However, the V&V approach is equally applicable to CFD simulations for other applications in fluids engineering such as aerospace, environmental, and automotive and also should be applicable to a fairly broad range of codes such as boundary element methods and certain aspects of large-eddy and direct numerical simula-

tions. The present papers are based on Stern et al. [3], but with improved presentation and discussion based on nearly two years experience with the present V&V approach, especially through the International Towing Tank Conference (ITTC) community and Gothenburg 2000 Workshop on CFD in Ship Hydrodynamics (Larsson et al.).

The specific objectives of the present work are: (i) to provide a documented solution following the methodology and procedures in Part 1; (ii) to address practical issues in V&V of CFD simulations for complex geometries (e.g., generation of systematic grids); and (iii) to provide analysis and discussion of V&V results for a practical application where interpretation is complicated due to variability in the order of accuracy. Verification and validation methodology and procedures are summarized in Section 2 followed by a description of the CFD code in Section 3. Next, geometry, conditions, and benchmark data are specified in Section 4 with issues related to grid studies for practical applications given in Section 5. V&V results for the total resistance and wave profile are presented in Sections 6 and 7, respectively. Finally, conclusions are given in Section 8.

2 Verification and Validation Methodology and Procedures

The V&V methodology and procedures set forth in Part 1 provide a pragmatic approach for estimating simulation errors and uncertainties. The philosophy is strongly influenced by EFD uncertainty analysis. The present approach allows for treatment of simulation errors as either stochastic or deterministic and properly takes into account uncertainties in both the simulation and the data in assessing the level of validation.

Contributed by the Fluids Engineering Division for publication in the JOURNAL OF FLUIDS ENGINEERING. Manuscript received by the Fluids Engineering Division November 4, 1999; revised manuscript received July 10, 2001. Associate Editor: P. E. Raad.

Methodology. The simulation error δ_S is defined as the difference between a simulation result S and the truth T and is composed of modeling δ_{SM} and numerical δ_{SN} errors ($\delta_S = S - T = \delta_{SM} + \delta_{SN}$) with the corresponding simulation uncertainty given by $U_S^2 = U_{SM}^2 + U_{SN}^2$. For certain conditions, both the sign and magnitude of the numerical error can be estimated as $\delta_{SN} = \delta_{SN}^* + \varepsilon_{SN}$ where δ_{SN}^* is an estimate of the sign and magnitude of δ_{SN} and ε_{SN} is the error in that estimate. The simulation value is corrected to provide a numerical benchmark S_C , which is defined by

$$S_C = S - \delta_{SN}^* \quad (1)$$

with error equation $\delta_{S_C} = S_C - T = \delta_{SM} + \varepsilon_{SN}$ and corresponding uncertainty equation $U_{S_C}^2 = U_{SM}^2 + U_{S_CN}^2$ where U_{S_C} is the uncertainty in the corrected simulation and U_{S_CN} is the uncertainty estimate for ε_{SN} .

Verification is defined as a process for assessing simulation numerical uncertainty U_{SN} and, when conditions permit, estimating the sign and magnitude δ_{SN}^* of the simulation numerical error itself and the uncertainty in that error estimate U_{S_CN} . Numerical error is decomposed into contributions from iteration number δ_I , grid size δ_G , time step δ_T , and other parameters δ_P , which gives the following expression for the simulation numerical uncertainty

$$U_{SN}^2 = U_I^2 + U_G^2 + U_T^2 + U_P^2 \quad (2)$$

For situations when the solution is corrected to produce a numerical benchmark S_C , the estimated simulation numerical error δ_{SN}^* and corrected uncertainty U_{S_CN} are given by

$$\delta_{SN}^* = \delta_I^* + \delta_G^* + \delta_T^* + \delta_P^* \quad (3)$$

$$U_{S_CN}^2 = U_{I_C}^2 + U_{G_C}^2 + U_{T_C}^2 + U_{P_C}^2 \quad (4)$$

Validation is defined as a process for assessing simulation modeling uncertainty U_{SM} by using benchmark experimental data and, when conditions permit, estimating the sign and magnitude of the modeling error δ_{SM} itself. The comparison error E is given by the difference in the data D and simulation S values

$$E = D - S = \delta_D - (\delta_{SMA} + \delta_{SPD} + \delta_{SN}) \quad (5)$$

where δ_{SM} has been decomposed into the sum of δ_{SPD} , error from the use of previous data such as fluid properties, and δ_{SMA} , error from modeling assumptions. To determine if validation has been achieved, E is compared to the validation uncertainty U_V given by

$$U_V^2 = U_D^2 + U_{SN}^2 + U_{SPD}^2 \quad (6)$$

If $|E| < U_V$, the combination of all the errors in D and S is smaller than U_V and validation is achieved at the U_V level. If $U_V \leq |E|$, the sign and magnitude of $E = \delta_{SMA}$ can be used to make modeling improvements. For the corrected approach, the equations equivalent to Eqs. (5) and (6) are

$$E_C = D - S_C = \delta_D - (\delta_{SMA} + \delta_{SPD} + \varepsilon_{SN}) \quad (7)$$

$$U_{V_C}^2 = U_{E_C}^2 - U_{SMA}^2 = U_D^2 + U_{SPD}^2 + U_{S_CN}^2 \quad (8)$$

Procedures. The overall CFD V&V procedures can be conveniently grouped into four consecutive steps: preparation, verification, validation, and documentation.

Verification is accomplished through parameter convergence studies using multiple solutions (at least 3) with systematic parameter refinement by varying the k th input parameter Δx_k while holding all other parameters constant. Iterative errors must be accurately estimated or negligible in comparison to errors due to input parameters before accurate convergence studies can be con-

ducted. Changes between medium-fine $\varepsilon_{k_{21}} = \hat{S}_{k_2} - \hat{S}_{k_1}$ and coarse-medium $\varepsilon_{k_{32}} = \hat{S}_{k_3} - \hat{S}_{k_2}$ solutions are used to define the convergence ratio

$$R_k = \varepsilon_{k_{21}} / \varepsilon_{k_{32}} \quad (9)$$

and to determine convergence condition where \hat{S}_{k_1} , \hat{S}_{k_2} , \hat{S}_{k_3} correspond to solutions with fine, medium, and coarse input parameter, respectively, corrected for iterative errors. Three convergence conditions are possible:

(i) Monotonic convergence: $0 < R_k < 1$

(ii) Oscillatory convergence: $R_k < 0$ (10)

(iii) Divergence: $R_k < 1$

For condition (i), generalized RE is used to estimate U_k or δ_k^* and U_{k_C} . For condition (ii), uncertainties are estimated simply by attempting to bound the error based on oscillation maximums S_U and minimums S_L , i.e., $U_k = 1/2(S_U - S_L)$. For condition (iii), errors and uncertainties cannot be estimated.

For convergence condition (i), generalized RE is used to estimate the error $\delta_{RE_{k_1}}^*$ due to selection of the k th input parameter and order-of-accuracy p_k

$$\delta_{RE_{k_1}}^* = \frac{\varepsilon_{k_{21}}}{r_k^{p_k - 1}} \quad (11)$$

$$p_k = \frac{\ln(\varepsilon_{k_{32}} / \varepsilon_{k_{21}})}{\ln(r_k)} \quad (12)$$

Correction of Eq. (11) through a multiplication factor C_k accounts for effects of higher-order terms and provides a quantitative metric to determine proximity of the solutions to the asymptotic range

$$\delta_{k_1}^* = C_k \delta_{RE_{k_1}}^* = C_k \left(\frac{\varepsilon_{k_{21}}}{r_k^{p_k - 1}} \right) \quad (13)$$

where the correction factor is given by

$$C_k = \frac{r_k^{p_{k_{est}} - 1}}{r_k^{p_k - 1}} \quad (14)$$

and $p_{k_{est}}$ is an estimate for the limiting order of accuracy as spacing size goes to zero and the asymptotic range is reached so that $C_k \rightarrow 1$. When solutions are far from the asymptotic range, C_k is sufficiently less than or greater than 1 and only the magnitude of the error is estimated through the uncertainty U_k

$$U_k = |C_k \delta_{RE_{k_1}}^*| + |(1 - C_k) \delta_{RE_{k_1}}^*| \quad (15)$$

When solutions are close to the asymptotic range, C_k is close to 1 so that δ_k^* is estimated using Eq. (13) and U_{k_C} is estimated by

$$U_{k_C} = |(1 - C_k) \delta_{RE_{k_1}}^*| \quad (16)$$

Alternatively, a factor of safety approach proposed in Roache (1998) can be used to define U_k and U_{k_C} .

Validation is accomplished through comparison of simulations with benchmark EFD data, including experimental uncertainty estimates U_D . If the three variables U_V , $|E|$, and U_{reqd} (programmatic validation requirement) are considered, there are six combinations. For three cases, $|E| < U_V$ and validation is achieved at the U_V level, but for only one of these $U_V < U_{reqd}$ so that validation is also achieved at U_{reqd} . In these cases, attempting to estimate modeling errors δ_{SMA} is not feasible from an uncertainty standpoint. For the three other cases, $U_V < |E|$ and using the sign and magnitude of E to estimate δ_{SMA} is feasible from an uncertainty standpoint. In one of these cases, $U_V < |E| < U_{reqd}$ so that

validation is successful at the $|E|$ level from a programmatic standpoint. Similar conclusions can be reached using the corrected comparison error and corrected validation uncertainty.

3 RANS CFD Code

Solutions are obtained with CFDShip-IOWA, which is a general-purpose, multi-block, MPI-based high-performance, unsteady RANS CFD code (Paterson and Sinkovits, [4]; Paterson et al. [5]; Wilson et al. [6]) developed for computational ship hydrodynamics. The three-dimensional unsteady incompressible RANS equations are solved in either Cartesian or cylindrical-polar base coordinate systems. The grid dynamically conforms to the solution of the exact kinematic free-surface boundary condition. Approximate dynamic free-surface boundary conditions provide boundary conditions for velocity and pressure. For production simulations, Reynolds-stress closure is accomplished using the standard linear stress-strain relationship and a variety of eddy-viscosity models including algebraic Baldwin-Lomax and two-equation $k-\omega$ and $k-\epsilon$ models. The solution scheme is based upon the PISO algorithm and is fully implicit. The convective and viscous terms are discretized with second-order upwind and second-order central differences, respectively. Although the code can be run in either steady state or time-accurate mode, a time-marching procedure was used to obtain steady-state RANS solutions for simulations in this paper. The pressure equation is obtained by taking the divergence of the momentum equations. Further description can be found at <http://www.ihr.uiowa.edu/~cfdship> where related references may be found in electronic form.

4 Geometry, Conditions, and Benchmark Data

Steady-state simulations are performed for the Series 60 cargo/container ship. The Series 60 was used for two of the three test cases at an international workshop on validation of ship hydrodynamics CFD codes (CFD Workshop Tokyo [7]). The conditions for the calculations are Froude number $Fr=0.316$, Reynolds number $Re=4.3 \times 10^6$, and model orientation with zero sinkage and trim. These are the same conditions as the experiments, except the resistance and sinkage and trim tests, as explained next. The variables selected for verification and validation are resistance C_T (integral variable) and wave profile ζ (point variable).

The benchmark data is provided by Toda et al. [8], which was also the data used for the Series 60 test cases at the CFD Workshop Tokyo [7]. The data include resistance and sinkage and trim for a range of Fr for the model free condition (i.e., free to sink and trim). Also, wave profiles, near-field wave pattern, mean velocities, and pressures at numerous stations from the bow to the stern and near wake, all for $Fr=(0.16, 0.316)$ and the zero sinkage and trim model fixed condition. The data also include uncertainty estimates, which were recently confirmed/updated by Longo and Stern [9] closely following standard procedures (Coleman and Steele [10]).

The resistance is known to be larger for free versus fixed models. Data for the Series 60 indicates about an 8% increase in C_T for the free versus fixed condition over a range of Fr including $Fr=0.316$ (Ogiwara and Kajatani [11]). The Toda et al. [8] resistance values were calibrated (i.e., reduced by 8%) for effects of sinkage and trim for the present comparisons.

5 Grids Studies With Systematic Refinement

Errors and uncertainties due to grid size are estimated using multiple solutions (at least 3) on systematically refined grids with constant refinement ratio, $r_k = \Delta x_{k+1} / \Delta x_k = \Delta x_{k+2} / \Delta x_{k+1}$. Although grid doubling ($r_G=2$) is typically used for simplicity, resolving similar physics and meeting near-wall spacing requirements for turbulence modeling can be prohibitively difficult, especially in 3D simulations. A more reasonable refinement ratio of $r_G=\sqrt{2}$ was recommended in Part 1 and is used here. Using $r_G=\sqrt{2}$ has the added benefit that the coarse grid can be easily generated by removing every other fine grid point.

Table 1 Grid dimensions and y^+ values for grid refinement studies

Grid	Grid Dimensions	Total Number of points	y^+
1	287x78x43	876,211	0.7
2	201x51x31	317,781	1
3	144x36x22	114,048	1.4
4	101x26x16	42,016	2

Grid studies were conducted using four grids, which enables two separate three-grid studies to be performed and compared. Grid study 1 (GS1) gives estimates for grid errors and uncertainties on grid 1 using the three finest grids 1–3 while grid study 2 (GS2) gives estimates for grid errors and uncertainties on grid 2 using the three coarsest grids 2–4. Grid dimensions and average y^+ values (for grid points closest to no-slip surface) are given in Table 1 and a comparison of the four grids at the free surface plane is shown in Fig. 1 along with computed wave elevation contours.

With grid refinement ratio $r_G=\sqrt{2}$, only grids 1 and 2 were generated manually using the commercial code GRIDGEN (Pointwise, Inc.). Grids 3 and 4 were obtained by removing every other point from grids 1 and 2, respectively (i.e., the grid spacing of grids 3 and 4 is twice that of grids 1 and 2, respectively). In an effort to keep the exact shape of the leading and trailing edges of the hull surface on all four grids, the single-block grid system is divided into three subblocks. The $j=1$ surface of one of the subblocks is body-fitted and defines the entire no-slip surface of the

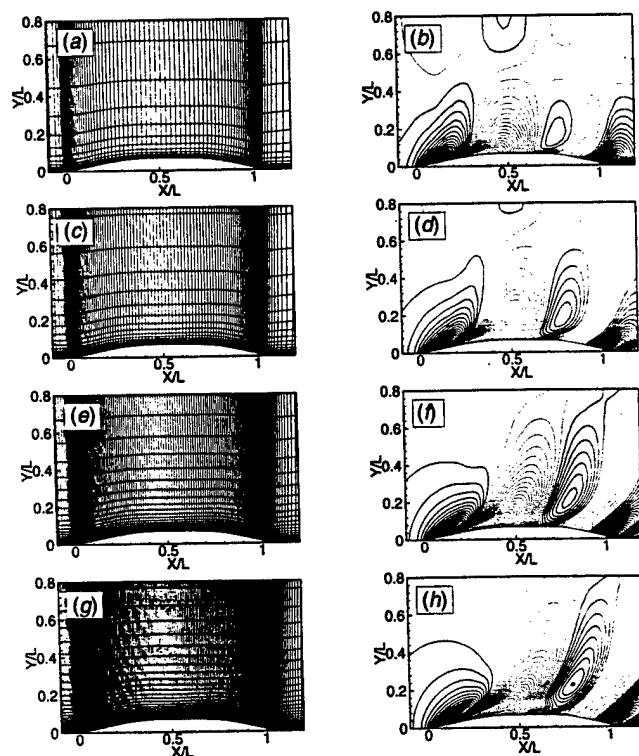


Fig. 1 Grids and computed wave contours on the free-surface plane from verification and validation studies for Series 60: (a) and (b) coarsest—grid 4; (c) and (d) grid 3; (e) and (f) grid 2; and (g) and (h) finest—grid 1. Ship leading and trailing edges at $X/L=0$ and 1, respectively.

ship from the leading to trailing edges. The $j=1$ surface of the other two subblocks, one upstream and one downstream of the ship hull, defines the symmetry plane using an H -type grid topology.

For grid 1 (i.e., finest grid), spacing along the edges of the computational block was controlled by specifying the grid distribution function (e.g., hyperbolic tanh or geometric series), grid spacing at the endpoint(s), and number of points. Grid clustering was used near the bow and stern in the ξ -direction, at the hull in the η -direction, and near the free surface in the ζ -direction. The faces of the subblocks were smoothed using an elliptic solver after which the coordinates in the interior were obtained using transfinite interpolation from the block faces. The three subblocks were then joined into a single block before simulations were performed.

Grid 2 was generated from grid 1 by using the same grid distribution function and by increasing the fine grid spacing Δx_{G_1} at the corners of the blocks and decreasing the number of fine grid computational cells (N_1-1) in each coordinate direction by a factor r_G

$$\Delta x_{G_2} = r_G \Delta x_{G_1} \quad (17)$$

$$N_2 = 1 + (N_1 - 1)/r_G \quad (18)$$

where Δx_{G_1} and Δx_{G_2} are the grid spacing and N_1 and N_2 are the number of points on grids 1 and 2, respectively. Finally, the faces of the blocks for grid 2 were then resmoothed using the elliptic solver and coordinates in the interior were obtained using transfinite interpolation (TFI).

For integer grid refinement ratio, this procedure results in a set of grids with systematic refinement (i.e., constant refinement ratio $r_G = \Delta x_{G_2}/\Delta x_{G_1} = \Delta x_{G_3}/\Delta x_{G_2} = \Delta x_{G_4}/\Delta x_{G_3}$). However, for non-integer refinement ratio r_G , Eq. (18) yields a noninteger grid number N_2 which obviously must be rounded to the nearest integer. This results in a difference in the actual r_{G_ACTUAL} and target r_{G_TARGET} refinement ratio. In other words,

$$r_{G_ACTUAL} = \frac{(N_1 - 1)}{\text{integer}[(N_1 - 1)/r_{G_TARGET}]} \neq r_{G_TARGET} \quad (19)$$

where the function "integer[]" is used to denote rounding of a real number to the nearest integer value.

The actual and target refinement ratios were compared by post-processing grids 1–3. Refinement ratio was computed at grid points along the intersection of the free- and no-slip surfaces which shows an average refinement ratio of $r_G = 1.39$ between grids 1 and 2 and $r_G = 1.44$ between grids 2 and 3. These values vary by 2% from the desired target value of $r_{G_TARGET} = \sqrt{2} \sim 1.4142$. However, inclusion of the effects of nonuniform grid refinement ratio for such small differences indicates $<1\%$ S_G differences in the estimates for numerical uncertainties (where $S_G = S_{G_1}$ is the solution on the finest grid), warranting the assumption of uniform grid refinement ratio. Because the volume grid is obtained using TFI from the elliptically smoothed faces of the blocks, larger deviations from uniform grid refinement ratio are possible in the interior.

Subsequent work has developed post-processing tools to automate generation of multiple grids with noninteger grid refinement ratio and to ensure uniform grid refinement ratio between multiple grids (Wilson et al. [11]). With this new procedure, the finest grid is trivially post-processed using a sequence of three, 1D interpolations to yield a medium grid with noninteger grid refinement ratio. This is in contrast to the approach used in this paper as described above for generation of the medium grid, which could become prohibitively difficult and time-consuming for large, multi-block grid systems with complex geometry.

6 Verification and Validation of Integral Variable: Total Resistance C_T

Friction and pressure stresses in the axial direction are integrated over the surface area of the Series 60 and summed to yield the total resistance coefficient C_T . The integration is performed in post processing using a second-order accurate method based on the trapezoidal rule. Results are analyzed and compared for both situations in which simulation numerical uncertainty is taken to be stochastic and U_{SN} estimated and when taken to be deterministic and δ_{SN}^* and U_{SCN} are estimated for grid studies GS1 and GS2, as discussed in Section 5.

Verification. For verification of the uncorrected solution, U_{SN} is given by Eq. (2), while for the corrected solution, δ_{SN}^* and U_{SCN} are given by Eqs. (3) and (4), respectively. Since steady-state simulations are performed, only contributions due to iteration number and grid size are considered (e.g., Eq. (2) simplifies to $U_{SN}^2 = U_I^2 + U_G^2$). The limiting order of accuracy is estimated using the formal order of accuracy of the CFD code (i.e., $p_{k_{est}} = p_{k_{th}} = 2.0$), which is realized for solution of simplified equations with uniform grids. For solution of the RANS equations on non-orthogonal stretched grids, values based on the formal order may be overly optimistic or not certain.

Iterative convergence is assessed through evaluation of the C_T iteration history and L2 norm of solution changes summed over all grid points. Figure 2 shows a portion of the iterative history for grid 1. The portion shown represents a computation started from a previous solution and does not include the total iterative history. Solution change drops four orders of magnitude from an initial value of about 10^{-2} (not shown) to a final value of 10^{-6} . The variation in C_T is about $0.14\% S_1$ (where S_1 is the solution on the finest grid) over the last period of oscillation (i.e., $U_I = 0.07\% S_1$). Iterative uncertainty is estimated as half the range of the maximum and minimum values over the last two periods of oscillation (see Fig. 2(c)). Iterative histories for grids 2–4 show iterative uncertainties of about 0.02, 0.03, and $0.01\% S_1$, respectively. The level of iterative uncertainties U_I for grids 2–4 are at least two orders of magnitude less than the corresponding grid uncertainties U_G , whereas the iterative uncertainty for grid 1 is only one order of magnitude smaller than the grid error. For all four grids, the iteration errors and uncertainties are assumed to be negligible in comparison to the grid errors and uncertainties for all four solutions (i.e., $U_I \ll U_G$ such that $U_{SN} = U_G$). Since iterative errors are negligible, correction of solutions for iterative error is not required.

Grid convergence is assessed through multiple C_T solutions on four systematically refined grids with constant refinement ratio (see Section 5). The total resistance C_T values on all four grids are given in Table 2 along with computed solution changes ϵ and benchmark EFD data for comparison. The convergence ratio $R_G(9)$, order of accuracy $p_G(12)$, and correction factor $C_G(14)$ are shown in Table 3. Since $0 < R_k < 1$, both GS1 and GS2 display monotonic convergence as given by condition (i), Eq. (10). However, the variability is large, i.e., the order of accuracy for GS1 is much greater than for GS2 and both are greater than $p_{k_{est}} = p_{k_{th}} = 2.0$. As a result, C_G is greater for GS1 than GS2. Although the fact that the order of accuracy does not approach $p_{k_{th}}$ with grid refinement is unexpected, in reality the estimation of $p_{k_{est}}$ for practical applications is not certain, as discussed previously.

Separate verification of the pressure C_P and friction C_F components of $C_T (= C_P + C_F)$ helps explain the variability displayed by p_G for C_T between GS1 and GS2. Note that in model-ship testing following Fr scaling, $C_{T_Ship} = C_R + C_{F_ITTC}$ where the residual resistance $C_R (= C_{T_Model} - C_{F_ITTC})$ and $C_{F_ITTC}(Re)$ is given by the ITTC model-ship correlation line evaluated for model and full scale Re . Table 2 includes C_P and C_F values along with C_R and C_{F_ITTC} for qualitative comparison. C_F comprises

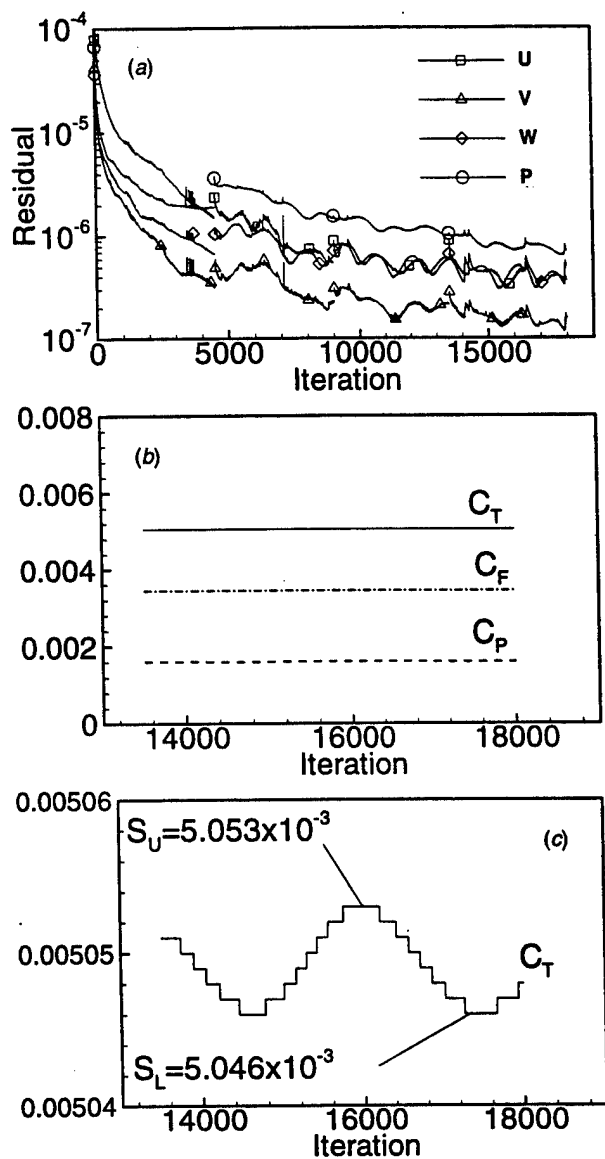


Fig. 2 Iteration history for Series 60 on grid 1: (a) solution change, (b) ship forces- C_F , C_P , and C_T and (c) magnified view of total resistance C_T over last two periods of oscillation

about 70% C_T and is convergent towards $C_{F_{ITTC}}$ (for GS1 within 1% $C_{F_{ITTC}}$). The C_P and C_F convergence ratio R_G , order of accuracy p_G , and correction factor C_G are shown in Table 4. For GS1, C_P is grid independent ($R_G = U_G = 0.0$) so that p_G cannot be estimated and C_F convergent but with $p_G > p_{k_{th}}$. For GS2, both C_P and C_F are convergent but with $p_G \gg p_{k_{th}}$ and $p_G > p_{k_{th}}$, respectively. For C_F , the trends with regard to variability are simi-

Table 2 Grid convergence study for total C_T , pressure C_P , and frictional C_F resistance ($\times 10^{-3}$) for Series 60

Grid	S_4 (grid 4)	S_3 (grid 3)	S_2 (grid 2)	S_1 (grid 1)	Data
C_T	6.02	5.39	5.11	5.05	5.42
ϵ		-10%	-5.2%	-1.2%	
C_F	1.88	1.61	1.60	1.60	$C_F = 2.00$
ϵ		-14%	-0.6%	0.0%	
C_P	4.14	3.69	3.51	3.45	3.42
ϵ		-11%	-4.9%	-1.7%	ITTC

% S_1

Table 3 Verification of $C_T (\times 10^{-3})$ for Series 60

Study	R_G	p_G	C_G
1 (grids 1-3)	0.21	4.4	3.7
2 (grids 2-4)	0.44	2.3	1.3

% S_1

lar as for C_T but with reduced magnitude. The fact that the C_P is grid independent so that p_G cannot be estimated using RE and C_F is monotonically convergent with $p_G > p_{k_{th}}$ partially explains the variability exhibited in C_T . Such complications should be expected for verification of integral variables comprised of multiple components, especially when components strongly depend on different physics.

Table 5 shows the estimated grid uncertainty $U_G(15)$, grid error $\delta_G^*(13)$, corrected grid uncertainty $U_{G_C}(16)$, and numerical benchmark $S_C(1)$. Uncertainty estimates based on the factor of safety approach are included for comparison. The grid uncertainty is less for GS1 than GS2 and the values (2% S_1 and 7% S_1 , respectively) are reasonable in consideration of the overall number of grid points used. The corrected grid uncertainty is also less for GS1 than GS2, but the difference is smaller than was the case for U_G ($\Delta U_{G_C} \approx 1\% S_1$). Similarly S_C , which according to RE should be grid independent, shows 3% difference when comparing GS1 and GS2. The factor of safety approach provides less conservative estimates, which is contrary to previous experience for analytical benchmarks.

Solutions on the next finer grid with $r_G = \sqrt{2}$ would require 2.4M grid points. U_G would likely be reduced to the current U_{G_C} levels, but with similar or greater levels for U_1 making it difficult to separate iterative and grid uncertainties. Therefore, from a resource point of view it may be sufficient to accept the current corrected solution S_C on the finest grid with associated corrected grid uncertainty U_{G_C} . This conclusion is supported by the overall verification results (i.e., four solutions decrease and converge monotonically with grid refinement and with positive $\delta_G^* > 0$) notwithstanding the variability exhibited in p_G which precludes complete confidence. Nonetheless, additional solutions are desirable for gaining experience and an understanding of the nature of the asymptotic range for practical applications and hopefully such solutions will show reduced variability.

Validation. The comparison error $E = D - S(5)$, validation uncertainty $U_V(6)$, experimental data uncertainty U_D , and simulation numerical uncertainty $U_{SN}(2)$ are shown in Table 6. Uncertainty due to the use of previous data U_{SPD} was not considered,

Table 4 Verification of C_P and $C_F (\times 10^{-3})$ for Series 60

Study	C_P			C_F		
	R_G	p_G	C_G	R_G	p_G	C_G
1 (grids 1-3)	0.00	-	-	0.33	3.2	2.0
2 (grids 2-4)	0.04	9.5	26	0.40	2.6	1.5

% S_1

Table 5 Errors and uncertainties for $C_T (\times 10^{-3})$ for Series 60

Grid	C_T uncorrected			C_T corrected		
	$U_G(C_G)$	$U_G(F_G)$	δ_G^*	$U_{G_C}(C_G)$	$U_{G_C}(F_G)$	S_C
1	2.1%	0.5%	1.2%	0.9%	0.1%	4.99
2	6.7%	5.6%	5.5%	1.1%	1.1%	4.83

% S_1

Table 6 Validation of uncorrected total resistance for Series 60

Grid	$E\%$	$U_v\%$	$U_D\%$	$U_{SN}\%$
1	6.8	3.1	2.5	1.9
2	5.7	6.7	2.5	6.3

%D.

so the validation uncertainty $U_V = \sqrt{U_{SN}^2 + U_D^2}$. Note that since iterative uncertainty was found to be negligible $U_{SN} = U_G$ and the data uncertainty was reported to be $U_D = 2.5\%D$.

For grid 1, $|E| > U_V$ such that C_T is not validated at the $|E| = 7\%D$ level; however, from an uncertainty standpoint, the sign and magnitude of E can be used to estimate δ_{SMA} and make modeling improvements. Further reduction of U_V requires reduction of U_{SN} and U_D since they are of similar magnitude. For grid 2, $|E| < U_V$ such that C_T is validated but at the larger validation uncertainty level of $U_V = 6.7\%D$ due to larger U_{SN} . Such large U_{SN} and therefore U_V precludes distinguishing δ_{SMA} from an uncertainty standpoint.

Table 7 is similar to Table 6, but for the corrected comparison error $E_C(7)$, validation uncertainty $U_{V_C}(8)$, and simulation numerical uncertainty $U_{S_{CN}}(4)$. In this case, $|E_C| > U_{V_C}$ for grids 1 and 2 such that neither is validated at the $U_V = 2.6$ and $2.7\%D$ levels, respectively. $U_{S_{CN}} \ll U_D$ shows that reduction of U_D by one order of magnitude is required to reduce U_{V_C} to the level of $U_{S_{CN}}$ and leads to the conclusion that the comparison error is largely due to modeling errors (i.e., $E_C \approx \delta_{SMA}$).

The overall conclusion for V&V of resistance is that C_T is not validated on the finest grid due to modeling errors of about $8\%D$. Likely modeling assumptions to consider are approximations of static sinkage and trim, free surface boundary conditions, and turbulence, which should be addressed for possible validation at about the $3\%D$ level. Reducing levels of validation uncertainty primarily requires reduction in experimental uncertainties; since, $U_D(=2.5\%D) > U_{G_C}(=1\%S_1)$.

7 Verification and Validation of a Point Variable: Wave Profile ζ

The wave profile is defined from the computed wave height at the intersection of the free- and no-slip hull surfaces from $0 \leq x/L \leq 1$. Wave elevation contours for the entire free-surface plane are shown in Figs. 1(b), (d), (f) and (h) while the wave profile on all four grids is shown in Fig. 3 including qualitative comparison with the benchmark EFD data. To facilitate the comparisons, the solutions from all four grids are interpolated onto the distribution for the data. Results are analyzed and compared for both situations in which simulation numerical uncertainty is taken to be stochastic and U_{SN} estimated and when taken to be deterministic and δ_{SN}^* and $U_{S_{CN}}$ are estimated for grid studies GS1 and GS2. Both point distributions and profile-averages of errors and uncertainties are discussed for verification and validation of the wave profile.

Verification. Evaluation of convergence ratio $R_G(9)$, order of accuracy $p_G(12)$, and correction factor $C_G(14)$, for point variables can be problematic when solution changes ε_{21_G} and ε_{32_G}

Table 7 Validation of corrected total resistance for Series 60

Grid	$E_C\%$	$U_{V_C}\%$	$U_D\%$	$U_{S_{CN}}\%$
1	7.9	2.6	2.5	0.8
2	11	2.7	2.5	1.0

%D.

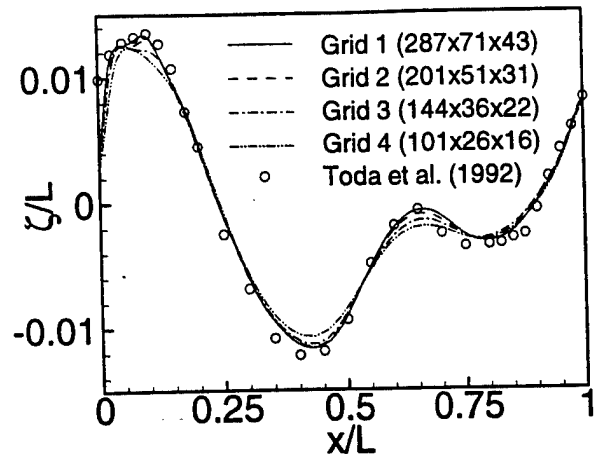


Fig. 3 Grid study for Series 60 wave profile

both go to zero so that their ratio is ill-defined. To overcome this problem, separate L2 norms of $\varepsilon_{G_{21}}$ and $\varepsilon_{G_{32}}$ are used to define ratios for R_G and p_G , i.e.,

$$\langle R_G \rangle = \|\varepsilon_{G_{21}}\|_2 / \|\varepsilon_{G_{32}}\|_2 \quad (20)$$

$$\langle p_G \rangle = \frac{\ln(\|\varepsilon_{G_{32}}\|_2 / \|\varepsilon_{G_{21}}\|_2)}{\ln(r_G)} \quad (21)$$

where $\langle \rangle$ and $\|\cdot\|_2$ are used to denote a profile-averaged quantity (with ratio of solution changes based on L2 norms) and L2 norm, respectively.

For verification of the uncorrected solution, Eq. (15) is used to estimate distributions of U_G at each point from the local solution change $\varepsilon_{G_{21}}$, where p_G is estimated from Eq. (21). Similarly, for the corrected solution, $\langle p_G \rangle$ is used to estimate δ_G^* and U_{G_C} at each point using Eqs. (13) and (16), respectively. An L2 norm of point distributions of errors and uncertainties are then used to assess verification levels and to judge if validation has been achieved globally. Iteration errors and uncertainties were found to be negligible in comparison to the grid errors and uncertainties for all four solutions, i.e., $U_I \ll U_G$ such that $U_{SN} = U_G$.

The profile-averaged convergence ratio $\langle R_G \rangle$, order of accuracy $\langle p_G \rangle$, correction factor $\langle C_G \rangle$, global grid uncertainty U_G , and corrected grid uncertainty U_{G_C} are shown in Table 8. Both GS1 and GS2 display monotonic convergence condition (i) from Eq. (10), but with $\langle p_G \rangle$ for GS1 greater than that for GS2 and both less than $p_{k_{th}}$, which in this case is consistent with expectations for solutions on stretched, curvilinear grids. The levels of U_G and U_{G_C} for GS1 are 1/2 those for GS2. Variability between GS1 and GS2 is absent and the trends are consistent with expectation. The distributions for U_G and U_{G_C} are discussed next in conjunction with validation.

Validation. Validation results with (U_V, U_{V_C}) and (E, E_C) based on L2 norms of point distributions are discussed first, followed by an examination of the actual point distributions. Profile-

Table 8 Profile-averaged verification results for wave profile for Series 60

Study	R_G	p_G	C_G	U_G	U_{G_C}
1 (grids 1-3)	0.64	1.3	0.56	2.0%	0.9%
2 (grids 2-4)	0.68	1.1	0.47	4.1%	2.2%

% ζ_{max} .

Table 9 Profile-averaged validation results for uncorrected wave profile for Series 60

Grid	$E\%$	$U_v\%$	$U_D\%$	$U_{SN}\%$
1	5.2	4.2	3.7	2.0
2	5.6	5.5	3.7	4.1

$\% \xi_{max}$

averaged validation results for the uncorrected and corrected wave profile are given in Tables 9 and 10, respectively. Values are normalized with the maximum value for the wave profile $\xi_{max} = 0.014$ and the uncertainty in the data is $3.7\% \xi_{max}$. For grid 1, $|E| > U_v$ such that the wave profile is not validated at the $|E| = 5.2\% \xi_{max}$ level; however the margin to achieve validation is small, i.e., $< 1\% \xi_{max}$. U_D is roughly twice U_{SN} . For grid 2, $E \sim U_v$ such that the solution is nearly validated at $|E| = 5.6\% \xi_{max}$ level. U_D and U_{SN} are of similar magnitude.

For grids 1 and 2, $|E| > U_{v_c}$ such that neither is validated at the $|E_c| = 5.6\%$ and $6.6\% \xi_{max}$ levels, respectively. Here again, the margin to achieve validation is fairly small (i.e., $< 2\%$ and $< 3\% \xi_{max}$ for grids 1 and 2, respectively). U_D is roughly twice and four times U_{G_c} for grids 1 and 2, respectively.

Distributions of $(E, \pm U_v)$ and $(E_c, \pm U_{v_c})$ vs. x/L are shown in Figs. 4(a, b) and 4(c, d) for grids 1 and 2, respectively. When E is within $\pm U_v$ or E_c is within $\pm U_{v_c}$, the solutions are validated at the levels of U_v or U_{v_c} , respectively. Since U_D is constant the variations in U_v and U_{v_c} are due to variations in U_G and U_{G_c} . In all cases, lack of validation is mainly due to under prediction of wave crests and troughs in the simulations. For grid 1, $U_{v_c} \sim U_D$ since $U_{G_c} \ll U_D$. Although modeling errors are relatively small (2% and $3\% \xi_{max}$ for grids 1 and 2), Fig. 4 clearly indicates where improvements are warranted.

The overall conclusion for V&V of the wave profile is that ξ is not validated due to modeling errors of about $6\% \xi_{max}$; however, in this case, U_v is relatively large compared to E making the

Table 10 Profile-averaged validation results for corrected wave profile for Series 60

Grid	$E_c\%$	$U_{v_c}\%$	$U_D\%$	$U_{SN}\%$
1	5.6	3.8	3.7	0.9
2	6.6	4.3	3.7	2.2

$\% \xi_{max}$

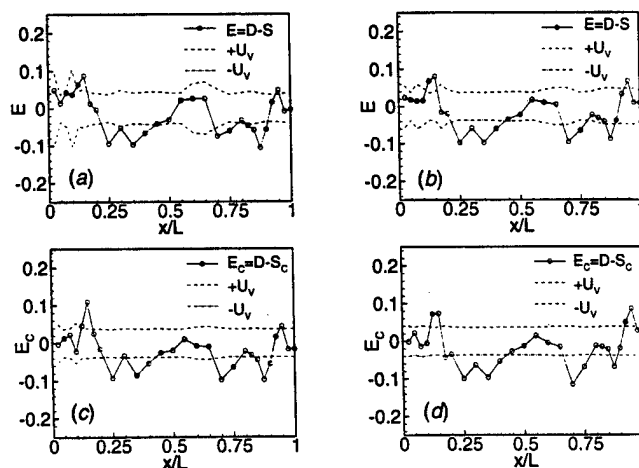


Fig. 4 Validation of wave profile for Series 60: (a) and (b) grid 1; and (c) and (d) grid 2. E and E_c values are normalized with the maximum value for the wave profile $\xi_{max} = 0.014$

margin for reduction in modeling errors small (i.e., $2\% \xi_{max}$). Modeling improvements should be made to increase simulation predictions at crests and troughs so that solutions are validated at about the $4\% \xi_{max}$ level. Reducing the level of validation uncertainty primarily requires reduction in experimental uncertainties; since, $U_D (= 4\% \xi_{max}) > U_{G_c} (= 1\% \xi_{max})$.

8 Conclusions

In Part 2 of this two-part paper, V&V results were presented for RANS simulation of the Series 60 cargo/container ship, which provides a documented solution following the methodology and procedures presented in Part 1 (Stern et al., [2]). Although there are many issues for practical applications, the methodology and procedures are shown to be successful in assessing levels of verification and validation and identifying modeling errors in some cases. For practical applications, solutions are far from the asymptotic range; therefore, analysis and interpretation of the results is shown to be important in assessing variability for order of accuracy, levels of verification, and strategies for reducing numerical and modeling errors and uncertainties.

Verification of the resistance (integral variable) and wave profile (point variable) indicates iterative uncertainties are much less than grid uncertainties, which are about $2\% S_1$ for the finest grid with 0.9M points. Solutions on the next finer grid with 2.4M points likely will reduce simulation numerical uncertainties to $< 1\% S_1$; however, iterative errors may be of similar order making it difficult to separate iterative and grid uncertainties. Therefore, from a resource point of view it may be sufficient to accept the current corrected solution (numerical benchmark) on the finest grid with corrected grid uncertainty $U_{G_c} = 1\% S_1$. Validation of the resistance and wave profile shows modeling errors of about $8\% D$ and $6\% \xi_{max}$, which should be addressed for possible validation at the $3\% D$ and $4\% \xi_{max}$ levels. Reducing the level of validation uncertainty primarily requires reduction in experimental uncertainties; since, $U_D > U_{G_c}$. The combination of a reduction of E (through reduction of modeling errors) and U_D will produce verified and validated CFD simulations with low levels of simulation modeling and numerical errors and uncertainties.

Future work will focus on both fundamental and practical V&V issues, especially for applications with complex geometry. Fundamental issues include the convergence of the power series expansion for numerical error, assumptions that the order of accuracy is constant for all solutions, and estimation of the limiting order of accuracy in the definition of correction factor. Issues with practical applications involve observed variability in order of accuracy estimates, existence of the asymptotic range, and generation of multiple grids and solutions with non-integer refinement ratio. The behavior of the asymptotic range was successfully demonstrated in Appendix A of Part 1 for simpler analytical benchmark problems. However, the existence and behavior of the asymptotic range for practical problems has not yet been demonstrated. Such an effort would require solutions on many more grids to properly assess variability in order of accuracy estimates and finer grids to ensure solutions are indeed in the asymptotic range. More experience is needed for additional practical applications and different CFD codes.

Acknowledgments

This research was sponsored by the Office of Naval Research under grants N00014-96-1-0018, N00014-97-1-0014, and N00014-97-1-0151 under the administration of Dr. E. P. Rood.

References

- [1] Mehta, U. B., 1998, "Credible Computational Fluids Dynamics Simulations," AIAA Journal, **36**, pp. 665–667.
- [2] Stern, F., Wilson, R. V., Coleman, H., and Paterson, E., 2001, "Verification and Validation of CFD Simulations: Part I—Comprehensive Methodology," ASME J. Fluids Eng., **123**, published in this issue, pp. 793–802.

- [3] Stern, F., Wilson, R. V., Coleman, H., and Paterson, E., 1999, "Verification and Validation of CFD Simulations," Iowa Institute of Hydraulic Research, The University of Iowa, IHR Report No. 407.
- [4] Paterson, E. G., and Sinkovits, R. S., 1999, "Performance, Scalability, and Portability of a MPI-based version of CFDShip-IOWA: Results of a NAVO PET Tiger-Team Collaboration," 9th DoD HPC Users Group Meeting, Monterey, CA, June.
- [5] Paterson, E. G., Wilson, R. V., and Stern, F., 1998, "CFDShip-IOWA and Steady Flow RANS Simulation of DTMB Model 5415," 1st Symposium on Marine Applications of Computational Fluid Dynamics, McLean, VA, 19–21 May.
- [6] Wilson, R., Paterson, E., and Stern, F., 1998, "Unsteady RANS CFD Method for Naval Combatant in Waves," Proc. 22nd ONR Symposium on Naval Hydro, Washington, DC, August.
- [7] CFD Workshop Tokyo 1994, Proceedings, Vol. 1 and 2, 1994, Ship Research Institute Ministry of Transport Ship & Ocean Foundation.
- [8] Toda, Y., Stern, F., and Longo, J., 1992, "Mean-Flow Measurements in the Boundary Layer and Wake and Wave Field of a Series 60 CB=.6 Model Ship—Part 1: Froude Numbers .16 and .316," *Journal of Ship Research*, 36, No. 4, pp. 360–377.
- [9] Longo, J. and Stern, F., 1998, "Resistance, Sinkage and Trim, Wave Profile, and Nominal Wake and Uncertainty Assessment for DTMB Model 5512," Proc. 25th ATTC, Iowa City, IA, 24–25 Sept.
- [10] Coleman, H. W., and Steele, W. G., 1999, *Experimentation and Uncertainty Analysis for Engineers*, 2nd Edition, Wiley, New York, NY.
- [11] Ogiwara, S., and Kajitani, H., 1994, "Pressure Distribution on the Hull Surface of Series 60 ($C_B=0.60$) Model," Proceedings CFD Workshop Tokyo, 1, pp. 350–358.
- [12] Wilson, R., Paterson, E., and Stern, F., 2000 "Verification and Validation for RANS Simulation of a Naval Combatant," Preprints of Gothenburg 2000 A Workshop on Numerical Ship Hydrodynamics.
- [13] Eca, L., and Hoekstra, M., 2000, "On the Application of Verification Procedures in Computational Fluid Dynamics," 2nd MARNET Workshop.
- [14] Roache, P. J., 1998, *Verification and Validation in Computational Science and Engineering*, Hermosa Publishers, Albuquerque, New Mexico.
- [15] Larsson, L., Stern, F., and Bertram, V., 2000, "Gothenburg 2000 A Workshop on Numerical Ship Hydrodynamics," Chalmers University of Technology, Gothenburg, Sweden, Sept. 2000.